Aus dem Institut für Neurophysiologie der Medizinischen Fakultät Charité – Universitätsmedizin Berlin

DISSERTATION

Gamma Oscillation-Induced Plasticity in Area CA3 of the hippocampus

zur Erlangung des akademischen Grades
Doctor medicinae (Dr. med.)

der Medizinischen Fakultät
Charité – Universitätsmedizin Berlin

vorgelegt von

Shota Zarnadze

aus Terjola, Georgien

Datum der Promotion: 26.02.2016

Table of Contents:

Abstract

Long-term potentiation (LTP) of synaptic transmission is crucial for learning and memory formation. However, most conventional LTP studies have been performed using high frequency stimulation of inputs while controlling postsynaptic cell activity allowing or preventing the generation of action potentials. The aim of this study was to investigate synaptic transmission changes induced during gamma frequency oscillations *in vitro*, which bear a close resemblance to the conditions under which LTP might occur *in vivo*.

Gamma frequency oscillations are associated with exploratory activity and have an important role in memory encoding. Another memory-relevant network pattern, sharp-wave-ripples (SWRs), is implicated in consolidation of previously acquired information. Yet, the interaction and interdependence of these different network oscillatory states have not been fully elucidated.

In our *in vitro* conditions, the neuronal network was capable of generating both SWRs and gamma rhythms allowing us to investigate synaptic properties and firing behavior of individual morphologically identified neurons during these rhythms and dynamic switching of their activity from one into another oscillatory state.

We uncovered gamma rhythm-induced plasticity changes in the CA3 network, including alterations in subsequent SWR activity. After gamma frequency oscillations, we observed significantly increased SWR-associated reappeared excitatory postsynaptic currents (r-EPSC) in pyramidal cells (PCs). These changes were expressed postsynaptically and mediated by metabotropic glutamate receptor 5 (mGluR5) activation. In contrast to EPSC, SWR-associated reappeared inhibitory postsynaptic currents (r-IPSC) in PCs increased moderately and did not depend on postsynaptic activity. Consequently, gamma rhythm-induced changes in SWR-associated postsynaptic currents were reflected in a significantly increased EPSC/IPSC ratio in PCs obviously favoring their excitation.

We further investigated gamma rhythm-induced synaptic plasticity in interneurons. Different interneuron types exhibited clear cell type-specific changes in their excitability, whereas parvalbumin-positive (PV+) interneurons showed raised excitability after gamma frequency oscillations, cholecystokinin-positive basket cells (CCK+ BC) demonstrated enhanced inhibition. These alterations were reflected in significant increase and decrease of the SWR-associated EPSC/IPSC ratio in PV+ and CCK+ interneurons, respectively.

Thus, gamma rhythm led to activity-dependent long-lasting alterations in the CA3 network and induced postsynaptically mediated mGluR5-dependent LTP of excitatory postsynaptic currents

in PCs. Cell type-specific contradirectional modifications of cell excitability in two distinct interneuron classes may account for a moderate increase in PC-IPSC, which, in turn, could serve the control of increased PC excitability. We propose that gamma rhythm-associated synchronization of network activity supports cell type-specific modifications of synaptic strength and may thereby lead to formation of memory traces.

Abstract in German

Die Langzeitpotenzierung (LTP) der synaptischen Signalübertragung ist grundlegend für Lernen und Gedächtnisbildung. Allerdings wurden die meisten konventionellen LTP-Studien mit einer hochfrequenten Stimulation des Eingangs bei gleichzeitiger Kontrolle der Aktivität der postsynaptsichen Zelle unter Ermöglichung oder Verhinderung der Generierung von Aktionspotentialen durchgeführt. Ziel der vorliegenden Studie war es, *in vitro* Veränderungen der synaptischen Übertragung induziert durch Netzwerkoszillationen im Gammafrequenzbereich zu untersuchen, die eine große Ähnlichkeit zu möglichen *in vivo* Bedingungen der LTP aufzeigen.

Oszillationen im Gammafrequenzbereich sind mit Erkundungsverhalten verbunden und spielen eine wichtige Rolle für die Kodierung von Gedächtnisinhalten. Eine weitere für das Gedächtnis wichtige Netzwerkaktivität stellen die sogenannten „Sharp-wave-ripples“ (SWRs) dar, die an der Konsolidierung vorher erworbener Informationen beteiligt sind. Allerdings sind Wechselwirkung und Abhängigkeit dieser unterschiedlichen Aktivitätsmuster nicht vollständig geklärt.

In unseren *in vitro* Bedingungen können beide Aktivitätsmuster, SWRs und Gamma Oszillationen, generiert werden, wodurch wir die synaptischen Eigenschaften und Entladungsmuster einzelner morphologisch identifizierten Neuronen während dieser Rhythmen untersuchen und deren dynamische Umschaltung zwischen den Rhythmen analysieren konnten.

Wir fanden durch Gamma Oszillationen induzierte Aktivitäsänderung des CA3 Netzwerkes in nachfolgender SWRs. In Pyramidenzellen (PCs) beobachteten wir im Zusammenhang mit den wiederkehrenden SWRs signifikant erhöhte erregende postsynaptische Ströme (r-EPSC). Diese Änderungen wurden postsynaptisch generiert und durch die Aktivität des metabotropen Glutamatrezeptors vom Typ 5 (mGluR5) vermittelt. Im Gegensatz zu den EPSC, vergrößerten sich die mit den wiederkehrenden SWRs verbundenen hemmenden postsynaptischen Ströme (r-IPSC) in PC nur moderat und waren unabhängig von einer postsynaptischen Aktivität. Somit spiegeln die durch Gamma Oszillationen induzierten Veränderungen der SWR-assoziierten Ströme einen signifikanten Anstieg des PC EPSC/IPSC-Verhältnisses wider, wodurch offensichtlich die PC-Erregbarkeit gefördert wird.

Zudem untersuchten wir Gamma induzierte synaptische Plastizität in Interneuronen. Verschiedene Interneuronengruppen wiesen dabei klare zelltypspezifische Veränderung der Erregbarkeit auf: Parvalbumin-positive (PV+) Interneurone zeigten nach dem Gamma-Rhythmus eine erhöhte Erregbarkeit, Cholecystokinin-enthaltenden Korbzellen (CCK+) eine verstärkte

Hemmung. Diese Veränderungen zeigten sich in den entsprechend signifikant veränderten SWR-assoziierten EPSC/IPSC-Verhältnissen.

Insgesamt führen Gamma Oszillationen zu aktivitätsabhängigen, lang anhaltenden Veränderungen im CA3 Netzwerk, inklusive einer postsynaptisch vermittelten mGluR5-abhängigen LTP der PC EPSC. Die entgegengesetzte Veränderung der Erregbarkeit zweier Interneurontypen kann verantwortlich für die insgesamt nur mäßige Verstärkung pyramidaler IPSC sein, was wiederum der Kontrollerhaltung über die erhöhte PC-Erregbarkeit dienen könnte. Unsere Ergebnisse legen nahe, dass die mit Gamma Oszillationen assoziierte Synchronisierung der Netzwerkaktivität zu zelltypspezifischer Veränderung der synaptischen Übertragungsstärke führen und dadurch zur Bildung von Gedächtnisspuren beitragen kann.

Introduction

1. Anatomy and connectivity of the hippocampus

The hippocampal formation (HF) is divided into three parts and includes the dentate gyrus (DG), hippocampus proper (HP) and the subiculum (SUB). The hippocampal proper in rodents is composed of three sub-regions: CA3, CA2 and CA1. The CA3 region can be divided into three distinct areas: CA3a adjacent to CA1, CA3c bordering the DG and CA3b located between these two areas [1, 2].

The HF has a laminated organization. Based on their cellular composition and arrangement of input-output projections, the most superficial layer of the hippocampus proper is subdivided into three strata: The stratum lacunosum moleculare housing the apical tufts of the apical dendrites, the stratum radiatum containing the apical dendrites of hippocampal neurons and the stratum lucidum composed of the mossy fiber input from the DG. The latter belongs, and is exclusively restricted, to the CA3 area. Below this layer is situated the stratum pyramidale composed of principal cells and interneurons. The deepest layer is referred to as the stratum oriens that contains the basal dendrites of PCs as well as somas and a mixture of input-output fibers of local interneurons [3].

The DG represents a three-layered structure consisting of the hilus, the granular cell layer and the molecular layer [4]. In the SUB, these three layers are the polymorphic layer, the PCs layer and the molecular layer [5].

The entorhinal cortex (EC) as the primary interface between the neocortex and HF is divided into two parts: medial (MEC) and lateral (LEC). The lamination of the MEC and LEC is similar and includes six layers: layer I is a molecular layer, layer II- the stellate cell layer, layer III – the superficial PC-layer, layer IV – the lamina dissecans, layer V – the deep PC-layer and layer VI – the polymorph cell layer [6].

2. Intrahippocampal connections

According to the standard model, the principal (granular) cells in the DG referred to as mossy fibers, form unidirectional projections to the CA3 region. The mossy fibers synapse proximal dendrites of principal cells as well as inhibitory interneurons in the stratum lucidum and are confined to the CA3 area. PCs in CA3 give raise to highly arborized axons that project to the CA1 cells forming Schaffer collaterals, CA3 neurons via recurrent collaterals as well as to the same region in the contralateral hippocampus via commissural projections [2]. Interestingly, the

intrahippocampal connections show a particular topology along the transverse axis. The distal CA3 targets the proximal part of CA1 and, conversely, the proximal CA3 projects to the distal CA1. Similarly, The proximal part of CA1 is connected to the distal SUB, whereas the distal CA1 synapse the proximal SUB [7].

However, in contrast to the standard unidirectional model, several backprojections have also been reported in the HF, for instance, from the CA3 to the hilus and DG, from the CA1 to the CA3 as well as from the SUB to the CA1 [8, 9, 10]. However, the functional implications of these connections remains to be determined.

3. Extrahippocampal connections

3.1. Input

The high-order associative neocortical sensory projections reach EC via the parahippocampal region. In particular, the perirhinal cortex (PER) projects to the LEC and the postrhinal cortex aims at the MEC. The EC connects the DG via strong projections generally known as the perforant path (PP) as well as the other sub-regions of HF [11, 12]. Importantly, the different layers of EC target at different areas of HF, i.e., the layer II projects to the DG and CA3 [13], whereas, layer III issues its connections to the CA1 and SUB [7, 14, 15]. The PP perforate the PC-layer of the SUB subsequently, crossing the hippocampal fissure or traveling via the stratum lacunosum moleculare of the HP and eventually reach the molecular layer of DG. In addition, there is an alternative way in which projections travel through stratum oriens of the SUB and HP without perforating the stratum pyramidale of the SUB. These projections cross the stratum pyramidale of the CA1 and terminate in its stratum lacunosum moleculare. This pathway is referred to as the temporo-ammonic tract [13].

The targets of the axons from layer II of MEC are located deeper in DG and CA3 area than those of the LEC and constitute altogether the outer two-third of the molecular layer of the DG and the entire radial dimension of the stratum lacunosum moleculare of the CA3. It is assumed that the projections to the DG and the CA3 originate as collaterals from the same neuron of layer II of EC [3, 13].

The layer III of the MEC and LEC targets CA1 and SUB and exhibits a remarkably different termination pattern along the transverse axis, namely, the LEC selectively aims at the distal part of CA1 and proximal part of the SUB. In contrast, the projection that arises from the MEC selectively targets neurons in the proximal CA1 and the distal SUB. They travel through the

stratum lacunosum moleculare of CA1 and stratum moleculare of the SUB end eventually terminate on the apical dendrites of the principal cells and interneurons [3, 14].

In addition to the EC, the direct connections to the HF from other extrahippocampal regions such as the perirhinal/postrhinal cortexes, pre- and parasubiculum as well as the reticulo-septal input have been described [14, 16, 17].

3.2. Output

The main output projections emerge from CA1 and SUB and they primarily target the deep layers of EC. Nevertheless, the existence of projections to the superficial layers have also been reported [10, 18].

The output organization mimics input, which means that the proximal part of CA1 and distal part of SUB are strongly connected to the MEC, whereas the distal part of CA1 and proximal part of SUB project to the LEC [3, 7, 19]. Additionally, projections from the CA3, CA1 and SUB to the pre- and parasubiculum as well as direct connections between the CA1/SUB and peri-/postrhinal cortexes have also been described [3].

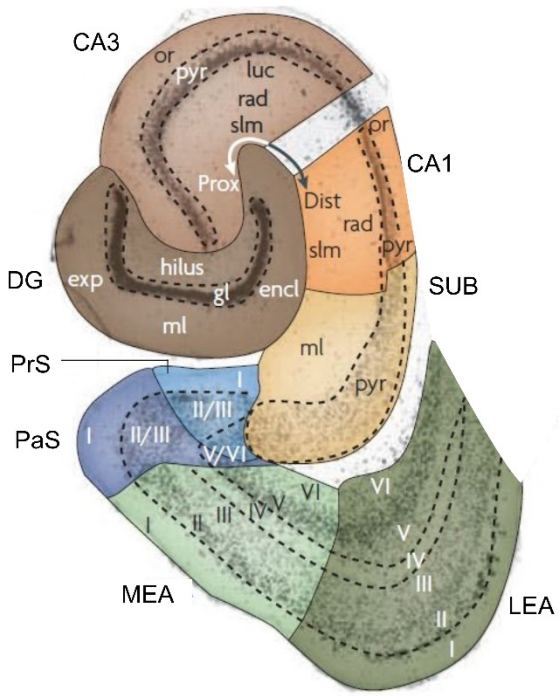

Figure 1.1. Hippocampal formation and entorhinal cortex in the rat brain. Cortical layers in a horizontal HF-EC combined slice. Cortical layers are indicated by Roman numerals. CA, cornu ammonis; SUB, subiculum; PrS, presubiculum; PaS, parasubiculum; MEA, medial entorhinal area; LEA, lateral entorhinal area; dist, distal; encl, enclosed blade of the DG; exp, exposed blade of the DG; gl, granule cell layer; luc, stratum lucidum; ml, molecular layer; or, stratum oriens; prox, proximal; pyr, pyramidal cell layer; rad, stratum radiatum; slm, stratum lacunosum moleculare; (Adapted from Van Strien, N.M; Cappaert, N.L.M and Witter, M.P; 2009; The anatomy of memory: an alternative overview of the parahippocampal-hippocampal network; Nature Reviews Neuroscience 10, page 274, Figure 1.C).

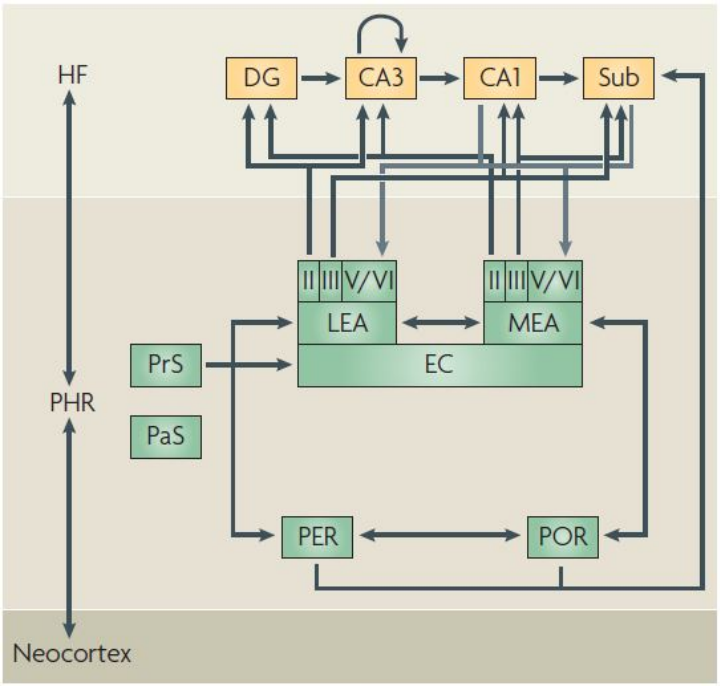

Figure 1.2. The parahippocampal–hippocampal circuitry. According to the standard view, neocortical projections connect the parahippocampal region (PHR), which in turn provides the main source of input to the HF. The PHR is aimed at the EC via two parallel projection streams: the perirhinal cortex (PER) is connected to the lateral entorhinal area (LEA), and the postrhinal cortex (POR) projects to the medial entorhinal area (MEA). The EC is bidirectionally connected to the PER and the POR. Furthermore, the EC receives input from the presubiculum (PrS). The EC gives rise the perforant pathway, which projects to all subregions of the HF. Projections to the DG and CA3 emanate from layer II of EC, whereas layer III is connected to CA1 and the subiculum (SUB). The DG granule cells give rise to the mossy fibre pathway, which targets CA3. The CA3 Schaffer collaterals project to CA1 and, lastly, CA1 projects to the Sub. Output from the HF arises in CA1 and the SUB and is directed to the PHR, in particular to the deep layers of the EC. The Roman numerals indicate cortical layers (From Van Strien, N.M; Cappaert, N.L.M and Witter, M.P; 2009; The anatomy of memory: an alternative overview of the parahippocampal-hippocampal network; Nature Reviews Neuroscience 10, page 276, Figure 3).

4. Hippocampal cells

4.1. Principal cells

Cellular architecture and organization of principal cells in the HF have been studied extensively over the past 100 years. As the first stage of the intrahippocampal trisynaptic loop, the DG is the target for the majority of entorhinal afferents. Principal cells in this region are the granule cells. These cells are characterized by two main radially orientated dendrites confined to stratum moleculare. The axons of mossy fibers originate from the opposite pole of cell soma. They are referred to as mossy fiber, enter the hilus and give rise to local collaterals remaining in hilar region [20]. The main axon of granule cells leaves the hilus entering the stratum lucidum and forms synapses on the PCs. The axon terminals exhibit large boutons called giant en passant boutons [21].

The principal cell type of the hilus is the mossy cell, which exhibit densely spiny dendrites and several thornlike excrescences. The dendritic tuft is mostly confined to the hilus [22]. Their axons terminate on the cells located in the inner one third of molecular layer of DG ipsi- and contralaterally. Additionally, they exhibit collaterals within the hilar region [22, 23].

The cell body of CA3 PCs are mostly located in the stratum pyramidale. Some dislocated PCs have also been described in the stratum radiatum [24, 25]. One or two prominent apical dendrites emerging from the soma are radially orientated in strata radiatum und lacunosum moleculare. Two to eight basal dendrites emerge from the base of the soma in the stratum oriens. Their terminal branches run toward the alveus. The entire dendritic tree exhibits thin spines. The proximal dendrites in the stratum lucidum are characterized by large complex spines, called thorny excrescences, which are formed by synaptic terminals of mossy fibers from granule cells of DG [1, 26]. The excitatory afferents of principal cells show a strictly laminated pattern. The stratum lucidum, as mentioned above, includes mossy fiber terminals, the stratum radiatum and the stratum oriens receive projections from other PCs from both ipsi- and contralateral hippocampus, which form so-called associational commissural collaterals. Apart from that, the stratum lacunosum moleculare comprising the most distal dendrites of PCs is innervated by direct projections from the EC [19, 27].

The axon of CA3 PCs emanates typically from the lower pole of the soma or one of the proximal dendrites. They project both to the ipsi- and contralateral hippocampus, thereby forming the commissural/associational pathway [28]. However, the CA3c region exhibits also collaterals projecting to the hilus and DG [28, 29]. The subregions of the CA3 area have a bias for certain

CA1 subregions. The CA3c, for instance, preferentially innervates the distal part of the CA1 close to the subicular border, whereas the axons originating from the CA3a terminate predominantly on the cells in the adjacent proximal CA1 segment. The cells from CA3b make synapses on the neurons in the middle part of CA1 region [28].

PCs in the CA1 region have a somewhat smaller cell body than those in CA3. They have small-caliber basal dendrites repeatedly bifurcating close to the soma running toward the alveus and a large-caliber apical dendrite extending into the stratum radiatum [30] bifurcating and forming a dendritic tuft in the stratum lacunosum molecurale.

The axon of CA1 PCs much the same as that of CA3 PCs emerges either from the base of the soma or from one of the proximal dendrites. The main collaterals enter the alveus and run toward the SUB, the entorhinal cortex or the fimbria/fornix. The CA1 PC-axons are characterized by a more prominent local arborization in the stratum oriens than in the stratum radiatum and a sparse recurrent connectivity at only 1 % [31].

It is worth noting that PCs in the CA2 region, which are the most overlooked area in the hippocampus, have been reported to lack mossy fiber input or thorny excrescences [1] . This region has been considered as a passive transient zone between CA3 and CA1. However, recent studies attempted to investigate specific features and cell connectivity of CA2 suggesting an afferentation by the supramammillary nucleus of the hypothalamus [32] along with a sparse innervation by the nucleus reuniens of the thalamus [33]. Nevertheless, the spatial coding properties of CA2 neurons, local field potential manifestation during different behavioral states in its neuronal circuits and the functional impacts of its lesion remain to be elucidated [34].

4.2. Diversity of hippocampal interneurons

The hippocampal interneurons exhibit a large degree heterogeneity. They can be classified into several classes based on their morphological features, expression of neurochemical markers and transcription factors as well as on their electrophysiological properties [21]. In contrast to principal cells, interneurons are characterized by extensive local axonal arborization enabling them to control the activity of large sets of pyramidal cells [21, 35, 36]. Over 21 interneurons classes have been described in the CA1 area [37]. According to one of the common classifications, interneurons are divided with respect to their axonal ramification pattern, including selective innervation of either principal cells or interneurons (interneuron-specific interneurons, ISI). The axons of principal cell-targeting interneurons spatially segregate different domains, either the soma or dendrites, of principal cells. Thus, there are perisomatic-targeting

interneurons such as BCs and axo-axonic (AAC) cells, which control the output whereas dendritic targeting cells, such as bistratified (BSC), trilaminar interneurons, oriens-lacunosum moleculare cells (O-LM), regulate efficacy and plasticity of inputs [21, 38, 39] .

4.2.1. Perisomatic-targeting interneurons

4.2.1.1. Basket cells

On the basis of their neurochemical content, the hippocampal BCs are divided into two classes: BCs containing a calcium binding protein parvalbumin (PV+ BCs) [40] and neuropeptide cholecystokinin (CCK+ BCs) [41]. These cells show a morphological resemblance in terms of their somata location as well as dendritic and axonal arborization patterns but they differ remarkably in their electrophysiological properties. Cell bodies of BCs are located predominantly in the stratum pyramidale. Exceptionally, they have been found in stratum radiatum. They have a bitufted dendritic tree and span all layers [42, 43]. BCs form synapses with the cell bodies and proximal dendrites of principal cells and other GABAergic interneurons [43, 44]. The extent of axon terminals is largely restricted to the stratum pyramidale [21]. Although the two populations of BCs containing either PV or CCK share several neuroanatomical characteristics, they have very different electrophysiological properties: PV-BCs display a fast-spiking firing pattern, are able to generate action potentials upon a depolarizing current injection at a very high frequency range of about 100 Hz without accommodation and are primarily activated by feedforward (FF) glutamatergic input with high temporal fidelity, while CCK+ BCs have a regular-spiking firing pattern with considerable accommodation and are best activated by temporal summation of convergent FF and feedback (FB) glutamatergic input [44, 45, 46].

4.2.1.2. Axo-axonic cells

Cell bodies of AACs are located in the stratum pyramidale or oriens. Most of the dendrites are vertically orientated spanning all layers. A few cells with horizontally orientated dendrites in the stratum oriens have also been found [47]. In contrast to PV-BCs, the apical dendrites often show extensive arborization in the stratum lacunosum moleculare [48, 49]. These cells receive input from all major afferent terminals [48, 50]. There is some evidence of gap-junction coupling of these cells in the PV+ interneuron network receiving inhibitory inputs from PV+ GABAergic interneurons [51, 52]. AACs do not give rise to any inhibitory connections to other PV+

interneurons but rather form 2-10 GABAergic synapses on single axon initial segments of up to 1200 PCs [50] controlling synaptic output of these cells. AAC show a fast-spiking discharge pattern and contain a high level of PV [44, 53].

4.2.2. Dendritic inhibitory interneurons

Principal cell dendritic targeting interneurons exhibit a high diversity in their morphology. With respect to the targeted dendritic segment and axonal ramification pattern, they could be divided into distal, such as Oriens-lacunosum moleculare (O-LM) cells, and proximal, such as BSCs, dendrite-targeting interneurons [21, 45].

4.2.2.1. Bistratified cells

Cell bodies of these cells are located in the stratum pyramidale or oriens. The radially orientated dendritic tree is largely confined to the stratum oriens and radiatum and rarely invades the stratum lacunosum moleculare [42, 43, 54]. BSCs have a typical axonal arborization in two adjacent layers (hence the name): stratum oriens and radiatum co-aligned with the Schaffer collaterals [38, 42]. The axons form synapses predominantly on shafts and spines of small-caliber dendrites and rarely on large-caliber apical dendrites or cell bodies of PCs [43, 54]. BSCs are believed to target other GABAergic interneurons via gap junctions and mutual inhibitory synapses [51, 52]. They have a fast-spiking firing pattern, are positive for PV, somatostatine and neuropeptide Y and express high levels of $GABA_A$-alpha1 subunit [44, 52, 54].

4.2.2.2. Trilaminar cells

Cell bodies and the sparsely spiny dendritic tuft are located in the stratum oriens. The Input from inhibitory and excitatory terminals expresses high levels of mGluR8 that makes them likely to be strongly modulated by glutamatergic transmission [55]. The excitatory input may derive from local PCs and the inhibitory input from ISI [55]. The axonal ramification pattern shows, as the name implies, a typical distribution to tree adjacent layers: the stratum radiatum, pyramidale and the oriens [55, 56]. The axon targets distal neighboring areas in the hippocampus [55, 56] and other brain areas. Trilaminar cells are connected to interneuron cell bodies and dendrites as well as to dendritic shafts and somata of PCs [55]. They have a fast-spiking firing pattern. The biochemical markers of these cells are widely unknown with the exception of high levels of muscarinic acetylcholine receptor (M2) [55, 57].

4.2.2.3. Oriens-lacunosum moleculare cells

The cell bodies are located in the stratum oriens close to the alveus. The dendritic tree is mainly confined to the stratum oriens. The axon originates from the soma or one of major dendrites [58]. The axon extends through the stratum pyramidale and radiatum and densely arborizes in the stratum lacunosum moleculare [45]. 3D reconstruction of these cells revealed that the axonal plexus is most extensively arborized in the longitudinal axis of the hippocampus [59]. The axon projects on distal dendrites of PCs and is co-aligned with the perforant path (PP) [45]. It receives excitatory input from PCs and mediate FB inhibition [60]. They innervate other interneurons as well [61]. O-LM cells show immunoreactivity for somatostatin, neuropeptide Y, mGluR 1 alpha and PV [40. 45, 49, 62].

5. Network oscillatory activity in the Hippocampus

By synchronized and coordinated activity, hippocampal neurons establish functionally specialized assemblies, which are able to generate several oscillatory bands in a behavior-dependent frequency range [63, 64]. Three types of hippocampal oscillatory activities have been described in *in vivo* [65]. Theta (5-10 Hz) and gamma (30-100 Hz) frequency oscillations have been observed during exploratory activity and rapid eye movement sleep occurring concurrently or separately [36]. Behavior-dependent occurrence of these rhythms suggests their fundamental role in encoding and retrieval of memory traces [66, 67], feature recognition, associative learning and processing of sensory information. The third type of behavior-dependent oscillatory activities, so-called sharp wave-associated ripples (100-300Hz), have been observed during slow wave sleep and consummatory activities [68, 69, 70]. Various *in vitro* models have been established to reproduce these rhythms in slice preparations in order to clarify the cellular and synaptic mechanisms underlying the rhythm generation [56, 59, 71, 72, 73].

Using novel techniques, the challenge of conjointly recording single neuron activity and extracellular filed potential oscillations *in vivo* and *in vitro* [49, 56, 59, 73, 74, 75] have been met, permitting to gain deeper insight into activity patterns of individual neurons during different rhythmic activities accompanying different hippocampal network states.

5.1. Gamma oscillations *in vivo* and *in vitro*

Hippocampal gamma oscillations in freely moving rodents have been reported to be mostly superposed on theta frequency oscillations. This highly synchronous local field activity can be generated in the DG requiring an extrahippocampal drive which may arrive from the EC.

Another gamma generator has been identified intrahippocampally in the CA3-CA1 areas. However, the exact underlying mechanisms of the emergence of gamma rhythms remain to be elucidated [66, 76], yet recent experimental evidence suggests that due to the particular morphological features (recurrent collaterals) of its principal cells, the CA3 region is likely to generate intrahippocampal gamma oscillations which then entrain the CA1 region via CA1 inhibitory network.

Two major forms of gamma frequency oscillation have been postulated in hippocampal slices: transient, lasting for a few seconds or minutes induced by tetanic stimulation (Wittington et al., 1997), high molarity of kainate (KA) [56, 59], potassium [78] or through pressure ejection of glutamate [39, 79] and persistent, lasting for hours induced by bath application of muscarinic acetylcholine receptor [80] and KA receptor [56, 59, 81] agonists, CCh and KA, respectively. These *in vitro* oscillations exhibit a considerable resemblance to them observed *in vivo* with respect to many of the features such as gamma phase relationship between PCs and perisomatic-targeting GABAergic interneurons [76, 82], loci of generation (CA3) and propagation [59]. Gamma frequency oscillation can be obtained from different hippocampal areas, including DG, CA3 and CA1 [59, 78, 79]. However, they differ in their features such as frequency and power, indicating different gamma current generators in the hippocampus. Gamma oscillations in the DG, for example, requires an extrahippocampal drive from the EC [66, 76], whereas these oscillations can be generated intrinsically by the interaction of CA3 PCs and GABAergic interneurons in the CA3-CA1 neuronal network [76]. Two major scenarios of interaction between PCs and interneurons have been proposed for gamma oscillations. According to the "pyramidal interneuron network gamma" theory, gamma frequency oscillations can be generated by reciprocal PC-interneuron interaction [77], whereas the "interneuronal network gamma" theory suggests a mutual inhibition between GABAergic interneurons [83, 84]. Observations *in vivo* are in agreement with *in vitro* investigations, suggesting the same underlying cellular mechanisms in the intact hippocampus and hippocampal slice preparation [76].

5.1.1. Firing patterns in gamma frequency oscillations

For generation of neuronal network oscillations, rhythmic synchronous activity of large sets of neurons is required. In order to uncover their role in field potential activity, the characteristic firing pattern during different oscillations has to be analyzed.

5.1.1.1. Principal cells

Although PCs in CA3 and CA1 share some morphological and electrophysiological properties, the population of these cells is not homogenous and displays important differences such as the existence of recurrent collaterals in CA3 but not CA1 PCs [39]. Even CA3 PCs show differences with respect to their connectivity pattern: Whereas CA3a and CA3b neurons form extensive recurrent collaterals targeting CA3 neurons, PC in the CA3c area project to the CA1 region [28]. This morphological diversity may be important for driving network oscillations [76]. PCs exhibit a low frequency firing pattern during gamma oscillations and peak activity of these cells precedes the peak of interneuron firing in the CA3 area *in vivo* [76]. Observations on the firing behavior of PCs during KA and CCh-induced gamma oscillations *in vitro* [56, 59, 73] revealed comparable firing properties during gamma activity obtained *in vivo* [76]. According to these observations, PCs generate action potentials around the negative peak of gamma cycles in the PCs layer and recruit local interneurons in the FB-manner so that the firing of PC precedes interneuron discharges [73]. Interneurons recorded during KA-induced gamma frequency oscillations *in vitro* receive a gamma frequency-modulated compound excitatory postsynaptic current (EPSC) [59]. Due to differentiation of hippocampal slices *in vitro*, one could assume that the strong EPSC on interneurons is mediated by local excitatory input from adjacent PCs. Considering the low frequency firing pattern of PCs during gamma oscillations, the question arises as to how PCs can generate this high frequency barrage of EPSC to discharge interneurons reliably. Although the exact source of this excitation remains to be uncovered, there is strong experimental evidence suggesting different underlying cellular and synaptic mechanisms for this observation. The high degree of PC-convergence onto single interneurons enables interneurons to receive multiple unitary EPSC on each gamma cycle. Furthermore, axonal spikes can be generated ectopically in the axon without invading the soma [85]. Recent experimental data have convincingly demonstrated that during gamma frequency oscillations, the frequency of action currents in axons recorded >600µm from the soma was higher by a factor of 4 to 5 than in the soma of CA3 PCs [86]. These results suggest that ectopically generated action potentials may propagate orthodromically and excite interneurons.

5.1.1.2. Interneurons

Hippocampal interneurons constitute a highly inhomogeneous population with respect to their morphological, electrophysiological and immunohistochemical characteristics. At least 21 classes of interneurons have been reported in the CA1 region [37]. Depending on their firing

pattern and targeted subcellular domain of principal cells, they could differently contribute to the generation of gamma frequency oscillations. However, little is known about deferent firing patterns and contributions of individual interneurons within hippocampal network *in vivo*. Fast-spiking interneurons in the stratum pyramidale may have a pivotal role in the gamma frequency activity since they have been reported to show a phase correlated firing to gamma oscillations discharging on every gamma cycle [76] and leading to the gamma-modulated postsynaptic somatic inhibition observed in PCs *in vivo* [76, 82]. Indeed, strong in vivo experimental evidence suggests that gamma oscillations can be suppressed by inhibiting and generated by driving PV+ interneurons [87].

Several classes of interneurons have been shown to be crucially involved in gamma rhythm generation *in vitro*. As an important player, perisomatic-targeting PV+ fast-spiking BC exhibits a tightly coupled firing pattern to every gamma cycle and generates a predominantly gamma frequency output [59, 73] and, by providing rhythmic inhibition, entrains hippocampal network in the gamma frequency band.

Another class of perisomatic-targeting BCs is negative for PV, but express CCK, have a regular-spiking firing pattern [44, 45, 46], fire out of phase of gamma oscillations, precede discharges of PC [88] and are supposed to even interfere with gamma synchronicity [89].

Selective expression of PV or CCK correlates well with presence or absence of cannabinoid receptor type 1 (CB1R), respectively. CB1R-positive BCs are characterized by a long membrane time constant, enabling them to integrate activity over longer intervals, whereas CB1R negative interneurons exhibit a fast membrane time constant, permitting generation of a narrow integration time window at about 3 ms [90]. Additionally, it has been found that PV+ BCs receive more excitatory but less GABAergic synapses than CCK BCs [91]. The weaker excitation received by CB1R-positive BCs requires the summation of FF- and FB-EPSPs in sequence to generate a spike, whereas CB1R negative interneurons are able to fire to only FF-EPSPs and mediate FF inhibition to their targets. Since FB-inhibition is important for gamma rhythm generation, CCK+ BCs are likely to be involved in the modulation of gamma oscillations [90]. This notion is supported by experimental evidence of suppression of gamma oscillations by cannabinoids through inhibition of presynaptic GABA release from CCK+ cell terminals [92]. However, according to other evidence, this effect could also be attributed to a presynaptic inhibition of glutamate release from CA3 PCs collaterals, which express low levels of CB1R as well [93].

Thus, PV+ cells are primarily activated by FF excitatory input in CA1 [90] and play a crucial role in the generation of gamma oscillations, whereas CCK+ regular-spiking BCs integrate FB and FF excitatory inputs over a longer time window and fire with less temporal precision and a high failure rate [46].

In contrast to PV+ BCs, PV+ axo-axonic cells demonstrate a weakly coupled firing pattern to the field gamma cycles in anesthetized animals [88]. By inhibiting axon initial segment, these cells could prevent back-propagation of ectopic action potentials in principal cells and thereby separate axonal from somatic activity to maintain functional polarization of hippocampal PCs during network oscillations [86].

Other classes of fast-spiking interneurons, such as BSCs and trilaminar cells, exhibit phase-locked fast-spiking firing patterns generated at every gamma cycle and make these neurons ideally suited to substantially contributing to the generation of local gamma rhythms [59, 73, 88]. Furthermore, collateral projections of trilaminar cells have been described in CA1, SUB as well as other brain areas [64], therefore it is possible that locally generated gamma rhythms can be efficiently transmitted to other brain regions. Electrophysiological properties such as generation of highly regular, short latency spike doublets [59] support this assumption.

In contrast, radiatum interneurons as well as distal dendrite targeting cells such as O-LM and R-LM interneurons show a weak coupling to the gamma oscillations *in vitro* and a low firing rate [73], pointing to their less importance for the gamma rhythm generation.

5.2. Theta Oscillations

Network oscillatory activity in the theta frequency range (5-10 Hz) has been observed during various types of locomotor activities [68] and rapid eye movement sleep [94]. According to one of the classical theories, GABAergic interneurons in the hippocampus receive cholinergic excitation from the septum and diagonal band of Broca which in turn inhibit rhythmically PCs [95]. The EC have been also implicated in the generation mechanisms [96]. Synchronous somatic inhibition and dendritic excitation of PCs have been suggested to be an important underlying mechanism for the theta rhythm generation. While PV+ neurons such as axo-axonic exert perisomatic inhibition, the EC provides rhythmic excitatory inputs to the apical dendrites of PCs [97]. However, there is ample experimental evidence to indicate that hippocampal CA3 and CA1 areas are capable of generating theta frequency oscillation intrinsically [56, 98]. Interestingly, a prerequisite for induction of precisely synchronized theta activity by application of KA in the CA3 area was a longitudinally orientated slice preparation. In this preparation,

axonal arborisation of O-LM cells, which have been reported to be instrumental in theta rhythm generation, is largely preserved [56].

5.2.1. Pyramidal cells

In vivo recordings demonstrated that CA1 PCs fire at the trough of theta oscillations during active exploration [99], whereas CA3 PCs firing is coupled with opposite theta phase, supporting the idea that CA1 neurons are likely to be recruited by rhythmic activity of CA3 cells [100]. Somatic firing has been reported in only few cases in *in vitro* experiments during mGluR activation induced theta rhythms with blockade of α-amino-3-hydroxy-5-methyl-4-isoxazolepropionic acid (AMPA) receptors. PCs demonstrated distal apical dendritic spiking along with compound somatic IPSC, whose pharmacological modulation altered the theta rhythm, suggesting a major importance of inhibitory network.

5.2.2. Interneurons

Both *in vivo* and *in vitro* experimental data convincingly demonstrate the critical involvement of O-LM interneurons in theta rhythm generation [49, 56, 59, 73, 96]. In contrast to perisomatic-targeting fast-spiking interneurons, these cells are characterized by prominent membrane potential oscillations in the theta frequency rage [101], a longer membrane time constant and afterhyperpolarization which seems to be a crucial factor for the firing pattern of O-LM cells [102]. During KA-induced theta and gamma oscillations, O-LM cells fire at the theta frequency range [56], providing a robust rhythmic inhibition to the apical dendrites of PCs. The preservation of extensively arborized axon of O-LM cells in the longitudinal slice preparation could underlie the prominence of theta rhythm in these slices [56].

5.3. Sharp wave-associated ripple activity

SWR represents a particular pattern of fast (~200Hz) network oscillations superimposed on slower sharp waves [72]. This synchronous local field activity has been observed during awake immobility and sleep and is likely to be associated with memory consolidation based on synaptic plasticity and transfer of new memory trace from the hippocampus to the neocortex [103]. The existence of multiple mutual excitatory connections between PCs in the CA3 area makes this region ideally suited for emergence of SWR by triggering synchronized activation and generating compound field EPSP underlying sharp waves [72, 104]. Another possible explanation is that synchronous GABA release from electrically-coupled interneurons may

underlie this local field activity [105]. In line with this tentative explanation, $GABA_A$ receptor antagonists and gap junction blockers abolished SWR activity [106, 107]. SWRs occur spontaneously in *in vitro* slices and have similar properties to those obtained *in vivo* [72]. The cellular and synaptic mechanism of the rhythm generation is not fully clarified.

5.3.1. Pyramidal cells

Several *in vivo* and *in vitro* experiments revealed a critical role of strong recurrent collaterals of CA3 PCs in the SWR initiation, which are transmitted via Schaffer collaterals to the CA1. However, only a small population of PCs has been reported to become active during SWRs *in vitro* [108]. Furthermore, non-participating PCs are inhibited during SWR [72]. According to a recently proposed model, SWRs are initiated by coincident firing of a sufficiently large number of PCs within a critical time window, which, in turn, recruit interneurons [109].

5.3.2. Interneurons

PV+ fast-spiking BCs and BSCs have been reported to show a phase-correlated firing behavior during SWRs *in vivo* [49, 75]. The importance of interneurons for SWR generation has been convincingly demonstrated in *in vitro* studies as well. A local injection of gabazine to block $GABA_A$-mediated perisomatic inhibition was sufficient to decrease SWR amplitude nearly to zero, highlighting a crucial contribution of PC perisomatic inhibition to generation of SWRs [109]. However, the two major classes of perisomatic-targeting interneurons, PV+ fast-spiking and CCK+ regular-spiking BCs, may differently contribute to SWR generation. Recent experimental data have demonstrated that after a blockade of PV+ fast-spiking BCs by pharmacological inhibition of P/Q type Ca^{2+} channels, SWR amplitude decreased and ripple activity vanished, whereas selective inhibition of CCK+ BCs outcome synapses by blockade of N-type Ca^{2+} channels had no influence on SWR parameters [109]. Furthermore, whilst CB1R-positive BCs and axo-axonic cell are weakly recruited, PV+ BCs generate significantly more action potentials during SWRs. In addition, PV+ BCs fire on the larger portion of SWR than CB1R-positive and axo-axonic interneurons [108] making it most likely that these perisomatic-targeting fast-spiking cells play a crucial role in SWR generation. These results are comparable with SWR-associated behavior of interneurons observed *in vivo* [75, 110], suggesting that the *in vitro* model is well suited for investigating the underlying synaptic mechanisms of SWR and firing properties of principal cells and different interneuron types.

6. Synaptic plasticity at hippocampal synapses

Hippocampal synapses can undergo activity-dependent bidirectional changes in synaptic strength. According to the Hebb's theory, synaptic connections are strengthened by coincident firing of inputs on a neuron or simultaneous firing of pre- and postsynaptic neurons [111]. Uncorrelated firing, however, induce long-term depression of synaptic strength [112]. Whereas these theories apply only to associative long-term synaptic plasticity, there are other forms of plasticity, whose rules and induction principles have been postulated later and differ from those of Hebbian plasticity. To these belong non associative or non Hebbian synaptic plasticity requiring activity in only one neuron as well as homeostatic and heterosynaptic plasticity.

The timescale of *in vitro* synaptic plasticity varies from the millisecond (short-term potentiation-STP and depression-STD) to the hour range (long-term potentiation-LTP and depression-LTD).

The major mediator for synaptic plasticity is calcium the level of which can determine the direction of changes in synaptic strength. For STP, for instance, presynaptic Ca^{2+} accumulation leads to an increased transmitter release through heightened probability of presynaptic vesicle depletion [113]. In general, most GABAergic synapses are characterized by a high initial transmitter release probability and exhibit STD, whereas glutamatergic synaptic short-term transmission can be facilitated or depressed [45, 114]. Furthermore, changes in Ca^{2+} concentration have been reported to determine the direction of LTP [115].

6.1. Synaptic plasticity in PCs

Hebbian or associative LTP requires coincident activity in the presynaptic and postsynaptic neurons and depends on the activation of N-methyl-D-aspartate (NMDA) receptors. At the mossy fiber-CA3 synapse, for instance, NMDA receptor, which acts as a coincidence detector for presynaptic release of glutamate and postsynaptic depolarization by back propagation of action potential, mediate substantial Ca^{2+} influx into the postsynaptic cell [116, 117]. Temporal order of pre- and postsynaptic spiking appears to be an important triggering signal for spike-timing-dependent plasticity (STDP) [118]. Indeed, STDP have been reported to be induced by presynaptic stimulation in stratum lucidum followed by a burst or single action potential with a time delay of 10 ms whereas a reversed spiking order with a time delay of 30 ms depressed synaptic strength. Blockade of postsynaptic NMDA receptors by applying the irreversible channel blocker MK-801 in these experiments have been reported to prevent LTP indicating the involvement of postsynaptic NMDA receptors in SDTP in CA3 neurons [119].

STDP has also been shown in paired recording from CA3 PCs at associational-commissural (A/C) synapses [120]. In addition, recurrent associative inputs have been reported to be capable of strengthening granule cell-CA3 connection important for pattern completion during the remapping of place fields [121].

Importantly, high frequency stimulation (≥10 Hz) in "pre-before-post" order leads to LTP, whereas "post-before-pre" firing at the frequencies between 0.1- 20 Hz downscale the synaptic strength leading to LTD [122]. In addition, the direction of synaptic plasticity have been reported to depend on the magnitude of Ca^{2+} transients: whereas low Ca^{2+} levels (180-500 nM) lead to LTD, induce higher levels (>500 nM) LTP [123]. However, regardless of temporal order of spiking, high frequency (≥40 Hz) pairing have been reported to fail in LTD induction. Indeed, although each postsynaptic AP precedes each presynaptic spikes by ~10 ms, it also follows presynaptic APs by ~15 ms so that the timing requirement for LTP are met [115, 122].

The CA3 network represents a highly associative neuronal circuit since three excitatory inputs converge on CA3 PCs: the Mossy fibers, A/C and temporoammonic projections [124, 125]. For each of these projections a different form of plasticity have been reported suggesting a crucial role of CA3 region for learning and memory. Whereas for the PP and A/C synapses pairing induced synaptic plasticity have been reported [126], exhibit mossy fiber synapsis other induction and expression mechanisms [125, 127, 128]. In addition, gamma frequency stimulation of mossy fibers and CA3 neurons have been suggested to induce LTP at recurrent synapses in CA3 [129], which is likely to account for associative memory encoding [130].

6.2. Synaptic plasticity in interneurons

Interneuron synaptic plasticity follows either Hebbian or anti-Hebbian rules depending on induction protocols e.g., whether a presynaptic stimulation is followed by postsynaptic depolarization and AP-generation or postsynaptic hyperpolarization, respectively. As in PCs, Hebbian LTP in interneurons is likely to depend on intact postsynaptic NMDA receptor activity. Here, too, NMDA receptor acts as a detector of coincidence of presynaptic glutamate release and postsynaptic depolarization to relieve the Mg^{2+} blockade from the channel with consecutive Ca^{2+} influx into postsynaptic cell [131]. Intriguingly, a large body of experimental evidence indicates that NMDA receptor-mediated excitatory current onto interneurons constitutes only a minor part of the total excitatory input and its main component is mediated by postsynaptic AMPA receptors which express low levels of GluR2 (one of its four subunits). The absence of GluR2 subunit determines Ca^{2+} permeability of these receptors (CP-AMPA) and inwardly

rectifying nature of their current, since they are blocked by intracellular polyamines at depolarized membrane potentials. On the contrary, AMPA receptors containing GluR2 subunit are Ca^{2+} impermeable (CI-AMPA) [116, 132]. It has been convincingly demonstrated that NMDA and CP-AMPA-mediated synaptic currents contribute to the total EPSC in a inversely correlated manner i.e. CP-AMPA reach synapses exhibit smaller NMDA-mediated components compared to CI-AMPA containing inputs [132, 133]. For instance, in CA3 region a significantly higher NMDA/AMPA receptor-mediated current ratio has been reported onto stratum lucidum interneuron synapses for PC input compared with mossy fiber synapses [134]. Further investigations of NMDA/AMPA receptor-mediated current ratio on PV+ interneurons revealed an input specificity and have been suggested to be significantly greater for FB compared to FF inputs pointing to the existence of more abundant NMDA receptors at FB synapses on PV+ interneurons [135].

In contrast to NMDA-dependent LTP, the calcium permeable AMPA (CP-AMPA) receptor dependent plasticity relies on increase of Ca^{2+} influx into postsynaptic cell whilst postsynaptic hyperpolarization or keeping the cells at or close to its RMP. Thus, if presynaptic firing is coupled to postsynaptic hyperpolarization, which keeps postsynaptic CP-AMPA receptors open, STDP referred to as anti-Hebbian synaptic plasticity will be induced by increased Ca^{2+} intracellular influx through these receptors [133, 136, 137]. Occurrence of „anti-Hebbian“ LTP have been reported in interneurons of both FF and FB inhibitory pathways such as O-LM, PV+ BCs, axo-axonic and ivy cells [133, 137, 138]. However, the „anti-Hebbian“ induction protocol have been reported to fail to elicit LTP in CCK+ BCs [137, 138].

Although it has been clearly demonstrated, that postsynaptic Ca^{2+} increase via CP-AMPA receptors is essential for LTP induction, the LTP expression has been suggested to have presynaptic character since in O-LM interneurons the association with changes in paired pulse ratio (PPR) and failure rate have been demonstrated pointing to a persistent increase in release probability. However, the exact biochemical cascade linking increased concentration of postsynaptic Ca^{2+} to increased presynaptic release probability, which may include a retrograde messenger, remains to be elucidated [138].

The importance of spike timing during LTP induction is widely accepted and believed to be a determining factor for the direction of changes in the synaptic strength. STDP can be triggered not only Hebbian but also anti-Hebbian induction protocols. Some authors report cells which are able to express STDP with both Hebbian and anti-Hebbian protocols. A typical example is the O-LM cell expressing high levels of both CP-AMPA receptors and mGluR1. Hebbian LPT is

sensitive for pharmacological blockade of mGluR1 whereas anti-Hebbian LTP can be prevented by applying of CP-AMPA receptor antagonists [136, 139].

However, the Hebbian form of mGluR-dependent plasticity is believed to be coupled to the voltage dependent Ca^{2+} channels and intracellular Ca^{2+} release from ryanodine-sensitive stores [139, 140]. Compelling evidence for changes in PPR and failure rate of EPSC has been demonstrated suggesting that mGluR-mediated LTP in interneurons is expressed presynaptically [133, 141]. Since the induction of this LTP form is mediated postsynaptically, the existence of a retrograde messenger have been supposed. Nitric oxide (NO) seems to be a potential candidate as the blockade of NO synthase prevented the LTP [141].

Evidence for importance of spike timing during mGluR-mediated LTP induction has been established in several studies. At excitatory synapses on CA1 O-LM cells, for instance, activation of VGCCs have been reported to play a critical role whilst postsynaptic spiking is required for mGluR-mediated Ca^{2+} influx through these channels [142]. Moreover, it has been demonstrated that associative plasticity at mossy fibre-BC synapses in DG induced by pairing with PP input was depending on postsynaptic spiking and requires precise timing [143].

A fundamental role of group I mGluRs for STDP have also been demonstrated in substantia gelatinosa neurons. This form of LTP was induced by presynaptic stimulation paired with postsynaptic spiking suggesting the requirement of cooperation of back propagating APs and stimulation induced presynaptic transmitter release. The magnitude of Ca^{2+} increase may determine the polarity of mGluR-mediated STDP. While low level Ca^{2+} elevation is believed to selectively activate phosphatase resulting in LTD, higher level of Ca^{2+} is required for activation of protein kinases leading to LTP. Correlated presynaptic stimulation and postsynaptic spiking are likely to induce mGluR-mediated Ca^{2+} release from inositol-1,4,5-trisphosphate gated Ca^{2+} stores which results in LTP [144].

Growing experimental evidence suggest that LTP in interneurons demonstrate cell type specificity. Whereas CCK+ BCs do not show any change in their excitatory synapses, exhibit PV+ interneurons a long-lasting increase of synaptic strength at PC/IN synapses [137, 138].

Cells expressing high levels of both group I mGluRs and CP-AMPA receptors such as O-LM interneurons have been reported to be capable of expression both Hebbian and anti-Hebbian LTP depending on the induction protocol. Hebbian LPT is sensitive for pharmacological blockade of mGluR1 whereas anti-Hebbian LTP can be prevented by applying of CP-AMPA receptor antagonists [136, 139].

Furthermore, specific learning rules at excitatory synapses on hippocampal PV+ interneurons have been reported. These interneurons receive two different inputs from either Schaffer collaterals or recurrent collaterals from local PCs, called FF or FB connections, respectively. The synapses made by both of them onto PV+ interneurons are equipped with both NMDA and CP-AMPA receptors. Interestingly, the ratio of NMDA/AMPA receptors differs in an input specific manner, which means, that it is almost two times higher at FB inputs indicating the abundance of NMDA receptors at FB-PV+ interneuron synapses. CP-AMPA receptor dependent STDP by anti-Hebbian induction protocol could be elicited at both FF and FB interneuron synapses showing sensitivity for applying of NASPM selective antagonist of CP-AMPA receptors, whereas NMDA-receptor dependent plasticity was triggered only at FB-interneurons synapses and was sensitive for APV [135].

Thus, NMDA-receptor dependent Hebbian plasticity occurring simultaneously in FB-PV+ interneurons and PCs could play at least two possible roles in the hippocampal network. First, it may rapidly counteracting the net increase in the excitatory drive of PCs. Second, LTP in interneurons may provide a “centre-surround” of target cells that sharpens memory traces. Furthermore, interneuron LTP may also serve the maintenance of temporal fidelity of action potential integration in PCs [131].

Goals of the thesis

The hippocampal network exhibits *in vivo* and *in vitro* network oscillations at different frequency range: theta, gamma and SWRs. However, underlying cellular mechanisms of transition from one oscillatory state into another in the same neuronal circuit is still ill defined. Furthermore, the interaction and interdependence of these rhythms at network and cellular level remains to be clarified. Therefore we aimed:

- to test, whether the two network patterns - gamma frequency oscillations and SWRs - are fully independent or interact with each other. For this purpose, we first developed *in vitro* conditions, which allowed reproduction of these two major network oscillatory rhythms, gamma and SWR activity in "submerged" slices. These models allowed insights into the dynamics of the cellular and synaptic mechanisms underlying those brain oscillations.
- to clarify the properties of certain cell types of the hippocampus, which enable the network to create a functional neuronal circuit capable of switching between different oscillatory states. Therefore, we recorded from morphologically identified PV+ fast-spiking BCs, BSCs, CCK+ regular-spiking BCs and PCs in hippocampal area CA3 during spontaneously occurring SWRs and pharmacologically (kainic acid, KA, 200-400 nM) induced gamma frequency oscillations. We recorded the cells in both voltage (cell-attached) and current clamp configuration and analysed their discharge pattern and their phase-relationship to the simultaneously recorded local field potential.
- to investigate the impact of gamma frequency oscillations on hippocampal network activities and test whether oscillations in the gamma frequency range promote lasting alterations in local field potentials of CA3 network. To clarify underlying mechanisms, we studied importance of different glutamate receptors for gamma activity-induced changes in local field activity.
- to examine whether gamma rhythm as a novel, relatively natural LTP induction paradigm elicits specific alterations in the synaptic strength of certain synapses on different types of neurons in the CA3 network. In particular, we tested whether ongoing gamma frequency oscillations facilitate changes in synaptic strength at glutamatergic excitatory as well as GABAergic inhibitory synapses and thereby influence the cell-excitability during reappeared SWRs (r-SWR) after gamma rhythm.
- to uncover the role of mGluR5 blockade on the gamma rhythm-induced change in excitatory synaptic transmission at PC-PC synapses.

Materials and methods

Experiments were performed on P18-P23 C57/Bl6 (for principal cells) and EGFP PV+ (for interneurons) transgenic mice, that expressed enhanced fluorescent protein under the control of the PV promoter [145]. All animal procedures were approved by the Regional Berlin Animal Ethics Committee, registration number T 0124/05, and in full compliance with national regulations.

1. Slice preparation

Mice were deeply anesthetized with a lethal dose of inhaled isoflurane, immediately decapitated rostral to the first cervical vertebra, the scalp was quickly incised in the middle between the nasal and occipital bones. The skull plates were cut through and immediately removed. Brain was quickly extracted, glued onto a mounting plate, incised in the middle between the hemispheres, transferred to the reservoir of the Vibratome and submerged into the oxygenized ice-cold artificial cerebrospinal fluid (ACSF). For tissue sectioning the Leica VT1200 (Nussloch, Germany) vibrating blade microtome was used, which minimizes damage to the upper and lower surfaces of the slice and ensures maintenance of cell morphology and viability. Transverse combined EC-hippocampal slices (400µm) were prepared and transferred to a holding interface chamber where they were continuously perfused with prewarmed (33± 1°C) and oxygenized (95% O2 and 5% CO2) ACSF containing (in mM): NaCl, 129; KCl, 3; NaH2PO4, 1.25; CaCl2, 1.6; MgSO4, 1.8; NaHCO3, 21; glucose, 10; Slices were allowed to rest at least 1 hour after the preparation before performing recordings. Each slice was transferred to a temperature controlled (33± 1°C) recording chamber with oxygenized ACSF. Neurons were visualized in DIC infrared video microscopy for patch-clamp experiments.

2. Extracellular field recordings

Extracellular recordings were obtained from the stratum pyramidale of the hippocampal CA3 area (Figure. 1, left, LFP-pipette). Kainic acid (400 nM, unless indicated otherwise) was applied in the bath to induce network gamma frequency oscillations. Field oscillations were low pass filtered at 2 kHz, digitized at 10 kHz (Digidata 1440A, Axon Instruments) and analyzed with the pClamp software package (notch filter 50 Hz; Axon Instruments). Oscillatory peak power and frequency was determined by averaging several consecutive fast Fourier transforms (FFT) obtained within a 30-60 second epoch. The student's t-test was used for statistical comparisons; differences were considered significant if $p<0.05$. Average values are expressed as the mean

±SEM. The spectral components of the local field potentials were analyzed with custom routines written in Matlab (The Mathworks, Inc.). Signals were zero-phase digital filtered from 2-300 Hz using an 8th order butterworth filter, 50 Hz components including their harmonics were removed through a second-order IIR notch filter. Recordings of gamma frequency oscillations were divided in consecutive 1s time bins. An FFT was calculated for each time bin and the frequency of the peak spectral amplitude was detected within each power spectrum. The FFT-based spectrogram (1 s time bins, hamming window, 50 % overlap) was computed for gamma frequency oscillations and a complex Morlet wavelet transform (cmor2-1) was used to display SWR (bandpass filter 100-300 Hz).

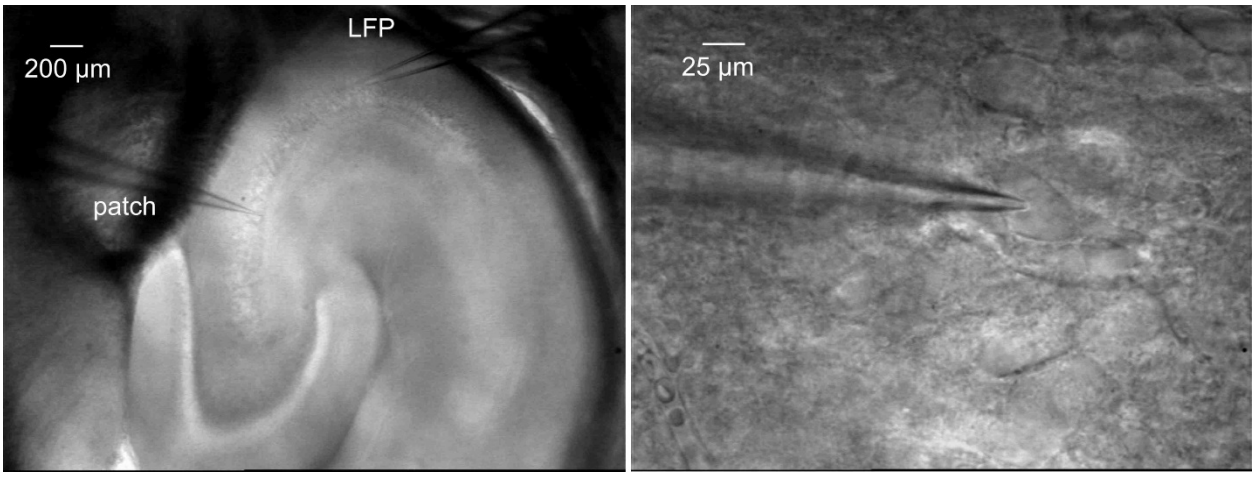

Figure 1. Visualization of hippocampal tissue and single cells by infrared differential interference contrast video microscopy. Hippocampal area CA3 with recording electrodes for local field potential (LFP) and single cell activity (patch) visualized using 4x (left) and 60x (right) objectives.

3. Patch-clamp recordings

All patch-clamp recordings in PCs and interneurons in the stratum oriens, pyramidale and lucidum of the CA3 area were performed simultaneously with extracellular field activity recordings. The cells were visualized by infrared differential interference contrast video microscopy (Olympus BX51WI microscope, Olympus corporation, Tokyo, Japan; VX55 CCD camera, TILL Photonics GmbH, Gräfelfing, Germany; Figure 1). Cells with intact cellular membrane and intracellular milieu were first recorded in the "cell-attached" configuration. The intrinsic and firing properties of cells were measured in whole-cell current- and voltage clamp mode. In order to minimize cytoplasmic dialysis, whole-cell recordings from interneurons were

performed with relatively high resistance pipets [146] filled with a solution containing (in mM): K-gluconate, 135; KCl, 5; ATP-Mg, 2; GTP-Na, 0.3; HEPES, 10; plus biocytin, 0.5 % (pH 7.4 and 290 mOsm). A Multiclamp 700B amplifier and pClamp software (Axon Instruments) were used for current- and voltage-clamp recordings. The holding potential in voltage-clamp mode was either -70 mV or 0 mV unless indicated otherwise. The seal resistance before establishing whole-cell mode was ≥2 GΩ.

The series resistance (range 12-18 MΩ) was not compensated but was monitored repeatedly during the experiment by measuring the amplitude of the capacitive current in response to a -10 mV pulse. Experiments in which the series resistance increased by >20% were discarded. Signals were low pass filtered at 5 kHz, digitized at 10 kHz (Digidata 1440A) and analyzed by using pClamp software.

The intrinsic properties of cells were obtained in whole-cell current-clamp mode. During estimating the resting membrane potential, no holding current was injected. The voltage responses to current injection (500ms; ±300pA, at 30pA increments) were analyzed to estimate the input resistance and membrane time constant. The input resistance was measured from the slope of the steady state responses in a linear region around, and including, the origin. For the analysis of "Sag", the ratio of the steady state to the peak voltage in response to hyperpolarizing current injection (-300pA, 500ms) was calculated. To analyze the amplitude and duration of action potentials (AP) as well as decay time constant and half-duration of afterhyperpolarization (AHP), stepwise increased constant depolarizing current were injected, inducing small (~5mV) graded membrane potential depolarization. Measurements were performed on the first AP. The AP-duration was measured at half duration. Interneurons demonstrated characteristic rapid-onset, deep spike AHP with a rapid and monophasic decay time. To estimate accommodation parameters, depolarizing current (up to 700 pA for 1s) pulses were injected for all stimulation intensities the difference between initial and steady state firing frequencies was calculated.

To facilitate identification of PV+ fast-spiking interneurons in CA3 network, we used transgenic mice in which the enhanced green fluorescent protein (EGFP) was specifically expressed in PV+ neurons using bacterial artificial chromosome (BAC) technology [145] enabling us to selectively target these interneurons under visual control using fluorescence microscope.

To analyze the involvement of neurons in generation of local field potentials, the number of phase coupled APs generated during an oscillatory cycle was calculated using custom routines written in Matlab (The Mathworks, Inc.) in current clamp mode with no current injection. We

analyzed two different parameters for each cell group: the firing rate implying the number of action potentials during (AP) one local field potential (LFP) episode coupled with ≥ 1 APs and the firing probability meaning the proportion of AP-coupled LFP episodes of the total number of these events.

EPSC and IPSC were measured by voltage clamping at a holding potential of the estimated reversal potential at - 70mV and 0mV. Local field potential (LFP)-associated EPSC and IPSC were detected by manually setting the threshold in the unfiltered LFP trace to trigger recording of over-threshold LFP events together with associated postsynaptic currents. The individual events (recorded for 30 to 60s) were overlaid for averaging and further calculating of area by offline analysis with the pClamp software. Signals were filtered at 5 kHz for whole-cell- and 1 kHz for LFP recordings with an external 8-pole Bessel filter (Applegarth Electronics, Oxford, UK) and digitalized at 10 kHz using an ITC-16 A/D board (Instrutech).

4. Immunostaining and morphological analysis

Slices with biocytin-filled cells were removed from the chamber and immersed overnight in a fixative solution containing 4 % paraformaldehyde (PFA) in 0.1 M phosphate buffer (PB). Slices were washed three times in 0.1 M PB and subsequently in 0.025 phosphate-buffered saline (PBS; pH 7.3). They were incubated in the PBS solution containing 1% Triton X-100, 10% goat serum, 2 drop Mouse on Mouse (M.O.M) blocking reagent per 2.5ml solution for 1 hour at the room temperature. To visualize PV+ and CCK+ cells, we used antibodies against PV (mause, Swant, Switzerland) and CCK (mause, CURE, Los Angeles, USA) diluted 1:5000 in PBS containing 5% goat serum and 1% Triton X-100. Slices were incubated with the primary antibodies for 48 hour at room temperature. After rinsing three times in PBS, sections were incubated in the PBS solution containing 0.5% Triton X-100, 5% goat serum, goat anti-mouse conjugated with Alexa fluor 546 (Invitrogen Corporation, Carlsbad, CA) for PV, Alexa fluor 568 (Invitrogen Corporation, Carlsbad, CA) for CCK diluted 1:500 and Alexa fluor 647 (in some experiments 350) conjugated avidin diluted 1:500 (Invitrogen Corporation) for visualizing biocytin filled neurons. 48 hour after incubation with the secondary antibodies, slices were mounted on glass slides in a glycerol-based, aqueous mountant Vectashield (Vector Laboratories, CA) under coverslips. Labeled cells were visualized using a 20x and/or 60x objectives on a confocal microscope system (Leica). To examine full extent of somato-dendritic compartments and axonal arborization, the intensity of Z-stack projections was optimized and the images were overlaid.

5. Biocytin staining

Slices with biocytin-filled cells were immersed overnight in a fixative solution containing 4 % paraformaldehyde (PFA) in 0.1 M phosphate buffer (PB). Slices were washed three times in 0.1 M PB. The avidin–biocytin complex reaction (Vectastain, ABC kit, Camon laboratory service) was allowed to occur overnight at 4°C in the presence of 0.3 % Triton X-100 (Sigma-Aldrich). Afterwards the sections were rinsed several times before development with 0.02 % diaminobenzidine in 0.1 M PB. The reaction product was intensified with 0.5 % OsO_4 and sections were mounted and coverslipped. Stained cells were reconstructed with the aid of a Neurolucida 3D reconstruction system (MicroBrightField, Inc).

Results

Chapter I

Hippocampal gamma oscillations influence network excitability and promote long-lasting changes in the network activity

1. Hippocampal gamma oscillations show temporal evolution during the course of network activity

We recorded local field potentials (LFP) in the stratum pyramidale of the hippocampal area CA3 during gamma frequency oscillations induced by bath application of kainic acid (KA, Figure 1.1.). Network oscillations were not constant but rather showed a temporal evolution over the course of induced gamma epoch (Figures 1.1.A and 1.1.B). Therefore we examined basic properties of the induced oscillatory network activity, including power and frequency, as well as their dynamics based on LFP spectral analysis (n=30). Analysis of the gamma activity pattern obtained from early gamma (~1-2 min after the onset of gamma frequency oscillations, 'e-gamma') and late gamma epochs (>4 min after the onset of gamma frequency oscillations, 'l-gamma') revealed a significant increase in the spectral power of gamma frequency oscillations (e-gamma: $2.25x10^{-4} \pm 0.45x10^{-4}$ mV^2/Hz, l-gamma: $7.0x10^{-4} \pm 1.58x10^{-4}$ mV^2/Hz, n=30, p=0.0057, Figures 1.2.B and 1.2.C) as well as a markedly higher auto-correlation (Figure 1.2.A) The frequency of gamma rhythms, in contrast, remained unchanged (e-gamma: 31.1 ± 0.9 Hz, l-gamma: 30.6 ± 0.8 Hz, n=30, p=0.68, Figure 1.2.D). A similar network dynamics was found for another pharmacological induced model of gamma network oscillations: carbachol (CCh) induced oscillations also displayed a significant increase in spectral power (e-gamma: $0.14x10^{-4} \pm 0.04x10^{-4}$ mV^2/Hz, l-gamma: $0.88x10^{-4} \pm 0.25x10^{-4}$ mV^2/Hz, n=16, p=0.004) with unchanged oscillatory frequency (e-gamma: 33.4 ± 1.4 Hz, l-gamma: 33.1 ± 1.3 Hz, n=16, p=0.87). Hence, gamma network oscillations induced by different pharmacologic agents display comparable temporal evolution, suggesting that modification is taking place in the network as a consequence of the oscillatory activity independent of the pharmacological agent applied.

We next examine whether the observed evolution of the oscillatory activity requires mGluR5- or NMDA receptor activation using antagonist of these receptors, 2-methyl-6-(phenylethynyl)pyridine, MPEP and AP5. Neither their separate nor combined application changed the power and frequency of l-gamma epoch (Figure 1.3, e.g. MPEP+AP5: $7.0x10^{-4} \pm$

$1.3x10^{-4}$ mV^2/Hz (33.1 ± 1.7 Hz), n=14, p=0.996 (p=0.15) with respect to normal l-gamma epoch above) precluding the involvement of these receptors in the temporal evolution of gamma oscillations.

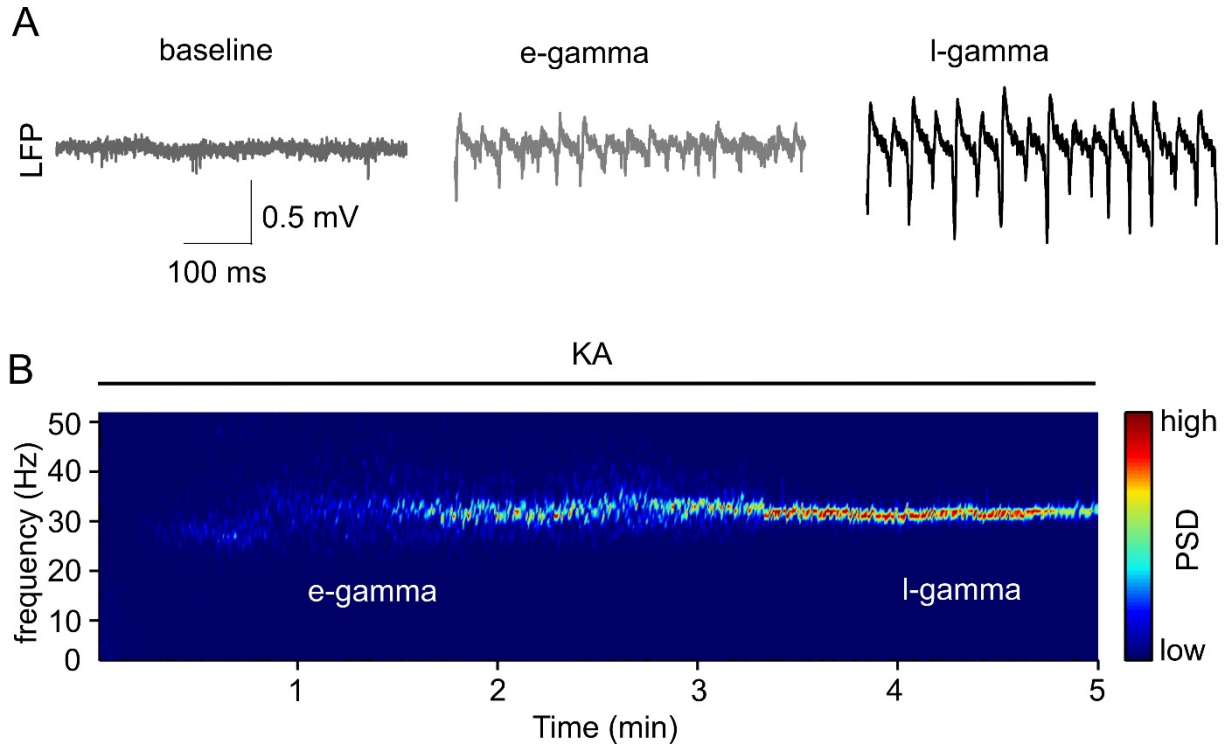

Figure 1.1. Dynamic of KA-evoked gamma oscillations. (A) Representative local field potential recordings ('LFP') obtained from the baseline ('baseline') and the early ('e-gamma') and late ('l-gamma') gamma activity following bath applied 400 nM KA. (B) The dynamics of KA-induced gamma frequency oscillations is exemplified by the spectrogram (color-coded power spectral density) of a continuous LFP recording.

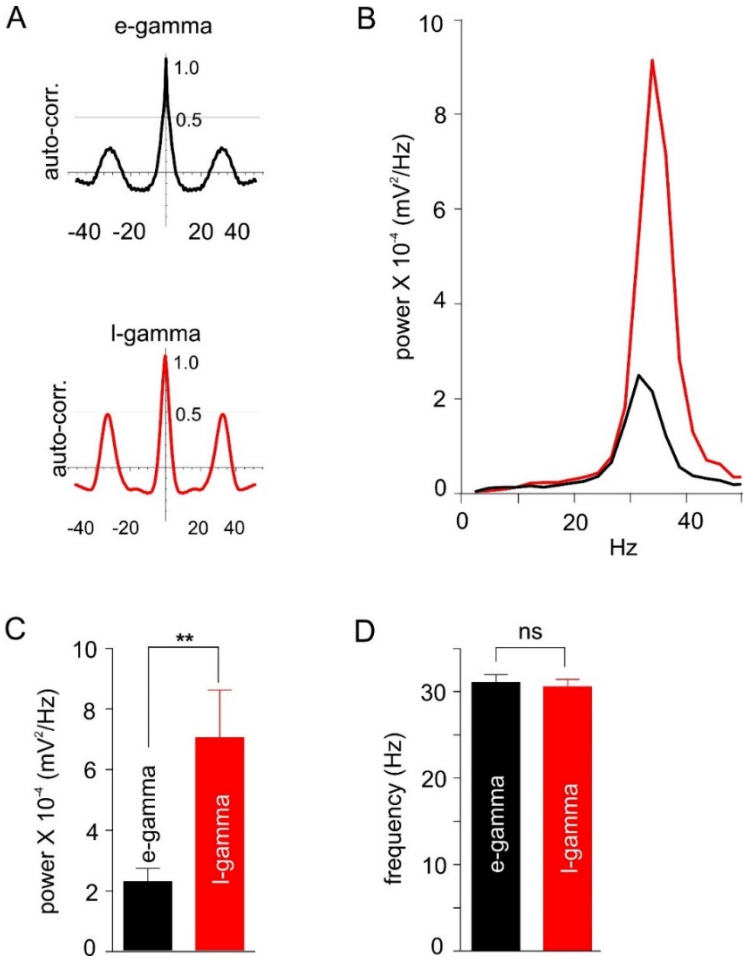

Figure 1.2. Auto correlation, power spectrum and frequency of e-gamma vs. l-gamma. (A) In comparison to the early period of gamma rhythms (black), the late period (red) display a markedly higher auto-correlation ('auto-corr.', left) as well as a higher spectral density (B, corresponding spectral analysis, right). (C) Summary bar charts of peak power as well as mean frequency (D) obtained from early and late gamma epochs (n=30). Note that the power but not the frequency of the LFP increases in the late period. Asterisks indicate the significance level ($p<0.01$, Student´s t-test).

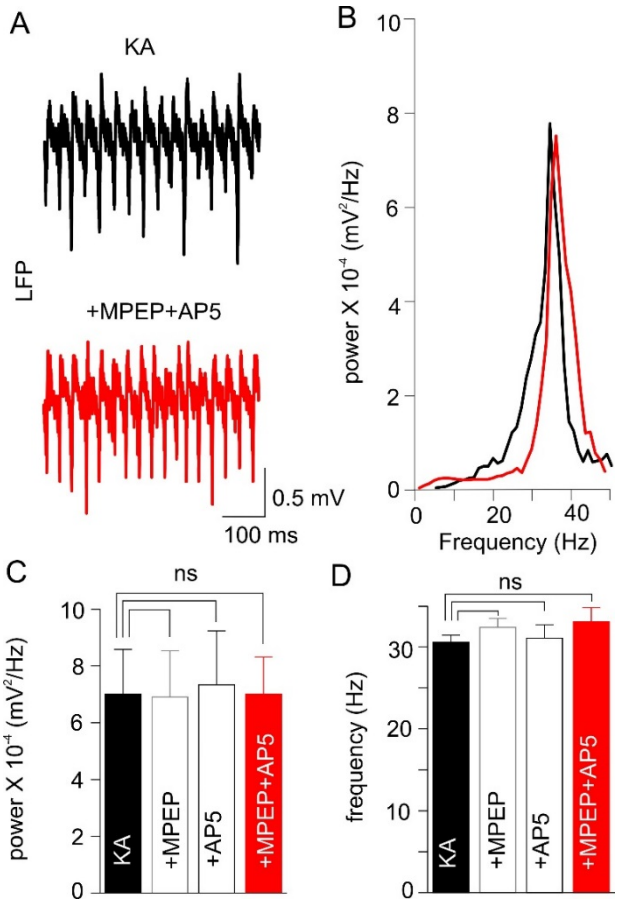

Figure 1.3. Pharmacological blockade of NMDA and/or mGluR5 receptors affects neither the power nor the frequency of gamma oscillations. (A) Example traces illustrating late gamma rhythms in the presence of KA ('KA', black) and KA+MPEP+AP5 ('+MPEP+AP5', red). (B) the corresponding spectral analyses. (C) and (D) Mean values of gamma epochs in KA (black bar, n=30), KA+MPEP (gray open bar, n=16), KA+AP5 (black open bar, n=14) and KA+MPEP+AP5 (red bar, n=14) illustrating that neither a separate nor a combined application of mGluR5 and NMDA receptor antagonists significantly affects the power or frequency of l-gamma oscillations.

2. Gamma frequency oscillations promote long-lasting changes in the network activity

To investigate the impact of the gamma frequency rhythm on hippocampal network activities we tested whether oscillations in the gamma frequency range promote the lasting alterations in LFP of CA3 network.

Therefore, we examined the readiness of CA3 network to generate gamma frequency episodes. For this purpose we first used lower concentrations of KA (10-50 nM) remaining either a) subthreshold (with no clear detectable spectral peak and/or a maximal spectral power value less than $1x10^{-5}$ mV^2/Hz) or b) just suprathreshold to induce brief 'weak' field gamma episodes (1. gamma, Figure 1.4.A). After this test period, 'conventional' gamma frequency oscillations were induced by high KA (400 nM) application, followed by KA washout achieving a complete disappearance of gamma-activity. Afterwards we tested again the oscillatory network behavior with low KA concentration as applied initially. Under this condition, we found that low concentrations of KA produced a) suprathreshold (power of gamma: $0.44x10^{-4}\pm0.11x10^{-4}$ mV^2/Hz, n=9) or b) significant stronger gamma oscillations than before (2. gamma, spectral power increase from $0.72x10^{-4} \pm 0.39x10^{-4}$ mV^2/Hz to $1.34x10^{-4} \pm 0.50x10^{-4}$ mV^2/Hz, n=10, p=0.003, Figure 1.4.B and C). However, the frequency of gamma oscillations remained unchanged (1.gamma: 25.90 ± 1.05 Hz, 2.gamma: 26.48 ± 0.80 Hz, n=10, p=0.52, Figure 1.4.D). These results altogether depict a clear impact of the preceding gamma episode on the subsequent network activity.

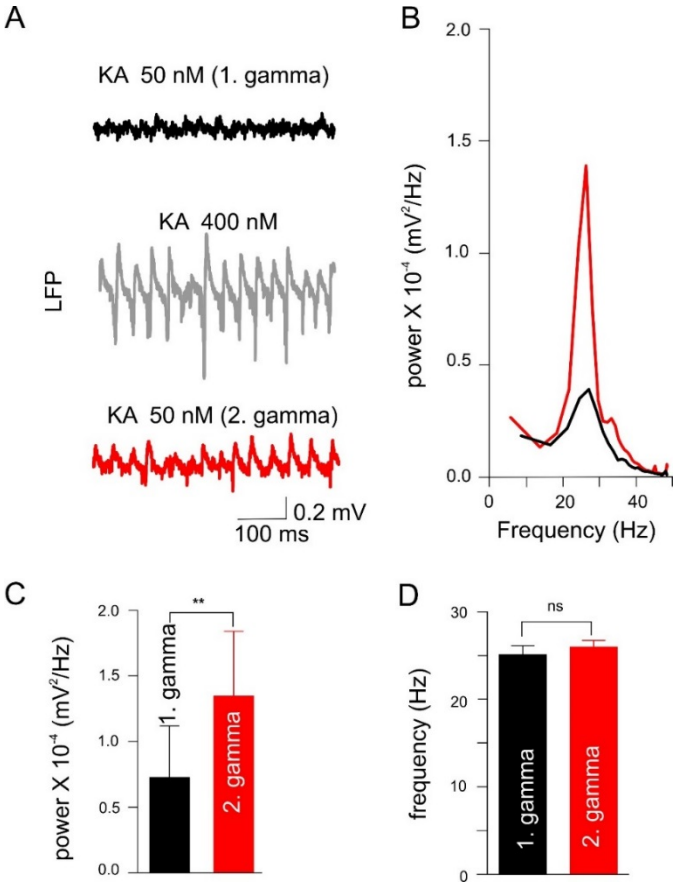

Figure 1.4. Readiness of CA3 network for generating local field potential oscillations is influenced by underwent synchronization in the gamma frequency range. (A) 'Weak' gamma episode (top, black: 1. gamma) induced by bath application of 50 nM KA becomes significant stronger (bottom, red: 2. gamma) after 'conventional' (middle, gray: 'KA 400 nM') gamma oscillations. (B) Corresponding spectral analyses. (C) and (D) Summary bar charts of peak power and frequency obtained before ('1.gamma') and after ('2.gamma') 'conventional' gamma.

Chapter II

Interaction and interdependence between two major network states: hippocampal gamma oscillations and sharp wave-ripples

We next examined the general potential of gamma frequency oscillations to affect subsequent network activities. Our *in vitro* model permitted the reproduction of two major network oscillatory rhythms in 'submerged' slices, gamma as well as SWR activity [147, 148], which enabled us to investigate the interaction and interdependence of these network activity patterns by monitoring local field potentials as well as analyzing cellular, synaptic and network mechanisms. Gamma frequency oscillations and SWR, which are generating during different behavioral states *in vivo* [149], reflect two "competing" mutually exclusive network states *in vitro*: the SWR oscillations occurred spontaneously (mean frequency: 1.33 ± 0.10 Hz, n=30), disappeared shortly (31.0 ± 2.8 sec, n=30) after bath application of KA and reappeared within a few minutes (14.6 ± 0.7 min, n=30) after KA washout (Figure 2.1.A). In order to examine the potential impact of gamma frequency oscillations on the subsequent SWR activity we compared basic properties of the SWR before and after intermediate gamma episode. In comparison to the SWR preceding gamma frequency oscillations the r-SWR exhibited a significant increase in SWR area (by 69.67 ± 15.07 %, n=30, $p<0.0001$, Figures 2.1.B and 2.2.A) but with a significant decrease in their incidence (from 1.3 ± 0.1 Hz to 0.9 ± 0.1 Hz, n=30, $P<0.0001$). In good agreement with these data, gamma oscillations induced by bath application of CCh also resulted in a significant increase in SWR area (by 21.0 ± 4.2 % of control, n=16, p=0.0002, Figure 2.2.B), confirming that gamma activity itself and not the pharmacologic agent is responsible for the network alterations. It should be also noted that in comparison to KA, CCh-triggered gamma frequency oscillations exhibited less spectral power (p=0.007) and accordingly induced smaller changes in SWR (p=0.02), suggesting an activity-dependent mechanism of oscillation-induced neuronal network plasticity.

To reveal the molecular mechanism underlying network plasticity, we tested whether the plasticity induced by gamma frequency activity requires activation of mGluR5 and NMDA receptor. First, we investigated the impact of mGluR5 on the long-lasting changes in the SWR activity. Bath application of a non-competitive mGluR5 antagonist 2-methyl-6-(phenylethynyl)pyridine MPEP during the course of gamma oscillatory activity significantly reduced the extent of this form of plasticity (by 83.41 ± 6.15 % of control n=16, $p<0.0001$, Figure 2.3.A and 2.4.B) without a significant impairment of the spectral power and frequency of

gamma oscillations (Figure 1.3.C and D). Similar, albeit less pronounced effect was observed following application of the NMDA receptor antagonist DL-2-amino-5-phosphonopentanoic acid (AP5, LTP reduction by 55.66 ± 8.93 %, n=13, p<0.0001, 2.3.B and 2.4.B). Finally, this form of plasticity was totally abolished using a joint application of mGluR5 and NMDA receptor antagonists (reduction by 91.8 ± 12.18 %, n=14, p<0.0001, Figure 2.4.A and B), again without a significant alteration in spectral power and frequency of gamma oscillations (Figure 1.3.C and D).

These results collectively suggest that gamma frequency oscillations influence the subsequent network dynamics through an mGluR5 and NMDA receptor-dependent mechanism in hippocampal area CA3.

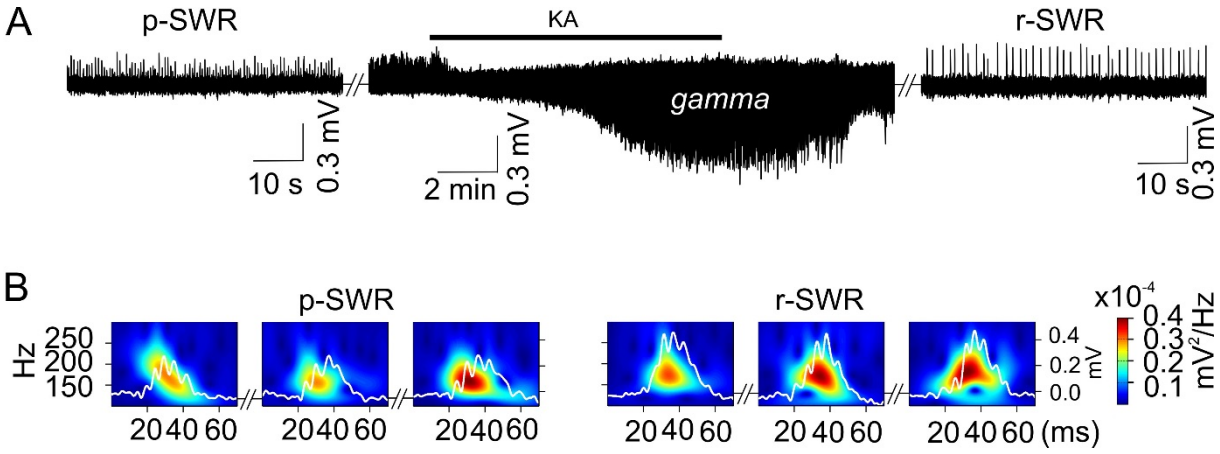

Figure 2.1. Network synchronization in the gamma frequency band induces long-lasting alterations in subsequent SWR episodes. (A) SWR recorded in the stratum pyramidale of the CA3 region occurred spontaneously (left), disappeared shortly after bath application of KA (middle) and reappeared with a significantly higher amplitude after KA washout (right). Note the persistent network gamma frequency oscillations for a few minutes after KA washout. (B) Example of the wavelet transform (color-coded power spectral density) for three consecutive highlighted SWR (white, right y-axis scaling) before (left panels, 'SWR') and after (right panels, 'r-SWR') the interposed gamma frequency oscillations.

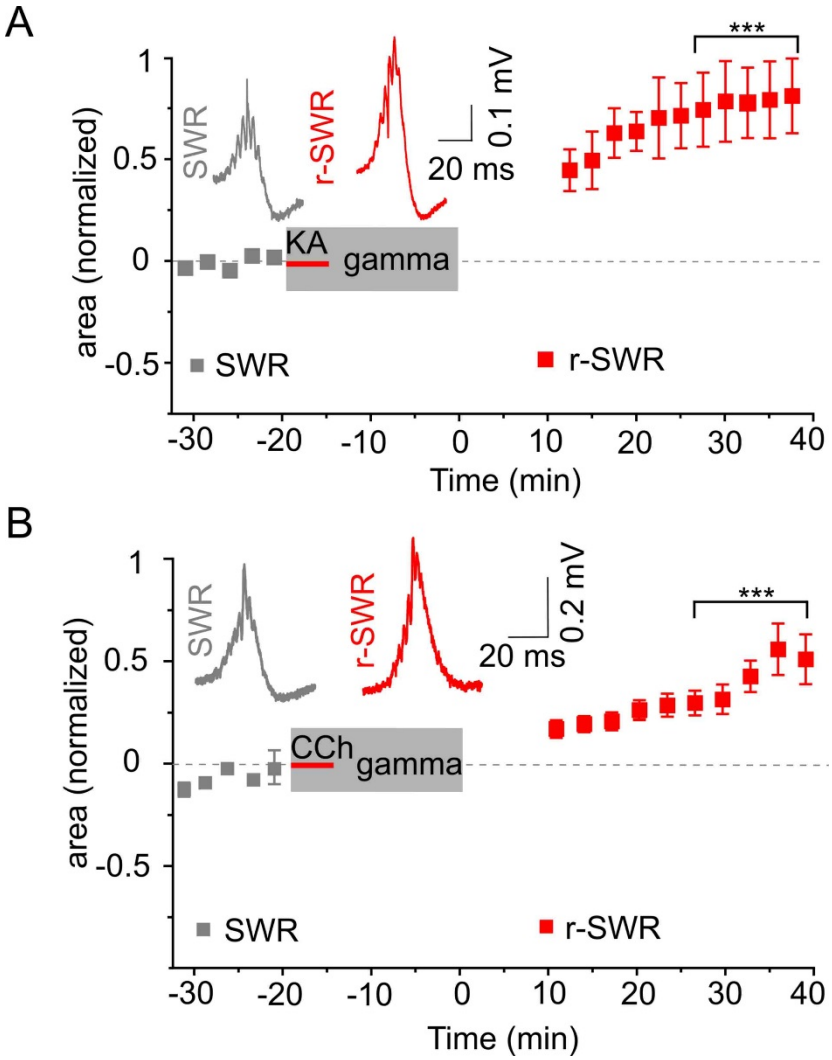

Figure 2.2. Gamma oscillation-induced SWR area increase does not depend on the pharmacologic agent used to trigger gamma rhythm. (A) After KA-induced gamma episode reappeared SWR areas (r-SWR, red squares) increased significantly compared to the SWR areas preceding gamma rhythms ('SWR', n=30, gray squares). (B) CCh-induced gamma oscillations induces a significant increase in r-SWR (red squares) area (n=16). The time courses of drug applications are depicted schematically. Examples of SWR and r-SWR activity (insert) obtained before (gray, 'SWR') and after gamma (red 'r-SWR) are displayed for KA (A) and CCh (B). Note that in comparison to KA, CCh triggered gamma frequency oscillations induce smaller changes in SWR area. The number of asterisks (Student´s t-test) indicates significance level.

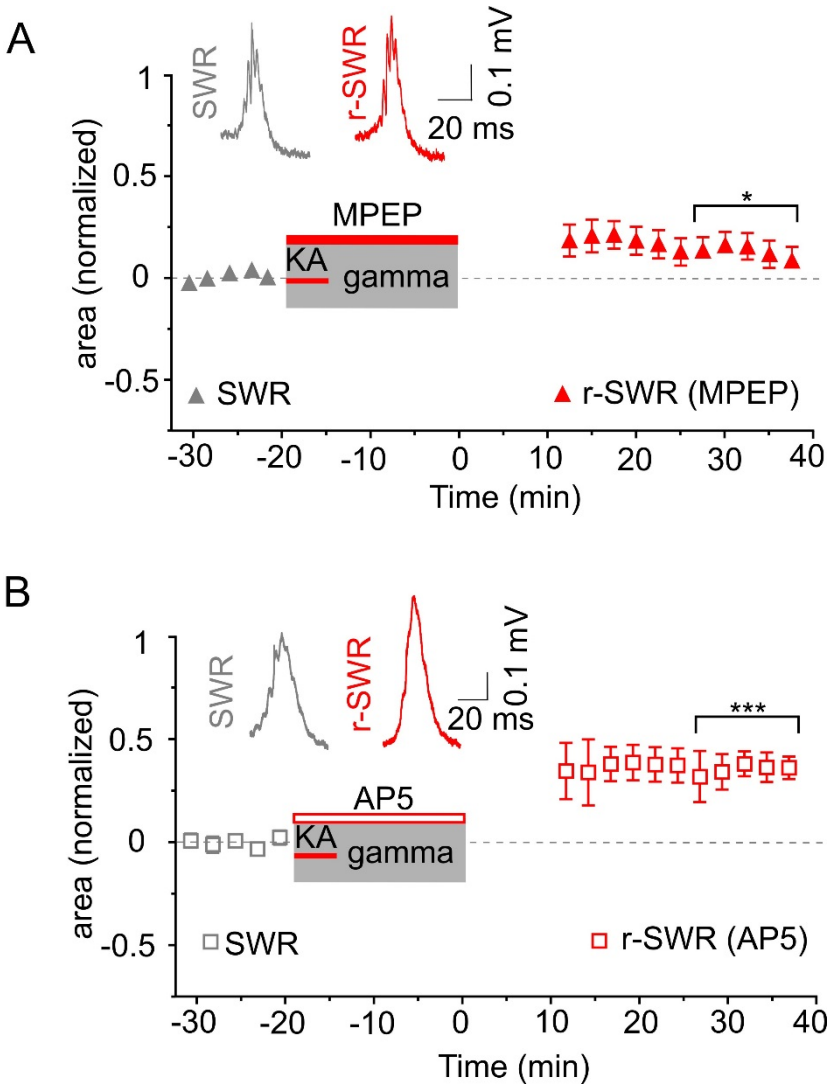

Figure 2.3. Blockade of mGluR5 or NMDA receptors during gamma frequency oscillations reduces gamma-induced LTP significantly. (A) After bath application of MPEP during gamma frequency oscillations LTP was reduced by ~80% (pre-gamma SWR-gray triangles, r-SWR-red triangles, n=16). (B) Blockade of NMDA receptors by bath applying of AP5 leads to the similar but lesser pronounced effect on the LTP (reduction by ~50%, pre-gamma SWR-gray open squares, r-SWR-red open squares, n=13). Inserts, representative example of SWR (gray) and r-SWR (red) with blocked mGluR5-(A) and NMDA receptor- (B) mediated transmission during gamma frequency oscillations. Significance level is indicated by the number of asterisks (Student´s t-test).

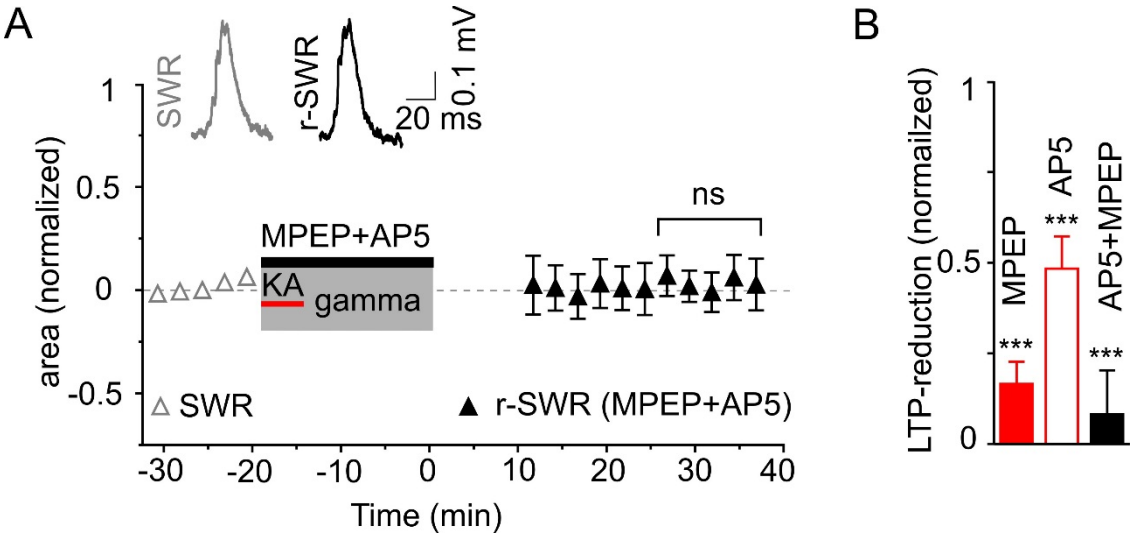

Figure 2.4. Joint application of mGluR5 and NMDA receptor antagonists during gamma frequency oscillations prevents LTP induction. (A) The area of SWR preceding gamma oscillations (gray open triangles) remains unchanged when during gamma rhythm both mGluR5 and NMDA receptors were blocked. Gamma-induced LTP of r-SWR with intact mGluR5 and NMDA receptor-mediated transmission was reduced by ~92 % (black triangles, n=14). Insert, representative example of pre-gamma SWR ('SWR', gray) and r-SWR (black) after gamma oscillations with blockade of mGluR5 and NMDA receptors. (B) Statistical analyses: LTP induced by gamma oscillations without antagonism of glutamatergic receptors is reduced significantly by administration of MPEP (red bar), AP5 (red open bar) and MPEP+AP5 (black filled bar). The number of asterisks indicates significance level (Student´s t-test).

Chapter III

Synaptic properties and firing patterns of anatomically identified principal cells and interneurons during different network states

1. Identification of individual neurons with distinct morphological properties in CA3

To explain cellular mechanisms of network oscillatory activity we recorded local field oscillations, CA3 principal cells as well as distinct types of GABAergic inhibitory interneurons simultaneously and analyzed their synaptic and firing properties during both SWR and gamma frequency rhythms. Initially, action currents were recorded in cell-attached mode during spontaneously occurred SWRs and subsequently recordings were continued in whole-cell mode to observe their firing behavior and SWR-associated postsynaptic currents of principal cells and distinct types of interneurons in hippocampal area CA3. Subsequent Induction of gamma frequency oscillations allowed us to observe the network oscillatory activity switch from SWR to gamma modus (Figure 3.1) and analyze gamma rhythm-associated input-output properties of the same cells, already recorded during SWRs. The biocytin filled neurons were post hoc anatomically identified and classified into four groups based on their dendritic and axonal arborization pattern as well as their neurochemical content: PCs (n=40), CCK+ BCs (n=12), PV+ BC (n=10) and PV+ BSCs (n=17) cells [21, 64].

The cell bodies of PCs were found in the stratum pyramidale. Their dendrites spanned all layers and their axons were found mainly in the stratum oriens (Figure 3.2.A).

The somata of BCs were predominantly located in the stratum pyramidale, the dendrites spanned all layers and axonal arborization was largely restricted to the stratum pyramidale. Whereas the BCs did not demonstrate substantially differences in terms of their morphological features, they fundamentally differed in their neurochemical content and electrophysiological properties (Figure 3.3 and 3.4).

Cell bodies of BSCs were located in the stratum pyramidale or oriens. The dendritic tree was largely confined to the stratum oriens and radiatum. Typical axonal arborization was found in two adjacent layers: stratum oriens and radiatum (Figure 3.4.Ai).

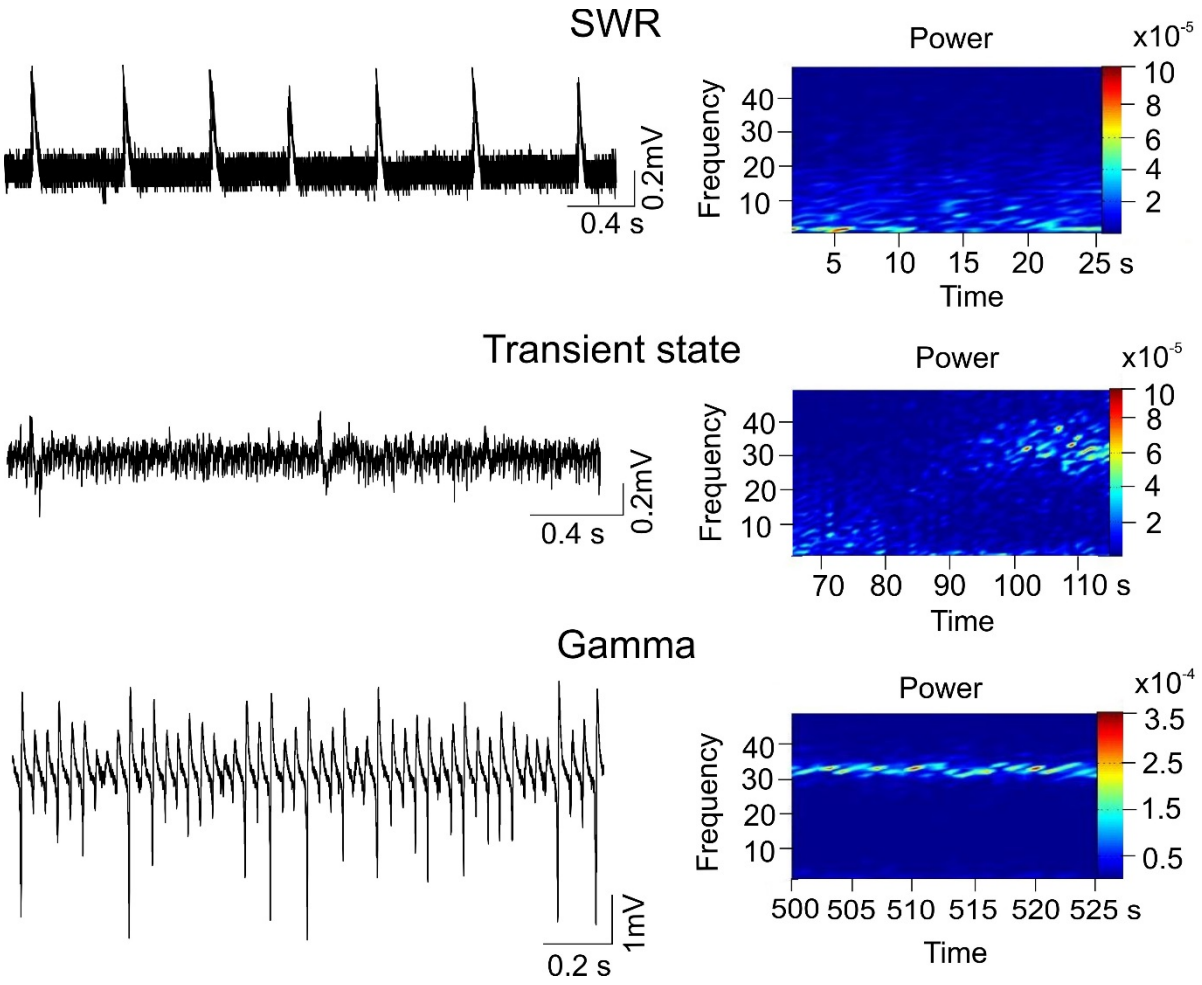

Figure 3.1. The network in the hippocampal area CA3 is capable of generating two different oscillatory activity patterns and dynamically switch between them. Right: example traces showing spontaneously occurred SWR activity (top), transient state (middle) and pharmacologically induced gamma frequency oscillations (bottom). Left: wavelet transform of sharp wave activity (top), transient state (middle) and gamma rhythms (bottom).

2. SWR-associated synaptic properties and firing behavior of distinct neurons in CA3

We first investigated SWR-associated EPSC and IPSC and calculate the EPSC/IPSC-ratio as an exit criterion for cell- excitability. For this purpose, the cells were held in the voltage clamp configurations at -70 mV and 0 mV, respectively. Comparison the SWR-associated EPSC to IPSC revealed a cell type-specific difference: the recorded PCs demonstrated significantly larger IPSC compared to EPSC (5.304 ± 0.860 vs. 13.650 ± 1.849 nA x ms; n=40 and n=21 for EPSC and IPSC, respectively; $p<0.0001$; Figure. 3.2.C and Ci), whereas EPSC and IPSC in the CCK+ interneurons did not differ significantly (6.895 ± 1.611 vs. 4.450 ± 1.126 nA x ms; n=10 and n=4, for EPSC and IPSC, respectively; p=0.382; Figure. 3.3.C and Cii). Compared to the PCs, EPSC and IPSC in the PV+ fast-spiking interneurons were inversely related: these cells received prominent EPSC and significantly lower IPSC during SWRs (8.563 ± 3.428 vs. 3.870 ± 1.834 nA x ms, n=6; p=0.034; Figure 3.4.C and Cii).

We next compared SWR-associated EPSC and IPSC as well as the EPSC/IPSC ratio between different cell classes. Statistical analyses revealed a highly significant difference in EPSC between PCs and PV+ interneurons (5.304 ± 0.860 nA x ms, n=40 and 15.250 ± 3.336 nA x ms, n=21, respectively, p=0.0005; Figure 3.5.A), whereas the difference in EPSC between PCs to CCK+BCs (6.895 ± 1.611 nA x ms, n=10) did not reach the significance level (Figure 3.5.A). However, PCs demonstrated significantly higher amount of SWR-associated IPSC (13.650 ± 1.849 nA x ms, n=21) in comparison to both CCK+ (4.450 ± 1.126 nA x ms, n=4, p=0.045) and PV+ interneurons (3.870 ± 1.834 nA x ms, n=6, p=0.012; Figure 3.5.B). Interestingly, the difference between these two groups of recorded interneuron was not significant in respect with both EPSC (p=0.105) and IPSC (p=0.820; Figure 3.5.A and B). Further analysis of the EPSC/IPSC ratio revealed again a cell type-specific difference. The lowest EPSC/IPSC ratio showed the PCs (0.413 ± 0.061, n=21) which differed significantly from those of both CCK+ (1.463 ± 0.574, n=4, p=0.007) and PV+ interneurons (2.817 ± 0.518, n=6, $p<0.0001$), whereas these two classes of recorded interneurons demonstrated no difference in this respect (p=0.125; Figure 3.5.C).

To test whether the cell type-specific EPSC/IPSC ratio determines different output properties of these cells, we further investigated their firing behavior during SWR activity. We analyzed two different parameters for each cell group: the firing rate, implying the number of APs during one local field potential (LFP) episode coupled with ≥ 1 APs and the firing probability, meaning the proportion of AP-coupled LFP episodes of the total number of these events.

Analysis of firing behavior of the recorded PCs revealed a predominant inhibition of spiking during SWR episodes so that the generation of APs was completely prevented after the peak of the SWR episode (Figure 3.2.C). Yet, very rarely we observed single APs on the ascending phase (probability 0.091 ± 0.014; n=20) in only 50% of recorded PCs, which can hardly be referred to as SWR-associated spikes but rather appear to be remnant APs survived due to insufficient inhibition by interneurons.

In contrast to PCs, GABAergic interneurons demonstrated a clear SWR-associated firing with a distinctly marked cell type specificity. Whereas CCK+ interneurons generated predominantly single AP on the ascending phase of the SWR episode (Figure 3.3.C), demonstrated PV+ fast-spiking interneurons multiple SWR-associated APs (Figure 3.4.C) over the entire time window of the SWR event (firing rate: 1.300 ± 0.112 vs. 3.106 ± 0.376; n=9 and n=20, p=0.004, for CCK+ and PV+ interneurons, respectively; Figure 3.3.Ci; 3.4.Ci and 3.6.A). Furthermore, whereas PV+ fast-spiking interneurons discharged on almost every SWR episodes, skipped CCK+ BC ~30% of these synchronous evens and demonstrated a significantly lower firing probability compared to PV+ fast-spiking interneurons (0.720 ± 0.014 vs. 0.945 ± 0.014; n=9 and n=20, p=0.005, for CCK+ and PV+ interneurons, respectively; Figure 3.3.Ci; 3.4.Ci and 3.6.B).

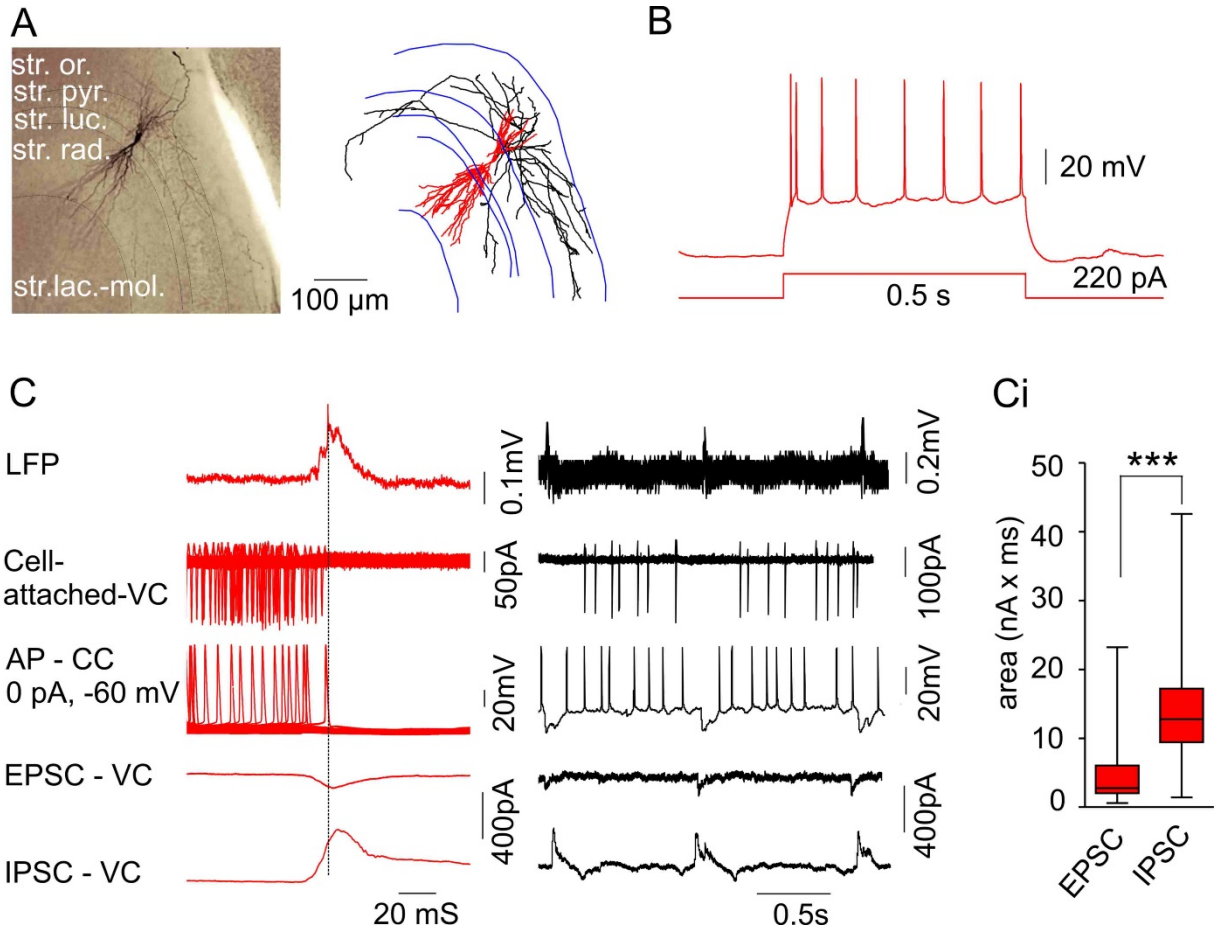

Figure 3.2. Morphological and electrophysiological properties of PCs during sharp wave-ripples. (A) Biocytin staining (left) and neurolucida reconstruction of a representative PC. (B) The regular firing pattern of this PC upon a depolarizing current injection. (C) Characteristic firing behavior and synaptic properties of PCs during SWR activity illustrated episodically (left, red traces) and dynamically (right, black traces). (Ci) SWR-associated excitatory (EPSC) and inhibitory (IPSC) postsynaptic currents of PCs. Note a prominent significantly higher IPSC in comparison with EPSC.

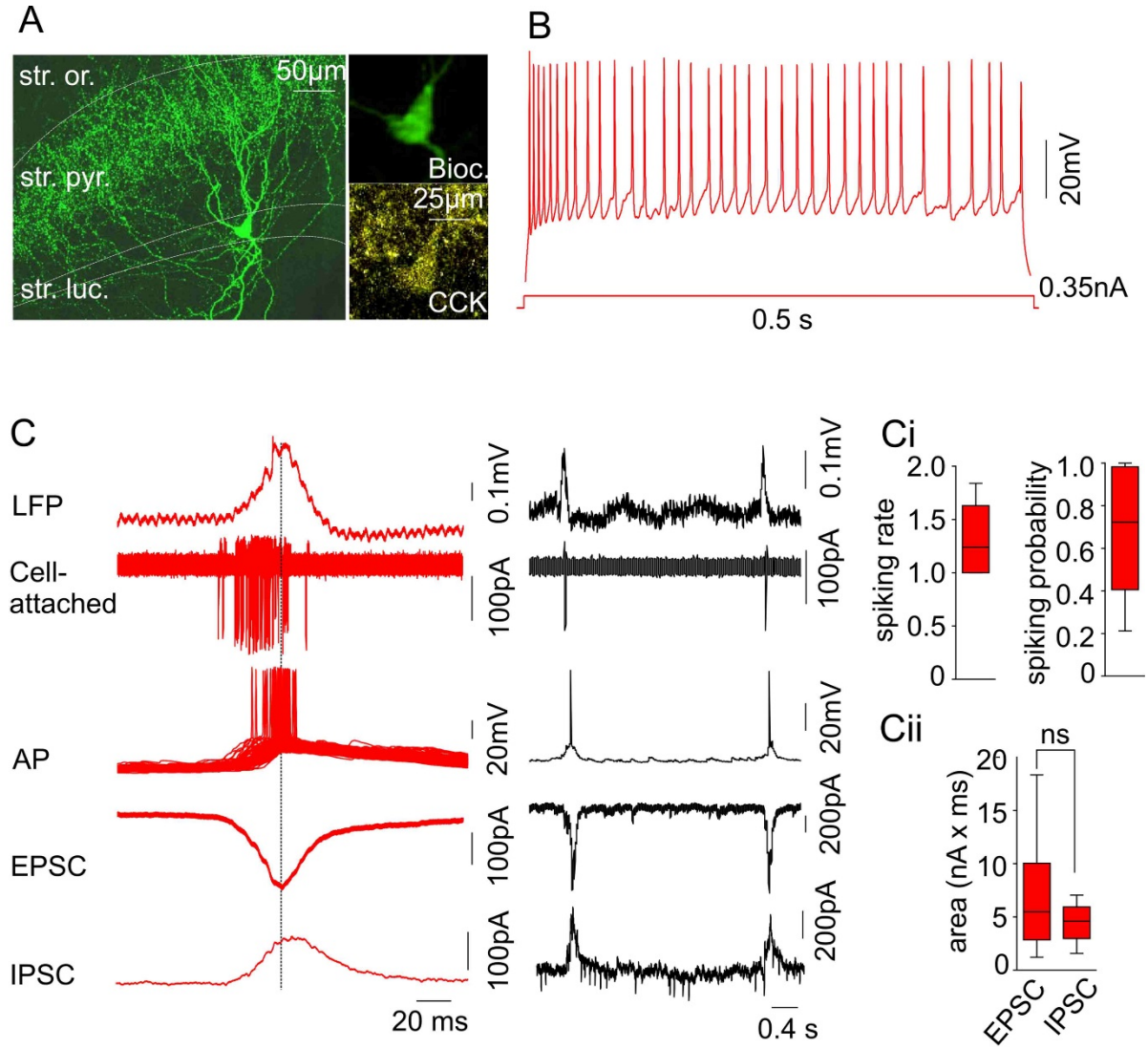

Figure 3.3. Morphological and electrophysiological properties of CCK+ regular-spiking BC during SWR activity. (A) Confocal image of a representative CCK+ regular-spiking BC filled with biocytin (left) and immuno-reactivity of the same cell for CCK (right). (B) Regular-spiking with characteristic accommodation upon a depolarizing current injection. (C) Firing behavior and synaptic properties during SWR activity, illustrated episodically (left, red traces) and dynamically (right, black traces), demonstrating predominant spiking of single APs on ca. 70% of all SWR episodes. (Ci) statistical analysis of firing rate and firing probability of CCK+BCs during SWR activity. (Cii). SWR-associated EPSC and IPSC with no significant difference in their strength.

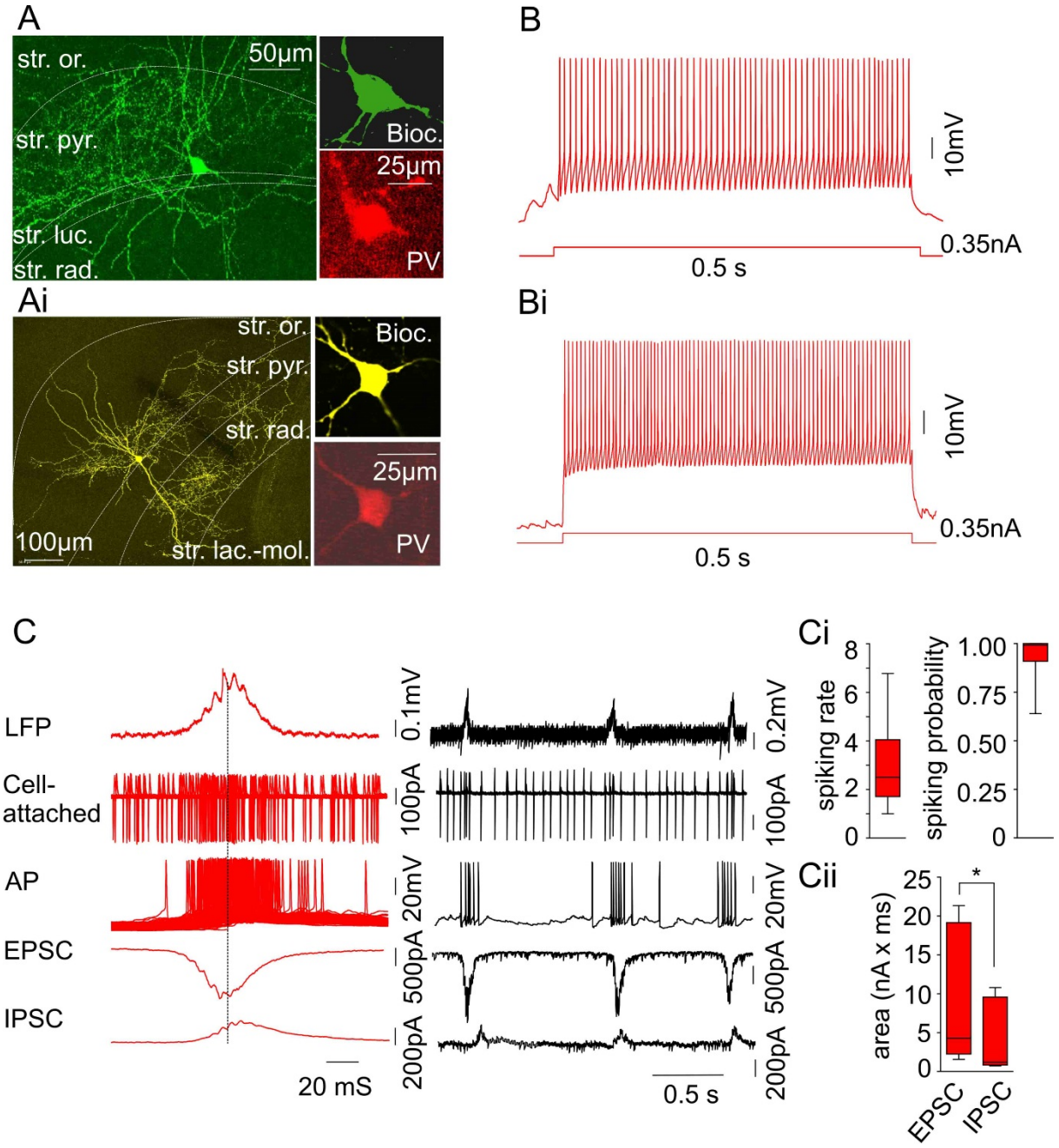

Figure 3.4. Morphological and electrophysiological properties of PV+ fast-spiking interneurons during SWR activity. Confocal image of a representative PV+ fast-spiking BC (A) and BSC (Ai) filled with biocytin (left) and immuno- reactivity of the same cells for PV (right). (B, Bi) Characteristic fast-spiking upon a depolarizing current injection. (C) Characteristic firing behavior and synaptic properties during SWR activity illustrated episodically (left, red traces) and dynamically (right, black traces) showing multiple APs on every SWR episode. (Ci) Statistical analyses of firing rate and firing probability of PV+ fast-spiking interneurons during SWRs. (Cii) SWR-associated EPSC and IPCS showing a prominent, significantly different EPSC compared to the IPSC.

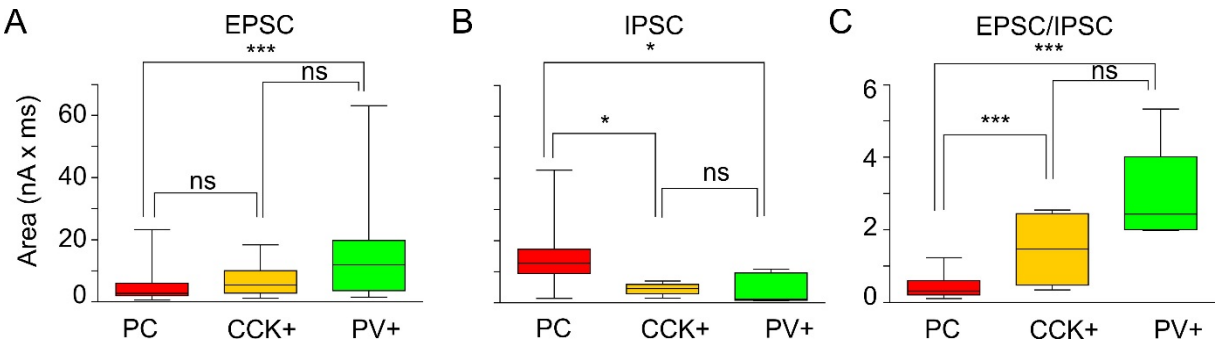

Figure 3.5. SWR-associated postsynaptic currents in three different classes of neurons in CA3. Statistical analyses of SWR-associated postsynaptic currents revealed a significantly higher EPSC (A) in PV+ fast-spiking interneurons in comparison with PC, whereas IPSC (B) in PCs was significantly higher than in interneurons. Accordingly, interneurons showed a significantly higher EPSC/IPSC ratio (C) than PCs.

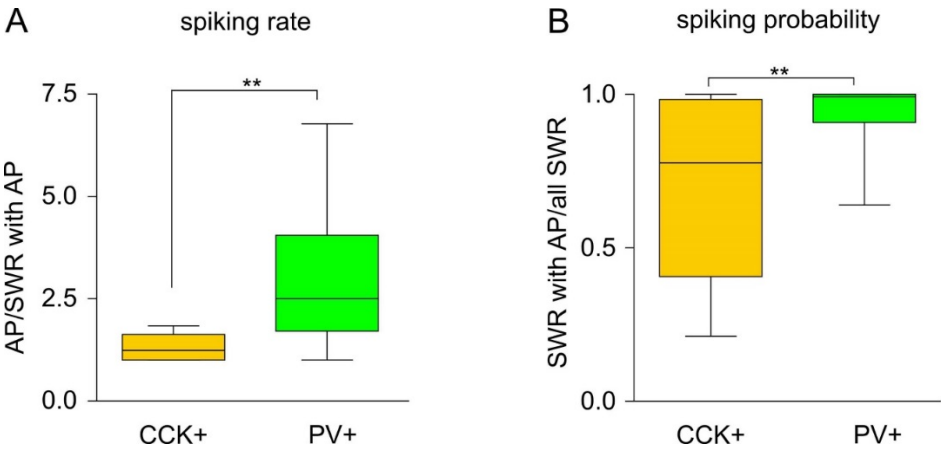

Figure 3.6. SWR-associated spiking rate and spiking probability of different classes of interneurons. Statistical analyses of SWR-associated spiking behavior of CCK+BC and PV+ fast-spiking interneurons revealed a significantly higher firing rate (A) as well as firing probability (B) of PV+ cells compared to CCK+ interneurons during network SWR activity.

3. Switching of cell type-specific activity of different neuronal classes from SWR into gamma frequency oscillations during transient state

To investigate cell type-specific behavior of different neurons, we continued recording after bath application of kainic acid (KA, 400nM, ascent scientific). A few seconds after KA application SWRs disappeared and all recorded cells with phase coupled spiking to SWR episodes changed their firing behavior.

All recorded PCs depolarized gradually during transient state and eventually reached a steady state (from -62.860 ± 1.791 mV to -50.380 ± 1.720 mV; n=21, $p<0.0001$; Figures 3.7.A and 3.7.B) once gamma frequency oscillations have been established. Moreover, they increased their spiking frequency during transient state (from 0.247 ± 0.101 Hz during SWR to 1.734 ± 0.209 Hz during transient state, n=16, $p<0.0001$, up to 3.819 ± 0.378 Hz during gamma activity n=16, $p<0.0001$; Figure 3.7.C). Similarly, all recorded CCK+BCs showed a significant depolarization during transient state (from -60.83 ± 1.621 mV to -52.83 ± 0.9458mV, n=6, p=0.0007; Figures 3.8.A and 3.8.B) and gradually increased their spiking frequency (from 0.283 ± 0.191 Hz during SWR to 3.333 ± 0.804 Hz during transient state, n=6, p=0.013 up to 9.183 ± 3.167 Hz during gamma frequency oscillations, n=6, p=0.070; Figure 3.8.C).

Although the extent of the transient state-associated depolarization in PV+ fast-spiking interneurons (from -67.170 ± 1.749 mV to -58.000 ± 1.981 mV, n=12, $p<0.0001$; Figures 3.9.A and 3.9.B) was not significantly different from other cell groups (p=0.171 and p=0.538 compared to PCs and CCK+BCs, respectively; Figure 3.10.A), they demonstrated the highest firing frequency during both transient states (increased from 0.483 ± 0.382 Hz during SWR to 10.490 ± 2.263 Hz during transient state, n=12, p=0.0006) and gamma oscillations (increased up to 28.97 ± 5.400 Hz, n=12, p=0.0049; Figure 3.9.C) which significantly exceeded the corresponding firing rate of both PCs (p=0.0001 and p=<0.0001 for transient state and gamma oscillations, respectively) and CCK+BCs (p=0.045 and p=0.026 for transient state and gamma oscillations, respectively; Figure 3.10.B).

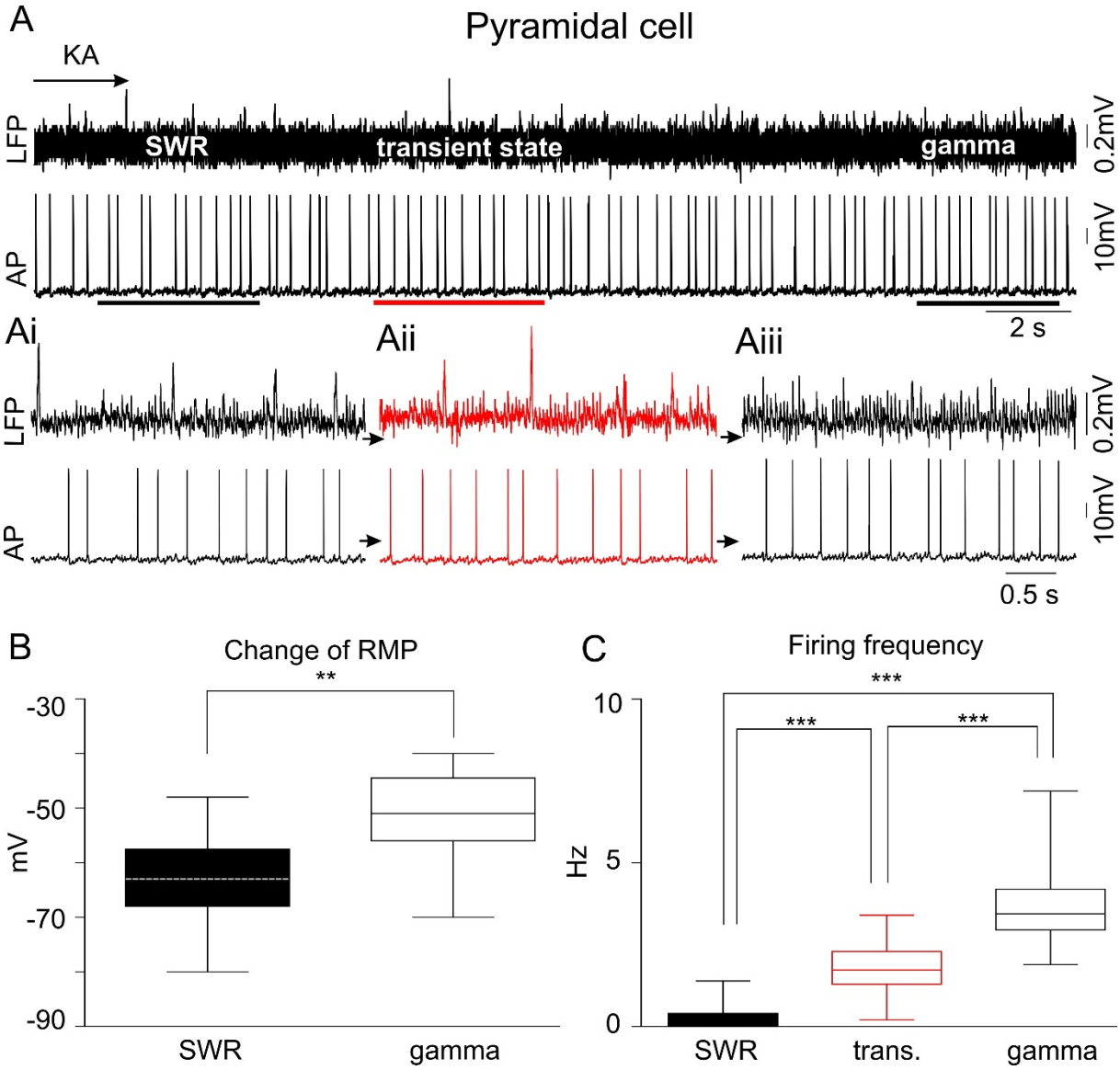

Figure 3.7. Dynamic change of firing behavior and resting membrane potential of PCs during transient state. (A) Simultaneously recorded LFP (top) showing dynamic switching from SWR into gamma frequency oscillations and spiking PC held at the RMP in current clamp configuration (bottom). SWR (Ai), transient state (Aii) and subsequent gamma oscillations (Aiii) with corresponding spiking pattern of PCs are illustrated with higher temporal resolution below. Statistical analyses of the RMP- (B) and firing frequency (C) changes of PCs during transient state revealed a significant depolarization as well as a gradual increase of spiking frequency while switching from SWRs into gamma frequency mode.

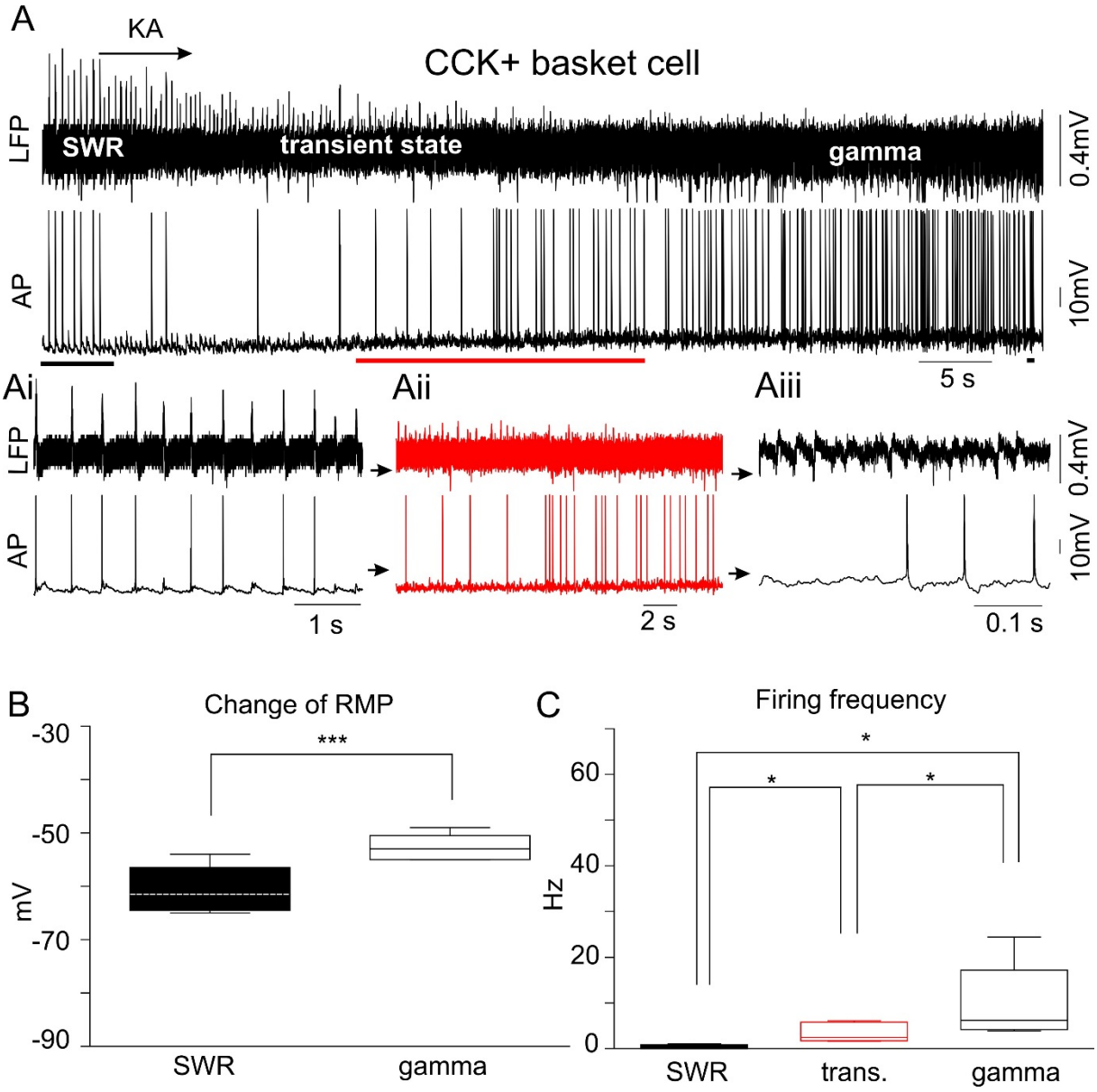

Figure 3.8. Dynamic change of firing behavior and resting membrane potential of CCK+BCs during transient state. (A) SWRs with subsequent transient state and gamma frequency oscillations (top) and simultaneously recorded cell spiking in the current clamp configuration at the RMP (bottom) illustrating dynamic switching of network and single cell activity from one into another oscillatory mode. High temporal resolution sequences of the same trace showing SWR (Ai), transient state (Aii) and gamma rhythms (Aiii) with corresponding characteristic cell-activity patterns. (B) Statistical analyses of RMP change showing a significant depolarization of RMP during transient state. (C) Statistical analyses of the firing frequency with significant increase during transient state and gamma frequency oscillations.

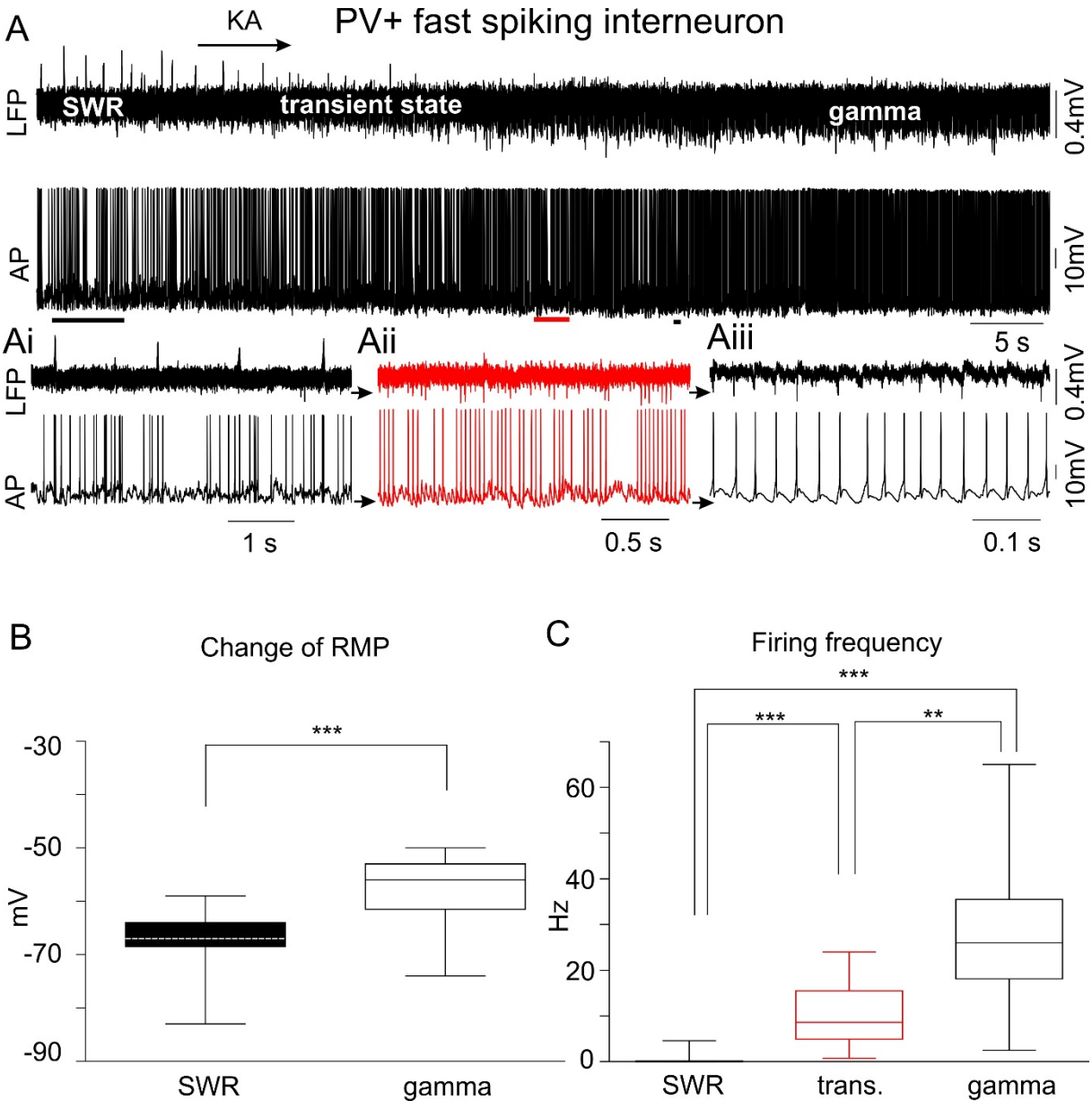

Figure 3.9. Dynamic change of firing behavior and resting membrane potential of PV+ fast-spiking interneurons during transient state. (A) Concomitant recording of LFP with SWR, transient state and gamma and corresponding single cell activity. Higher temporal resolution sections for SWR (Ai), transient state (Aii) and gamma rhythms (Aiii) with accompanying spikes illustrate characteristic changes in firing behavior of these cells. Statistical analyses revealed a significant RMP depolarization (B) as well as a gradual increase in firing frequency (C) along with dynamic changes in network activity from SWR to gamma frequency mode.

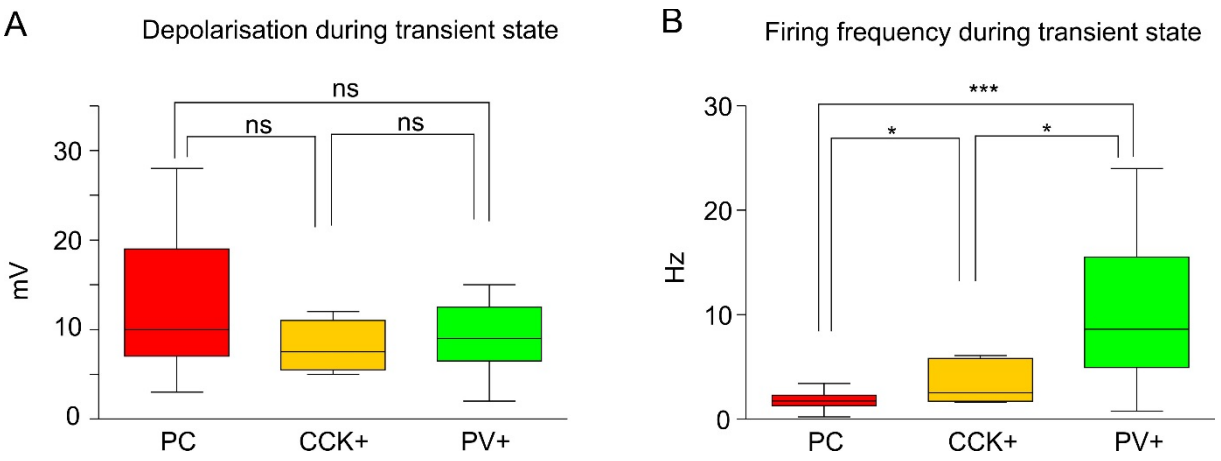

Figure 3.10. Comparison of changes in resting membrane potential and increased firing frequency of different neuron classes during transient state. Statistical analyses of the RMP and firing frequency revealed no cell type-specific differences in the extent of transient state-related depolarization (A), nevertheless interneurons fired at a significantly higher frequency compared to PCs during transient state, whereas PV+ fast-spiking interneurons demonstrated the highest firing frequency during transient state.

4. Gamma rhythm-associated cell specific synaptic and firing properties of individual morphologically identified neurons in CA3

Further analysis of synaptic currents during gamma oscillations revealed a significant difference between PCs and interneurons.

The recorded PCs received a significantly smaller amount of gamma-associated EPSC compared to CCK+BCs (0.640 ± 0.090 nA x ms, n=23 vs. 1.918 ± 0.827 nAxms, n=5, p=0.0043, PCs and CCK+BCs, respectively; Figures 3.11 and 3.14.A) and PV+ fast-spiking interneurons (2.175 ± 0.456 nA x ms, n=17, p=0.0005; Figure 3.14.A), whereas gamma-associated IPSC exhibited no significant cell type-specific difference (p=0.43 PCs vs. CCK+BC and p=0.452, PCs vs. PV+ fast-spiking interneurons; Figure 3.14.B). Nevertheless, the difference in EPSC appears to be essential for different excitability of these cell classes during gamma oscillations. Indeed, the PCs showed the lowest EPSC/IPSC ratio (0.388 ± 0.053, n=6) compared to the CCK+BCs (2.060 ± 0.631, n=3, p=0.005) and PV+ fast-spiking interneurons (2.145 ± 0.547; n=6, p=0.0096; Figure 3.14.C). It is worth noting that the comparison of gamma oscillation-associated synaptic currents and the EPSC/IPSC-ratio between these two different interneuron classes did not reveal a significant difference (Figure 3.14).

Similar to SWR, gamma frequency oscillations were accompanied by different firing behavior in a cell specific manner. Again, the PCs showed a lowest firing rate (1.001 ± 0.002; n=25; Figures 3.11 and 3.15.A) as well as firing probability (0.132 ± 0.020; n=25; Figures 3.11 and 3.15.B) compared with CCK+BC (1.073 ± 0.036 and 0.511 ± 0.085, n=12, p=0.013 and p<0.0001 for the firing rate and firing probability, respectively; Figure 3.12 and 3.15) and PV+ fast-spiking interneurons which showed the highest firing rate (1.598 ± 0.201; n=15, p=0.0005 and p=0.013 compared to the PCs and CCK+BCs, respectively; Figure 3.13 and 3.15A) and firing probability (0.884 ± 0.036, n=15, p<0.0001 and p=0.0002 compared to the PCs and CCK+BCs, respectively; Figure 3.13 and 3.15.B) during gamma frequency oscillations. Since we did not observed any differences in the synaptic currents and the EPSC/IPSC ratio between these two different interneuron classes, the cell-specific difference in spiking during gamma rhythms might be attributed to the different intrinsic properties of these interneurons.

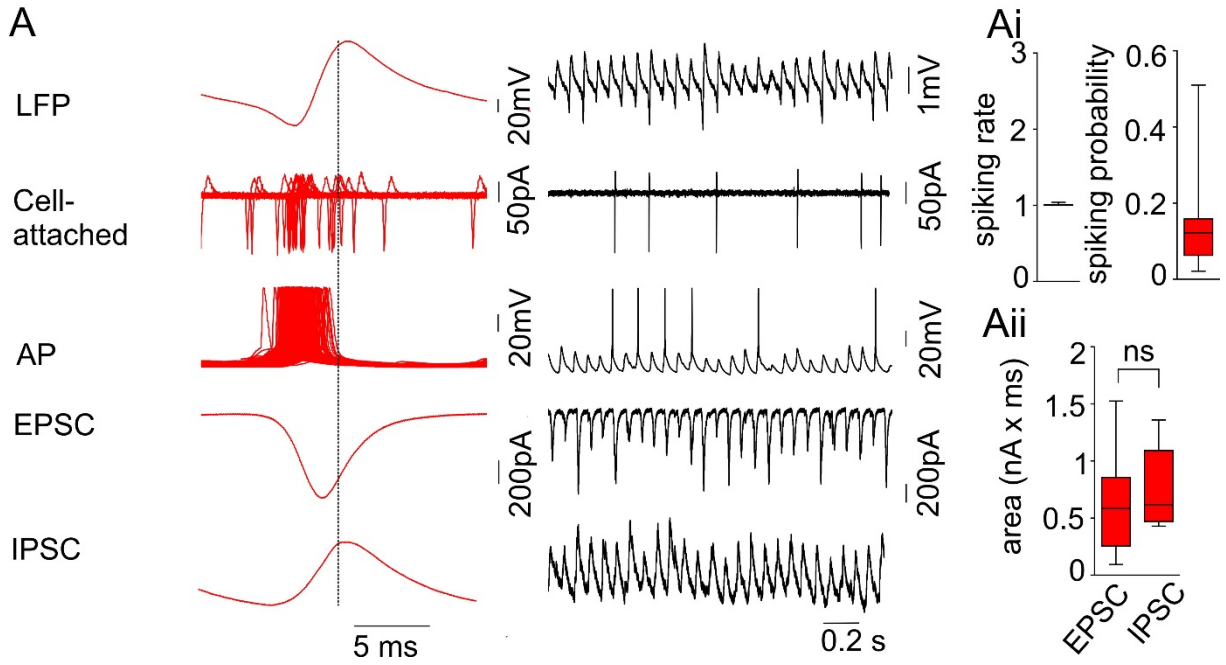

Figure 3.11. Synaptic and firing properties of PCs during gamma oscillations. (A) simultaneously recorded LFP and single cell activity in cell attached and whole cell mode with spikes and gamma-associated EPSC and IPSC illustrated episodically (left) and dynamically (right). (Ai) statistical analysis of gamma-related firing rate and firing probability of PCs. (Aii) statistical analyses of gamma-associate EPSC and IPSC revealed no significant difference.

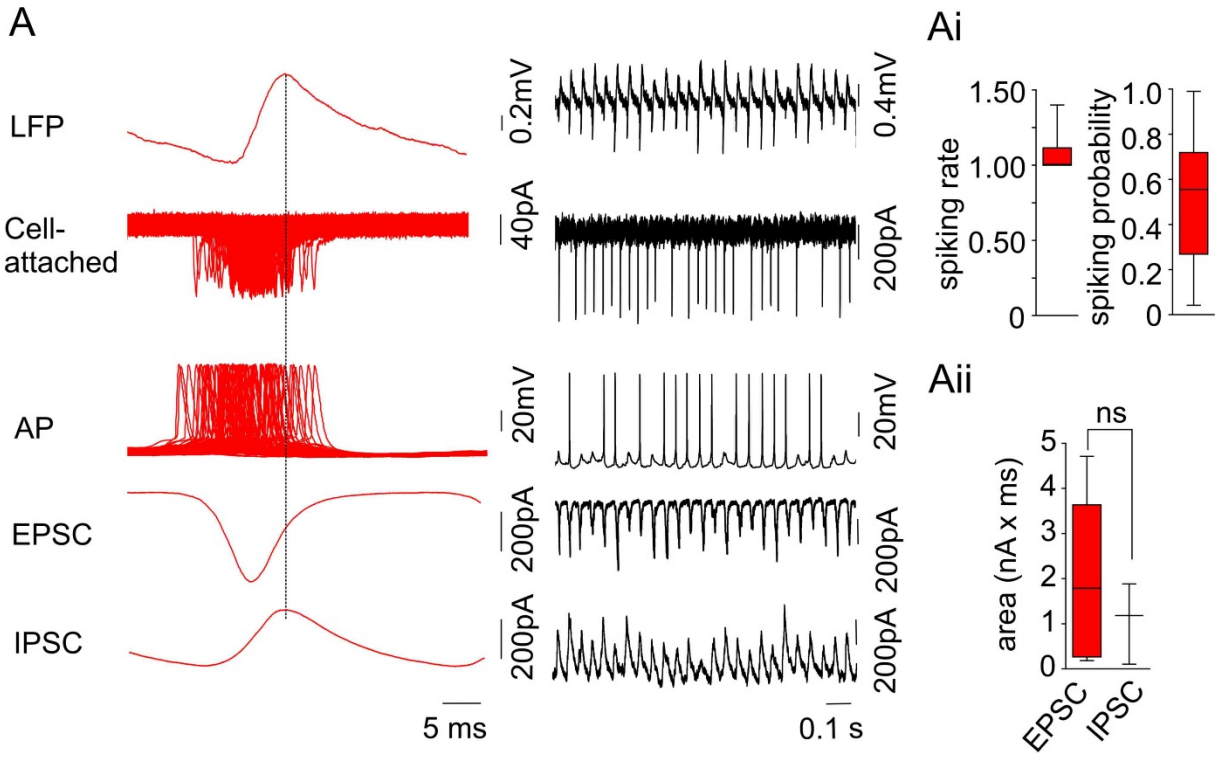

Figure 3.12. Firing behavior and synaptic properties of CCK+BCs during gamma rhythms. (A) Concomitantly recorded gamma oscillations and spiking activity as well as gamma-associated synaptic currents of CCK+BCs (A) illustrated episodically (left) and dynamically (right). (Ai) characteristic firing rate and firing probability of CCK+BCs during gamma frequency oscillations. (Aii) Gamma-related EPSC and IPSC do no differ significantly from each other.

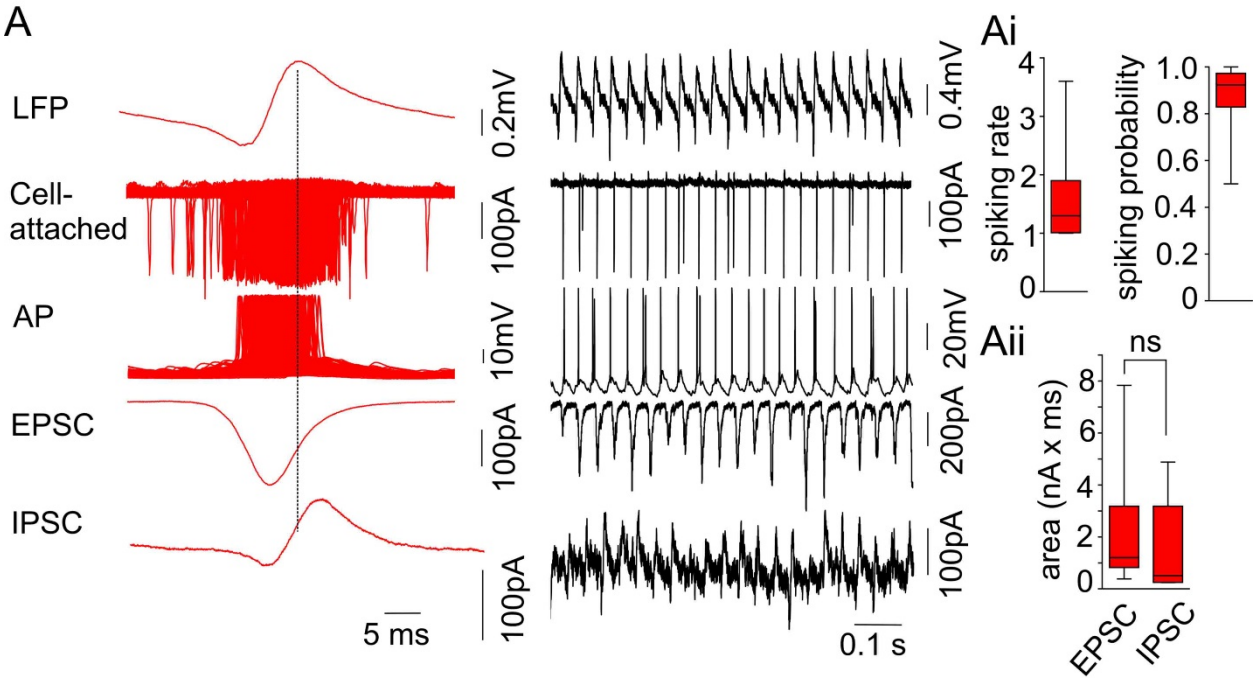

Figure 3.13. Typical firing behavior and synaptic properties of PV+ fast-spiking interneurons during gamma oscillations recorded in cell attached and whole cell mode. (A) Characteristic firing pattern and gamma-related postsynaptic currents illustrated episodically (left) and dynamically (right). (Ai) statistical analyses of gamma-related firing rate and firing probability of PV+ fast-spiking interneurons demonstrated single or double spikes at almost every gamma oscillatory cycle. (Aii) Gamma-associated EPSC and IPSC show no significant difference in their strength.

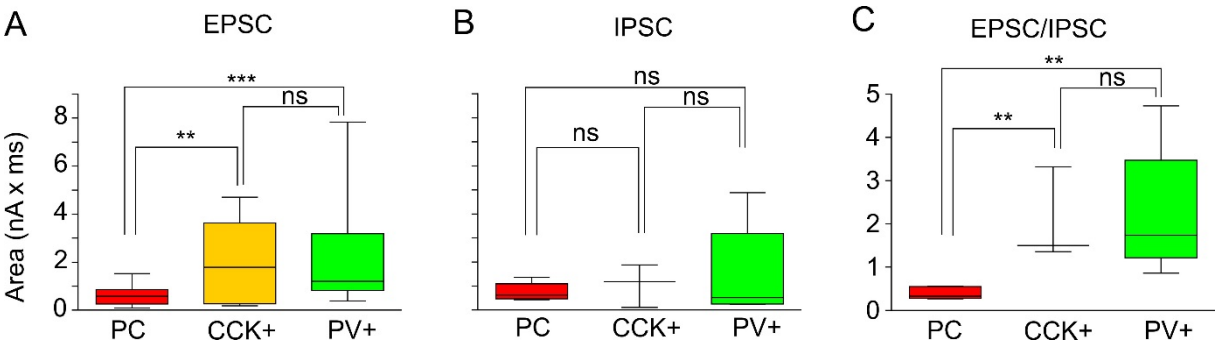

Figure 3.14. Gamma rhythm-associated synaptic properties of three different neuronal classes in CA3. Statistical analysis of cell type-specific EPSC (A), IPSC (B) and EPSC/IPSC ratio revealed a significantly higher gamma-related EPSC in interneurons in comparison with PCs, whereas gamma-associated IPSC did not show any cell type-specific difference. Accordingly, the EPSC/IPSC ratio in interneurons was significantly higher compared with principal cells. However, there was no difference between these two interneuron groups with respect to these parameters.

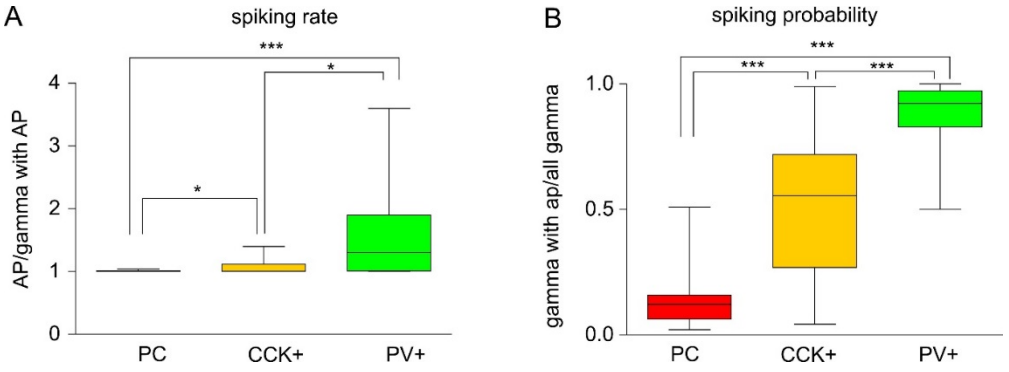

Figure 3.15. Statistical analyses of gamma-related spiking behavior of distinct neurons in CA3. Cell type-specific differences with significantly higher firing rate (A) and firing probability (B) in interneurons than in PCs, with PV+ fast-spiking interneurons firing a significantly higher number of spikes per single gamma cycle in a significantly higher proportion of these synchronous events than CCK+BC.

Chapter IV

Cellular mechanisms of gamma frequency oscillation-induced LTP in CA3

The previous observation on gamma rhythm-induced and mGluR5/NMDA receptor-mediated network plasticity, including increased subsequent SWR activity in CA3, motivated us to elucidate the underlying cellular mechanisms of these changes. Moreover, we intended to clarify whether cell type-specific activity clearly demonstrated by recorded PCs and different interneurons classes during gamma rhythm would result in distinct cell type-specific changes in their excitatory and inhibitory synaptic strength. For this purpose, we analyzed and compared SWR-associated EPSC and IPSC recorded before and after gamma rhythm (EPSC vs. r-EPSC and IPSC vs. r-IPSC) for each cell groups to detect potential long-lasting changes in synaptic transmission at the PC/PC, IN/PC as well as PC/IN and IN/IN synapses. Finally, we calculated the cell type-specific EPSC/IPSC ratio and analyzed changes in this ratio after gamma oscillations, which may imply gamma-induced excitability changes in different cell groups.

1. Gamma rhythm-induced long-lasting changes in excitatory and inhibitory synaptic currents in CA3 principal cells

We first examined activity-dependent changes in synaptic strength at PC-PC excitatory synapses and interneuron-PC inhibitory synapses by comparing SWR-associated EPSC with r-EPSC in whole cell mode in PCs. These cells were held at their resting membrane potential (RMP) and allowed to generate APs during gamma rhythm (see method). Analysis of EPSC revealed a significantly increased area of r-EPSC (by 104.2 ± 21.18%, n=14, p=0.0003, Figure 4.1.A) along with increased area of corresponding SWR events. In contrast, the PCs held in "voltage clamp" at -70 mV to avoid spike generation during gamma frequency oscillations, exhibited, parallel to the corresponding SWR area increase, a significantly reduced r-EPSC area (by 40.62 ± 7.68%, n=13, p=0.0002, Figure 4.2.A), suggesting postsynaptic induction mechanisms of this plasticity form which may essentially depend on PC spiking behavior during gamma rhythm.

To test the causality between long-lasting alterations in network excitability reflected in increased r-SWRs, which was largely dependent on mGluR5-mediated transmission and increased r-EPSC in PCs, we analyzed the effect of mGluR5 blockade on r-EPSC by application of MPEP and observed no increase in its area (LTP reduction by 95.21 ± 7.03%, n=4, p=0.0009, Figure 4.3). Thus, MPEP administration fully prevented gamma-induced increase in excitatory

synaptic strength suggesting a pivotal role of mGluR5-mediated synaptic transmission for LTP induction.

We next analyzed gamma rhythm-induced alterations in inhibitory synaptic transmission at IN/PC synapses. Cells allowed to spike during gamma rhythm demonstrated a moderate but still significant increase in the area of SWR-associated r-IPSC (by 32.81 ± 12.90%, p=0.039, n=8, Figure 4.1.B). Analysis of the EPSC/IPSC ratio in PCs revealed a significant increase after gamma rhythm (by 44.38 ± 14.62%, p=0.019, Figure 4.1.C). However, changes in IPSC were independent of postsynaptic activity, as r-IPSC increased significantly (by 30.33 ± 7.30, n=6, p=0.0089, Figure 4.2.B), even if the postsynaptic cells were prevented from spiking during gamma rhythm by holding in "voltage clamp" at -70mV.

These results suggest collectively that gamma-induced long-lasting increase in SWR-associated EPSC in PC is mediated postsynaptically and depends on intact mGluR5 activity, whereas changes in SWR-associated IPSC do not require postsynaptic spiking und may, therefore, derive from activity dependent plastic changes in presynaptic inhibitory interneurons. Thus, in the next set of experiments we investigated the same parameters of synaptic transmission at PC/IN and IN/IN synapses in two different interneuron classes: PV+ fast-spiking interneurons and CCK+ regular-spiking BCs.

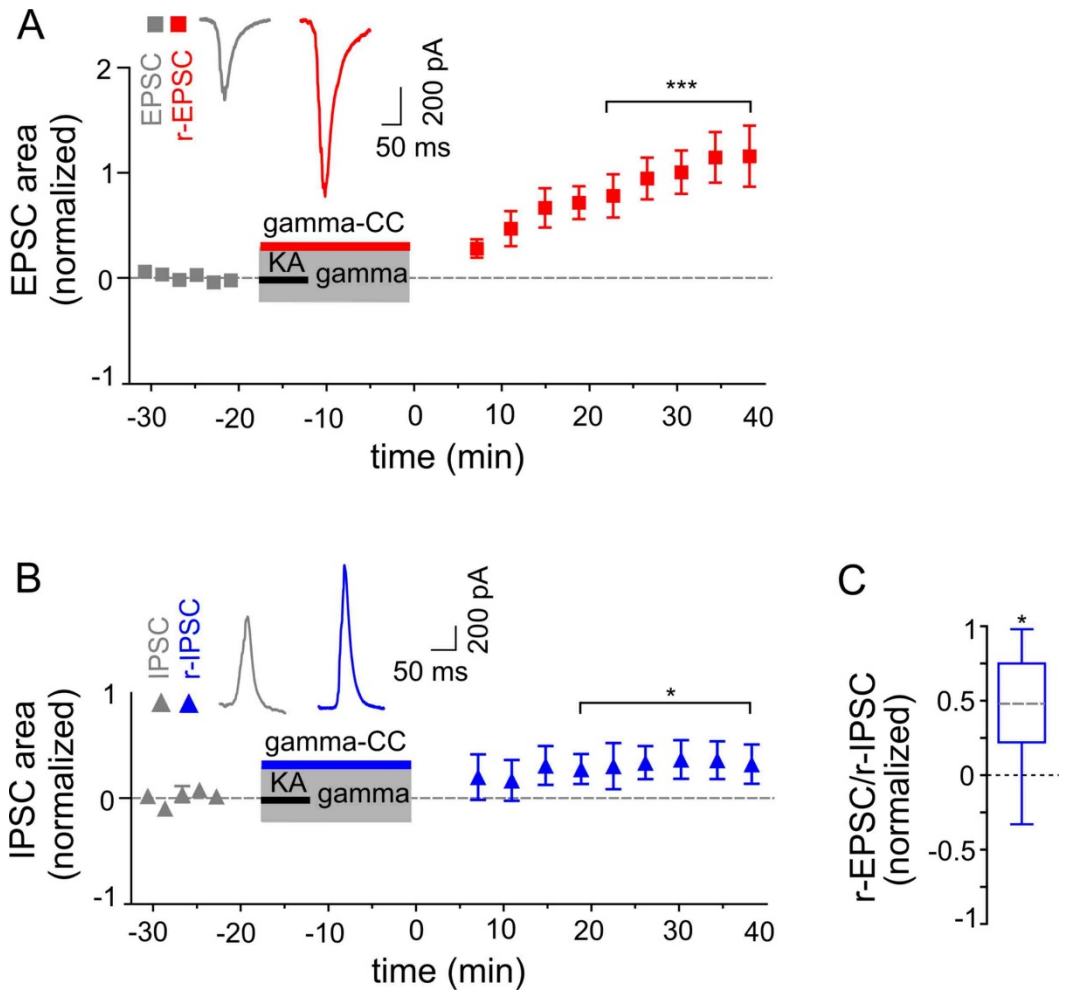

Figure 4.1. Gamma frequency oscillations elicit long-lasting changes in PC/PC and IN/PC synaptic transmission. (A) Normalized SWR-associated EPSC area before (gray squares) gamma oscillations increased significantly after (r-EPSC, red squares) gamma rhythm. Insert, representative examples of EPSC (gray) and increased r-EPSC (red) after gamma rhythm. (B) Moderately but still significantly changed area of inhibitory postsynaptic current (pre gamma IPSC, gray triangles) after gamma frequency oscillations (r-IPSC, blue triangles) in IN/PC synapses. Insert, representative examples of IPSC (gray) and r-IPSC (blue). Application time of KA and run duration of gamma frequency oscillations are indicated by the black horizontal line and the gray box, respectively. (C) Long-lasting changes in the EPSC/IPSC ratio after gamma frequency oscillations show significantly increased excitability of PCs demonstrating long-lasting synaptic potentiation of excitation induced by network activity in the gamma frequency range.

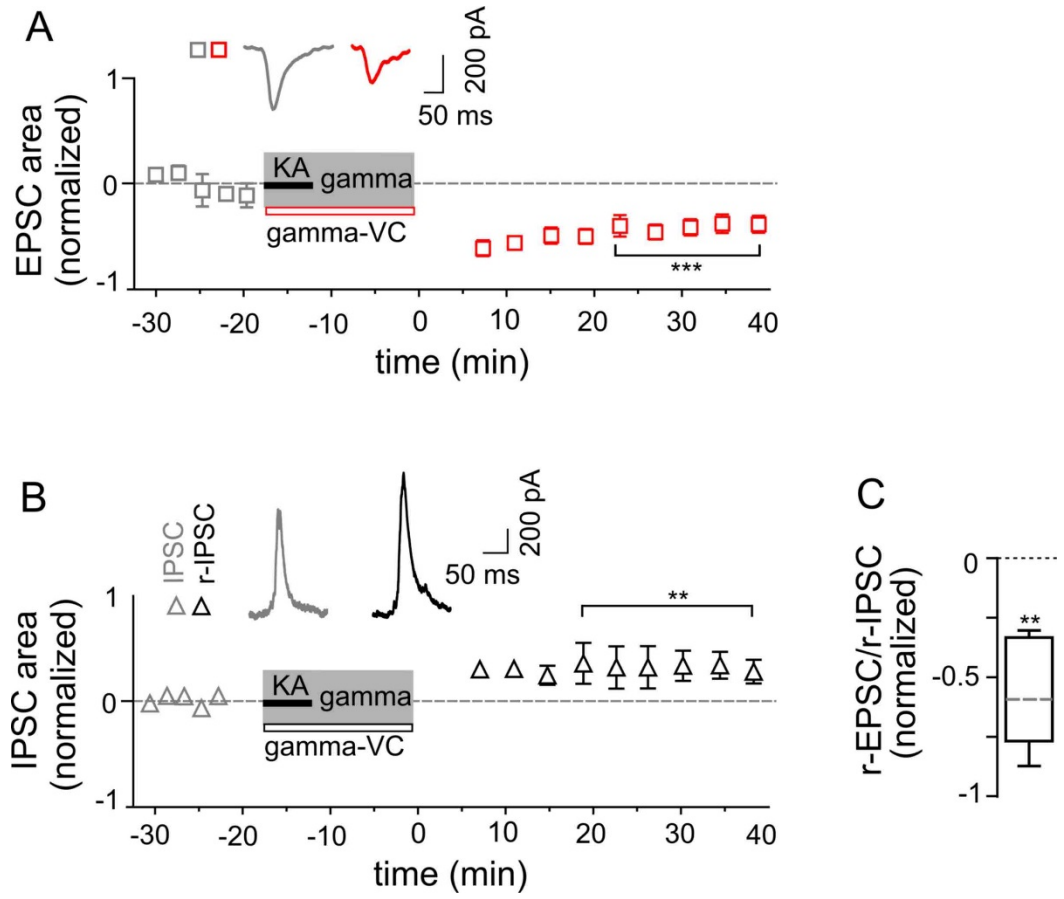

Figure 4.2. Long-lasting increase in EPSC after gamma frequency oscillations is mediated postsynaptically. (A) Normalized area of SWR-associated EPSC before (gray squares) gamma oscillations decreased significantly after (r-EPSC, red squares) gamma rhythm if the cell was voltage clamped at -70 mV during network activity in the gamma frequency band. Insert, representative examples of EPSC (gray) and decreased r-EPSC (red) after gamma rhythm. (B) Prevention of spiking by voltage clamping at -70 mV during gamma rhythm did not affect the increased r-IPSC in PCs. Insert, representative examples of IPSC (gray) and r-IPSC (black) (C) significant reduction of the EPSC/IPSC ratio in PCs prevented from spiking during gamma rhythm.

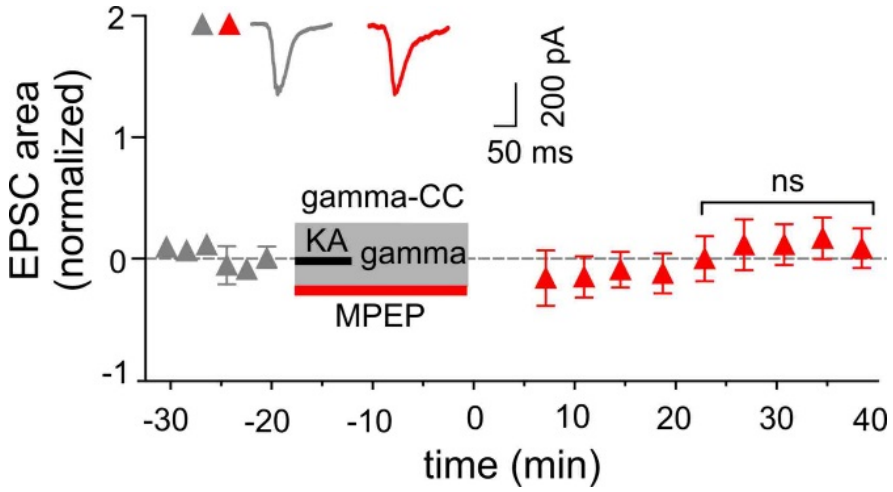

Figure 4.3. Long-lasting increase in EPSC after gamma frequency oscillations depends on metabotropic glutamate receptor 5 activation. (A) Administration of MPEP during gamma rhythm prevented increase in EPSC (EPSC before gamma, gray triangles vs. r-EPSC, red triangles). Insert, representative examples of corresponding EPSC (gray) and r-EPSC (red). KA and MPEP application time is depicted with the black and red horizontal lines, respectively and gamma duration – with the gray box.

2. Gamma rhythm-induced contra-directional long-lasting changes in synaptic currents in PV+ fast-spiking interneurons and CCK+ regular-spiking BCs in CA3

To uncover the source of changed SWR-associated IPSC in PCs, we investigated synaptic currents in two major interneuron classes: PV+ fast-spiking interneurons, including BCs and BSCs, and regular-spiking CCK+ BC. As observed previously, these interneurons exhibit distinct firing patterns during gamma frequency oscillations and therefore are likely to demonstrate differential gamma-induced changes in their excitability. Similar to PCs, we recorded in interneurons SWR-associated EPSC and IPSC in whole cell configuration at -70 mV and 0 mV, respectively and estimated finally the EPSC/IPSC ratio to evaluate cell excitability.

As expected, PV+ fast-spiking interneurons demonstrated significantly increased EPSC (by 103.40 ± 21.79%, n=10, p=0.0011, Figure 4.4.A), whereas CCK+ regular-spiking interneurons exhibited no significant changes in their excitatory synaptic strength (reduced by 0.13 ± 10.60% of control, n=8, p=0.991, Figure 4.5.A). Note that PV+ fast-spiking interneurons demonstrated a strongly gamma phase correlated firing pattern with significantly higher gamma-associated firing rate and firing probability compared to CCK+ BC (Chapter III.4.). Similar to EPSC, gamma rhythm-induced changes in IPSC were expressed in a clear cell type-specific manner. However, cells with increased EPSC showed a slight but not significant reduction of IPSC (by 27 ± 11.23, n=4, p=0.096, Figure 4.4.B), whereas interneurons with unchanged EPSC exhibited significantly increased IPSC (by 61.05 ± 15.95%, n=5, p=0.019, Figure 4.5.B). The cell type-specific opposite changes in EPSC and IPSC resulted in a contra-directional change in the EPSC/IPSC ratio. Whereas PV+ fast-spiking interneurons changed this ratio in favor of excitation (from 3.17 ± 0.74 up to 7.29 ± 1.71, n=4, p=0.0371, Figure 4.6.A), showed CCK+ regular-spiking BCs its significant reduction, favoring the inhibition (from 2.14 ± 0.39 to 1.21 ± 0.26, n=5, p=0.0238, Figure 4.6.B).

These data demonstrate that in the CA3, gamma rhythm induces a cell type-specific synaptic plasticity expressed as r-EPSC and r-IPSC changes in opposing direction in interneurons, which are differentially involved in the generation of network gamma oscillations. Thus, the CA3 network appears to selectively favor potentiation in excitatory input of interneurons, which are relevant for network rhythm generation.

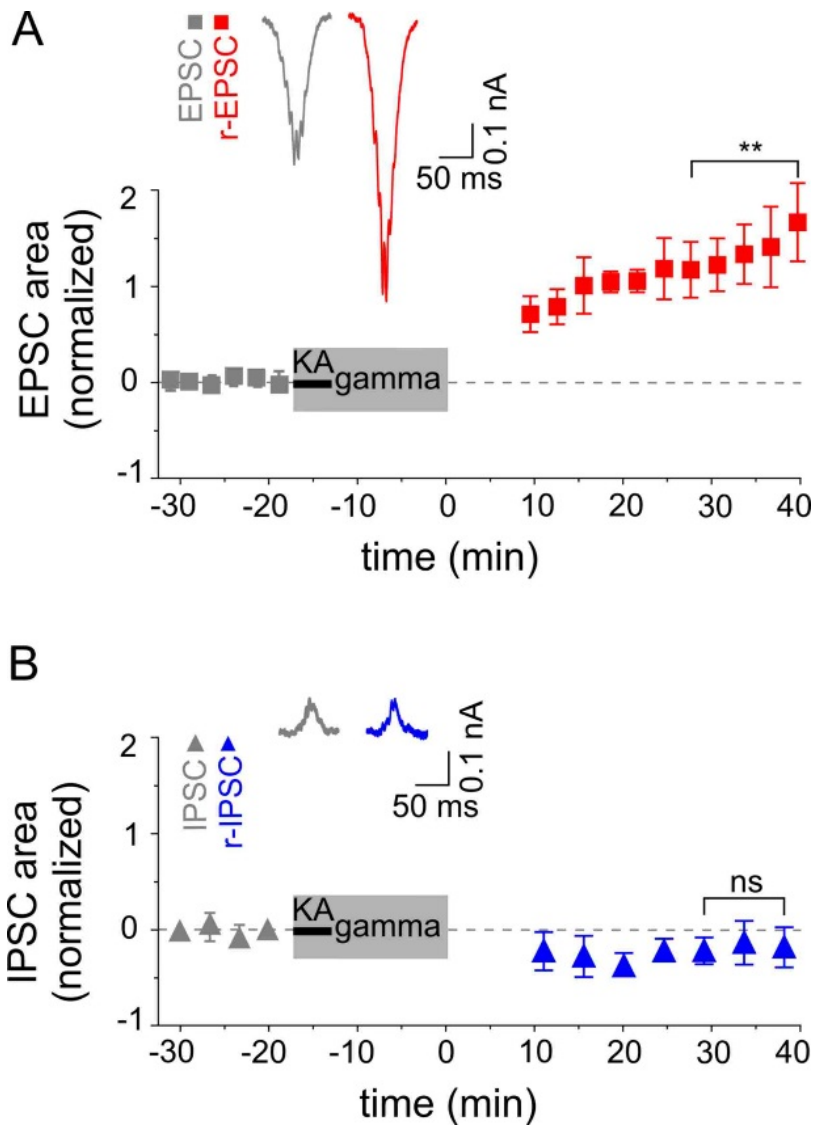

Figure 4.4. PV+ fast-spiking BCs and PV+ BSCs exhibit significant long-lasting potentiation of glutamatergic synaptic transmission, whereas GABAergic synaptic strength does not change significantly. (A) r-EPSC (red squares) shows a significant increase in area compared with EPSC (gray squares) obtained before gamma frequency oscillations. Insert, representative examples of EPSC and r-EPSC (gray and red traces, respectively). (B) r-IPSC (blue triangles) do not express significant changes in area compared with pre-gamma IPSC (gray triangles). Insert, representative examples of IPSC and r-IPSC (gray and black traces, respectively).

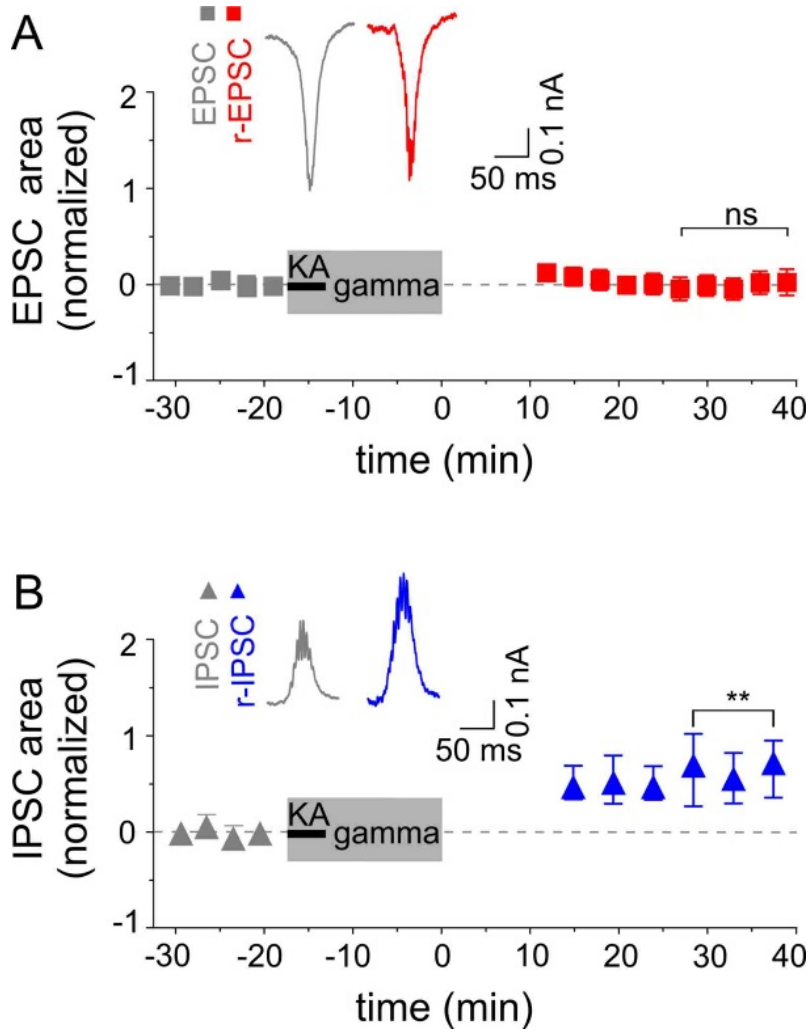

Figure 4.5. CCK+ regular-spiking BC show no long-lasting potentiation of excitatory synaptic strength, they do show such potentiation of inhibitory synaptic strength. (A) r-EPSC (red squares) show no significant changes in area compared with EPSC (gray squares) obtained before gamma frequency oscillations. Insert, representative examples of EPSC and r-EPSC (gray and red traces, respectively). (B) r-IPSC (blue triangles) express a significant increase in area compared with pre-gamma IPSC (gray triangles). Insert, representative examples of IPSC and r-IPSC (gray and blue traces, respectively).

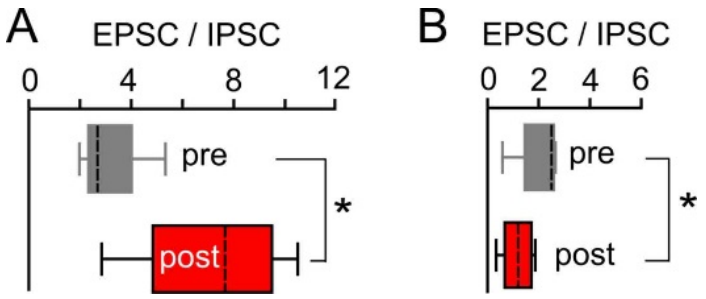

Figure 4.6. PV+ fast-spiking interneurons and CCK+ regular-spiking BCs show contra-directional changes in the EPSC/IPSC ratio after gamma frequency oscillations. (A) PV+ fast-spiking interneurons exhibit significant gamma rhythm-induced changes in the EPSC/IPSC ratio in favor of excitation. (B) In comparison to PV+ fast-spiking interneurons, CCK+ regular-spiking BCs show significant contra-directional changes in the EPSC/IPSC ratio in favor of inhibition.

Discussion

It is widely recognized that brain oscillations play a crucial role in long-term memory. In particular, oscillations in the gamma frequency range have been implicated in the processes of memory encoding [150]. The hippocampus is an important structure for memory consolidation and spatial orientation [150, 151, 152]. However, it remains unknown whether and if so, how gamma frequency oscillations promote the formation of long-lasting synaptic plasticity within the hippocampal circuit. Neuronal plasticity in the hippocampal network has been extensively studied using various induction tools, including electrical stimulation of different input/outputs and/or chemical stimulation of various receptors [124, 152, 153], however, the role of network oscillatory activity in LTP induction still remains to be elucidated.

This study was focused on the role of the gamma rhythm in activity-dependent modifications of neuronal activity. We used an *in vitro* model, which allowed us to reproduce both SWRs and gamma frequency activity in 'submerged' slices [147, 148] and observe the interaction and interdependence of these network activity patterns. These rhythms have been reported to constitute two different network states associated with different behavioral activity *in vivo* [149]. Gamma oscillations are associated with alert and exploratory behavior, periods essential for encoding of new information, whereas the SWRs represent a network state associated with memory consolidation [154, 155].

Our data demonstrate that oscillations at the gamma frequency range can directly induce activity-dependent changes in the hippocampus. We recorded local field potential in the stratum pyramidale of the area CA3 during gamma frequency oscillations and observed gradual changes in gamma power in the course of time. Gamma rhythm recorded >4 min after onset of gamma frequency oscillations referred to as 'late gamma' epochs showed a significantly higher power spectrum and auto-correlation in comparison with 'early gamma' recorded between ~1 and 4 min after gamma onset. To test whether temporal evolution of gamma rhythm depends on the pharmacological agent or takes place as a consequence of the oscillatory activity, we compared network dynamics of two different pharmacologically induced (KA- vs. CCh) models of gamma oscillations. We observed comparable effects of both agents. These results suggest a network activity-associated mechanism rather than specific pharmacological agent dependent changes responsible for the temporal evolution of the network activity in the gamma frequency range. Neither mGluR5 nor NMDA receptor antagonists affected gamma temporal evolution, excluding their contribution to the gradual increase observed in the spectral power of gamma frequency

oscillations. Thus, we assume that reinforced synchronization by gradually increasing recruitment of neurons, which appears to be independent of mGluR5 and NMDA receptor-mediated transmission, may account for temporal evolution of gamma oscillations.

Furthermore, gamma oscillatory activity influenced the readiness of CA3 network to generate the next gamma epoch. Application of low KA concentrations, which initially failed to induce gamma frequency oscillations, was sufficient for induction of gamma activity once applied again after preceding 'conventional' gamma oscillations have completely disappeared. These results suggest a clear reinforcing impact of the preceding gamma episode on the subsequent network activity facilitating generation of the next gamma epoch.

To examine the general potential of gamma frequency oscillations to affect subsequent network activities, we investigated another major rhythm, the SWR, and compared basic SWR properties before and after the intermediate gamma episode. Under our *in vitro* experimental conditions, SWRs occurred spontaneously, disappeared shortly after onset of the gamma rhythm and reappeared a few minutes after gamma oscillations had decayed. Thus, SWRs and gamma frequency activity represent two 'competing' network states *in vitro*. Although under our experimental conditions these two network patterns never took place concurrently and appear to be mutually exclusive rhythms, they are not fully independent: plastic changes initiated in the network through persistent gamma activity are reflected in an altered field SWR pattern. In comparison to the SWR preceding gamma frequency oscillations, the r-SWR exhibit a significant and long-lasting increase in area. In good agreement with these data, gamma oscillations induced by bath application of an alternative drug, CCh, also resulted in a significant increase in SWR area, confirming that gamma activity itself and not the pharmacological agent is responsible for the network alterations. It is worth noting that in comparison to KA, CCh-triggered gamma frequency oscillations exhibited less spectral power and accordingly induced smaller SWR area changes, suggesting again that the gamma oscillations and not the pharmacological agents themselves [156] may account for the observed network plasticity.

To uncover the molecular mechanisms underlying the network plasticity, we tested the role of mGluR5- and/or NMDA receptor activation using antagonists of these receptors, 2-methyl-6-(phenylethynyl)pyridine (MPEP) and DL-2-Amino-5-phosphonopentanoic acid (AP5), respectively. MPEP led to a more pronounced reduction of LTP compared to AP5, whereas a joint administration of both drugs abolished this form of plasticity. These results suggest that gamma frequency oscillations induce long-lasting modifications in the CA3 network, which depend on intact mGluR5 and/or NMDA receptor-mediated transmission.

To elucidate the mechanisms of gamma oscillation-induced changes in the local field network activity at the cellular level, we next investigated synaptic properties and firing behavior of anatomically identified individual neurons during different network states: SWR, gamma frequency oscillations as well as transient state between them. Analysis of synaptic currents revealed that PCs received prominent, significantly stronger SWR-associated IPSC compared with EPSC. Accordingly, we observed an inhibition of spiking in PCs during SWRs so that the generation of APs was completely prevented after the peak of the SWR episodes. Yet, very rarely, we observed single spikes on the ascending phase, which appear to be remnant spontaneous APs surviving due to insufficient SWR-associated inhibition at the initial phase of SWR episodes.

The importance of interneurons in the generation of SWRs has been demonstrated in both *in vivo* [49, 75] and *in vitro* [109] studies. Several studies have reported cell type-specific differences between PV+ and CCK+ interneurons in terms of their firing behavior and importance for SWR generation [108, 109]. Importantly, PV+ fast-spiking interneurons have been thought to be crucial players in the rhythm generation, since the selective inhibition of these cells resulted in a power decrease of SWs and disappearance of ripples, whereas inhibition of CCK+ cells did not affect these parameters [109].

In our study, the recorded CCK+ regular-spiking BCs and PV+ fast-spiking interneurons exhibited a higher excitability during SWRs, compared to the PCs. In contrast to the PCs, all interneurons demonstrated a clear phase-correlated spiking with SWR episodes. However, the interneurons showed strong cell type-specific differences in terms of their firing behavior. Whereas CCK+ BCs showed an SWR-associated single spike firing and moderately pronounced firing probability (~70%), PV+ fast-spiking interneurons exhibited a significantly higher spiking rate with multiple SWR-associated APs (~3 per SWR episode) and firing probability (~95%). Furthermore, we observed a cell type-specific difference between interneurons in terms of the temporal correlation with the SWR episode. Whilst CCK+ BCs spiked preferentially on the ascending phase, PV+ fast-spiking interneurons showed discharges during the entire time window of the SWR episode. In good agreement with our results, PV+ interneurons have been reported to fire on the larger portion of SWRs (firing probability) and generate significantly higher number of APs during single SWR episode than CCK+interneurons [108], suggesting again a pivotal role of PV+ fast-spiking interneurons in SWR generation.

Interestingly, analyses of postsynaptic currents and the EPSC/IPSC ratio in our study did not reveal any differences between these two interneuron classes.

Investigation of changes in membrane potential and firing behavior after KA application revealed significant differences among the recorded cell types. The firing frequency of PV+ fast-spiking interneurons increased to a significantly higher degree compared to PC and CCK+ BCs and achieved the gamma frequency range, so that during gamma rhythm these cells demonstrated a strongly phase-correlated firing on almost every gamma cycle with highly recurrent spike doublets. PCs showed a significantly lower firing probability along with the smallest gamma-associated EPSC compared to the GABAergic interneurons, whereas the analyses of gamma-associated IPSC revealed no cell type-specific differences. As expected, the EPSC/IPSC ratio in interneurons was significantly higher than in PCs. However, whereas the cell type-specific difference with respect to their synaptic currents in GABAergic interneurons did not reach the significance level, PV+ fast-spiking interneurons showed a significantly higher gamma-related spiking probability compared to CCK+ BCs. Different signaling characteristics in these interneuron classes with a high gamma fidelity activation of PV+ fast-spiking interneurons and less precisely timed and unreliable recruitment of CCK+ BCs might be determined by cell type-specific differences in spatiotemporal processing of synaptic currents due to distinct membrane resistance, membrane time constant and dendritic diameter [90, 132]. However, less is known about active membrane properties of different interneuron classes. Due to their output properties including high reliability and precise timing of spike generation during gamma rhythms, PV+ fast-spiking interneurons are suggested to provide a regular phasic inhibition, which may restrict the firing of PCs into a narrow time window. As these interneurons have been reported to be highly interconnected by both chemical synapses [157, 158] and gap-junctions [157], they may easily synchronize their activity and boost the generation of gamma rhythms [132]. In contrast, CCK+ BCs generate APs sporadically with less temporal precision predominantly on the ascending phase of the gamma cycle. The cells are suggested to provide an out-of-phase inhibition to PCs and interfere with gamma synchronization [88].

Our results demonstrate that gamma frequency oscillations induce long-lasting alterations of SWR-associated excitatory and inhibitory synaptic currents in PCs and interneurons in a cell specific manner (chapter IV).

Different forms of plasticity have been reported for the excitatory inputs converging on CA3 PCs: the mossy fibers, the A/C and the PP inputs. While the PP and A/C synapses show pairing-induced synaptic plasticity [126], other induction and expression mechanisms exist at mossy-fiber synapses [125, 127, 128]. Interestingly, activation of mossy fibers and CA3 neurons in the gamma frequency range induces LTP at recurrent CA3 synapses [129] that could be the substrate

of autoassociative memory encoding [130]. However, these and similar studies on hippocampal neuronal plasticity have considerable methodological limitations. Although CA3 PCs and their afferent neurons exhibit a sparse firing rate *in vivo*, LTP is usually induced by high-frequency electrical stimulation of the afferent input [144]. Furthermore, an isolated stimulation of different inputs is far from their physiological activity patterns in the intact hippocampal network. Therefore, we used gamma frequency oscillations as a physiological paradigm for LTP induction to uncover network-dependent cell-specific mechanisms, which have not been reported so far.

Our data demonstrate a long-lasting increase in the area of r-EPSC in PCs held in current-clamp mode during gamma oscillations (see method). This increase is temporally tightly correlated with an increase in the corresponding filed SWR area, suggesting a causal relationship. Conversely, r-EPSC in PCs held in voltage-clamp mode at -70 mV during gamma oscillations decreased rather than increased, suggesting that this form of plasticity is mediated postsynaptically and its induction is dependent on spiking.

The cell assembly theory formulated by Donald Hebb in his 1949 book "The organization of behavior", which highlighted the importance of correlated activity of multiple neurons for strengthening their connections [111], gave rise to numerous studies attempting to uncover cellular and molecular mechanisms underlying synchronization-induced changes in signal transmission by concurrent activity of synaptically connected neurons leading to memory formation. Indeed, growing evidence suggest that precise synchronization of neuronal activity is likely to support storage of information and improve memory performance [150, 159]. The cellular and synaptic mechanisms proposed to explain how neuronal synchronization, in particular, in the gamma frequency range, support long-lasting strengthening of synaptic weight rely on the principles of spike timing dependent plasticity (STDP) for induction of which the certain order as well as exact timing of action potential generation in a critical time frame (~10-20 ms) in pre- and postsynaptic neurons represent crucial factors [160]. Given the frequency of the gamma rhythm, it seems obvious that gamma frequency oscillations, which represent a synchronous rhythmic activity arising from strong perisomatic inhibition of local principal cells, set a narrow time window in which PCs are allowed to spike [56, 59, 161]. Thus, if activity of PCs follows the "pre-before-post" principle, network synchronization in the gamma frequency band will provide a sufficient narrow time frame as a necessary prerequisite for STDP induction. To exemplify this mechanism, one should consider that synchronously activated neurons spike during an earlier phase of the gamma cycle than "weakly activated" cells [162], which could represent common targets of "well synchronized" neurons and therefore receive an enhanced

excitatory current by temporal integration of their input arriving over a small time scale [163]. Thus, the prerequisites for the STDP-induction, including firing in a "pre-before-post" order within a specific time window, which is ensured by gamma oscillations and broadly corresponds to the half duration of the gamma cycles, are met and the synapses between these neurons are likely to undergo plastic changes, including strengthening of their weight. According to the classical view, for the STDP induction, elevation of Ca^{2+} level in the postsynaptic cell through activation of NMDA receptors is required [120, 160, 164]. NMDA receptors act as coincidence detectors for pre/post activity. They are blocked by the Mg^{2+} [165], which is relieved by the back propagating action potential (BAP)-mediated postsynaptic depolarization. However, the BAP can effectively unblock NMDA receptors and facilitate Ca^{2+} influx only if it arrives milliseconds after presynaptic input-mediated EPSC [166], which requires activity of connected neurons in the "pre-before-post" order within a critical time window of ~20ms [164, 167]. Interestingly, one recent study showed that in the hippocampal synapses of adult rats, NMDA receptor-mediated STDP cannot be induced by the single spike pairing paradigm but requires postsynaptic spikes in ~ >4Hz [168]. The administration of NMDA receptor antagonist or selective mGluR5 blocker prevented the STDP-induction. Thus, mGluR5 is thought to gate NMDA receptor-mediated STDP [168]. Importantly, several studies highlight the crucial role of mGluR5 receptors in potentiating not only NMDA receptor currents in principal cells [169, 170], but also spike-mediated long-lasting strengthening of glutamatergic synapses on interneurons [171].

In good agreement with the results on the LFP changes, bath application of MPEP prevented the increase and, in fact, resulted in a slight, albeit not significant reduction in r-EPSC area of CA3 PCs. These data provide direct evidence that at PC-PC synapses in area CA3, during gamma rhythms, a mGluR5-dependent increase in excitatory synaptic strength takes place. The network alterations described above reflect these changes in a tight temporal correlation, suggesting their causality for LTP induction.

Thus, mGluR5 appears to be a key factor for the observed long-lasting plastic alterations in the CA3 network.

Group I mGluR family comprises mGluR5 and mGluR1, which are preferentially located on the postsynaptic membrane of CA3 PC dendrites [172]. Activation of group I mGluRs increases intracellular Ca^{2+} concentration via at least two major distinct mechanisms: Ca^{2+} release from intracellular pools and potentiation of NMDA receptor currents [169, 170]. NMDA receptor carry a substantial fraction of the total synaptic charge [173] and recent studies suggest that activation of mGluR5 may modulate NMDA receptor-mediated synaptic currents [168, 174, 175]. In the hippocampus mGluR5-mediated potentiation of NMDA receptor currents has been

elegantly demonstrated at the mossy fiber-CA3 synapse [128, 176]. Consistent with these observations, our results demonstrate a fundamental role of both mGluR5 and NMDA receptors in LTP induction, since the joint blockade of these receptors abolished LTP.

Interestingly, mGluR5 activation-mediated potentiation of NMDA component of EPSC has been reported in numerous cellular studies of different brain regions [177, 178, 179, 180], and is suggested to be crucial for long-term plasticity and learning [181]. Furthermore, alterations in mGluR5-mediated regulation of NMDA receptor function may underly cognitive deficits in schizophrenia. Indeed, the blockade of mGluR5 by selective antagonist MPEP resulted in deterioration of cognitive impairment in an animal model of phencyclidine-induced NMDA hypofunction-mediated schizophrenia [182]. Conversely, mGluR5-mediated potentiation of NMDA receptor current could ameliorate the symptoms of schizophrenia, making mGluR5 a novel target to increase NMDA receptor function in the treatment of schizophrenia [183]. In addition to schizophrenia, mGluR5-mediated transmission has been reported to play an important role in autistic spectrum disorder such as tuberous sclerosis. Humans with this disorder often have associated symptoms including epilepsy and mental disability. Treatment with an mGluR5- positive allosteric modulator led to improvement of cognitive function in an animal model of this disease [184]. Furthermore, in line with our finding, impairments of both LTP and spatial learning as well as place field encoding of novel environments induced by mGluR5 antagonists have been reported [185, 186]. Thus, our results further highlight mGluR5 in the general context of memory processing and neuronal plasticity.

In contrast to the postsynaptically-mediated potentiation of PC excitatory currents, inhibitory currents changed only to a miner degree and these alterations were independent of postsynaptic activation. To clarify underlying cellular mechanisms, we aimed to investigate SWR-associated synaptic properties of two major interneuron classes: CCK+ regular-spiking BC and PV+ fast-spiking interneurons comprising BCs and BSCs. These interneurons demonstrated distinct LFP-associated firing patterns, suggesting their unequal contributions to LFP generation and attracted therefore our particular attention. Thus, we examined their specific roles in the changed network excitability after gamma frequency synchronization of neuronal activity.

Due to the lack of dendritic spines and Ca^{2+}/calmodulin-dependent protein kinase II (CaMKII) alpha, which are essential for synaptic plasticity in PCs, excitatory synapses on interneurons were previously believed not to be able to undergo plastic changes in their strength [187, 188]. However, more recent studies demonstrated that, firstly, dendrites of many interneurons are not completely devoid of spines and, secondly, the existence of spines is not of decisive importance for synaptic plasticity. Furthermore, the absence of CaMKII alpha does not exclude the existence

of an alternative, closely related kinase or alternative biochemical cascade [138]. Currently, compelling evidence suggests that excitatory synapses on interneurons can undergo plastic changes and that there are various underlying mechanisms for different forms of their plasticity [171]. Several studies suggest, for instance, a Hebbian induction rule for LTP in glutamatergic synapses on hippocampal interneurons requiring presynaptic spiking during postsynaptic depolarization [189]. However, the induction protocols used in these studies are hardly comparable with physiological activity patterns of neurons. Furthermore, in different studies the pre- and postsynaptic activities are controlled through experimentations in various ways. The presynaptic stimulation, for instance, varies from low frequency to 'theta-bust' up to high frequency tetanisation, whereas the activity of postsynaptic cells is differentially controlled as well, allowing them to depolarize as a result of presynaptic spiking or generate action potentials by depolarization via recording pipette.

We took advantage of using gamma rhythm as a tool for LTP induction, since it represents a close approximation to physiological network activity during exploration *in vivo* [36], and examined long-lasting changes in SWR-associated EPSC and IPSC in interneurons initiated by gamma rhythm. We observed divergent forms of synaptic plasticity in these two interneuron types induced by gamma frequency synchronization of the network activity. PV+ fast-spiking interneurons demonstrated a significant increase in EPSC after gamma oscillations along with a slight albeit not significant reduction of IPSC. However, CCK+ regular-spiking interneurons did not show changes in their EPSC after gamma rhythm, but they demonstrated a significantly enhanced inhibitory synaptic strength. The EPSC/IPSC ratio as the physiological correlate of neuronal excitability demonstrated contra-directional changes in these two major interneuron classes. Whereas PV+ fast-spiking interneurons showed synaptic current changes in favor of excitation, CCK+ regular-spiking BCs exhibited a reinforced inhibition after gamma frequency oscillations. Thus, enhanced excitability of PV+ fast-spiking but not CCK+ regular-spiking interneurons may account for reinforced IPSC in PC.

Although the mechanisms of interneuron plasticity have not been fully explained in a consistent way so far, emerging evidence suggests some cell type-specific differences in its induction and expression rules.

Whereas NMDA receptors are widely recognized to have a pivotal role in plasticity of PC excitatory synapses, they appear to play a minor part in glutamatergic synapses on interneurons. Indeed, only a small population of hippocampal interneurons have been reported to show NMDA receptor dependent plasticity on their excitatory synapses [135, 190]. This form of LTP has been

induced, for instance, at the Schaffer collateral synapses on a subset of interneurons in stratum radiatum by delivering low frequency presynaptic stimulation synchronously with postsynaptic depolarizing steps or continuous depolarization allowing postsynaptic spiking by presynaptic stimuli. Although the "pre-before-post-spiking" order has not been tested explicitly, a postsynaptic insertion of AMPA receptors has been proposed to account for this phenomenon, suggesting induction and expression rules of NMDA dependent plasticity, which have been reported in PCs [189, 190]. Interestingly, one recent study reports input-specific induction rules of synaptic plasticity at excitatory synapses on PV+ interneurons made by FF vs. FB inputs [135]. The authors suggest the existence of a Hebbian form of plasticity, which implies correlated spiking in "pre-before-post" order within a critical time window, only at FB but not FF synapses on PV+ interneurons. This form of plasticity was abolished by application of NMDA receptor antagonist AP5 and not associated with significant changes in PPR pointing to a decisive role of NMDA receptors for its induction and postsynaptic modifications for its expression. A straightforward explanation for the input specificity of NMDA receptor dependent Hebbian plasticity at excitatory synapses on PV+ interneurons would be an unequal distribution of these receptors between different inputs [135].

NMDA-independent LTP includes activation of either CP-AMPA receptors or group I mGluRs and have been demonstrated in various interneuron types [131].

The induction and expression rules of CP-AMPA receptor-mediated LTP display essential differences from those of NMDA-receptor dependent LTP. The particular features of these receptors, including polyamine block at depolarized membrane potentials, determine its inwardly rectifying character and require prevention of postsynaptic spiking by holding the cell either at the resting membrane potential or more hyperpolarized in order to avoid depolarization dependent inhibition of Ca^{2+} influx in the postsynaptic cell [131, 138]. Since the induction requirement of CP-AMPA receptor-mediated LTP differ diametrically from conventional Hebbian rules implying postsynaptic spiking while presynaptic stimulations, this form of LTP have been referred to as „anti-Hebbian" LTP [131].

Growing evidence has demonstrated LTP at excitatory synapses on GABAergic interneurons the induction of which has been convincingly shown to depend on activation of group I mGluRs comprising mGluR1 and mGluR5 subtypes. Several channels and intracellular messenger pathways have been proposed to account for mGluR activity dependent elevation of intracellular Ca^{2+} including AMPA receptors, transient receptor potential (TRP) channels, voltage gated Ca^{2+} channels as well as intracellular calcium stores [174]. Pharmacologically induced mGluR

dependent LTP has been reported to occur by activation either mGluR5 or mGluR1 [191]. For instance, whereas mossy fiber stratum lacunosum moleculare interneuron synapses in CA3 show mGluR1 dependent LTP, mGluR5 dependent LTP has been shown to exist at excitatory synapses in fast-spiking interneurons in the neocortex [192, 193].

Although Ca^{2+} influx in the postsynaptic cell is obviously required for mGluR-mediated LTP, the source of Ca^{2+} seems to differ depending on the cell type. Whereas L-type Ca^{2+} and TRP channels have been reported to be necessary for LTP at synapses on CA3 stratum lacunosum moleculare and CA1 oriens/alveus interneurons, respectively [142, 192], Ca^{2+} release from intracellular stores appears to be essential for LTP in neocortical fast-spiking interneurons [193].

In order to induce NMDA receptor- or mGluR-mediated STDP at excitatory synapses on GABAergic interneurons, following requirements have to be met: spiking in "pre-before-post" order within a critical time window of ~20ms as well as correlated firing at a sufficiently high frequency, which may ensure dendritic depolarization and support back propagating spikes to reach distal dendrites (boosting of back propagation of spikes) [115, 122].

During gamma oscillations, which provide a high frequency natural stimulation and set an optimal time window required for STDP, only interneurons appear to undergo LTP at their excitatory synapses, which fire at a high frequency and ensure thereby a high rate coincident firing of pre- and postsynaptic cells within this critical time window. As demonstrated in our results, PV+ fast-spiking interneurons and CCK+ BCs exhibit substantial differences with respect to their firing patterns during gamma frequency oscillations. Whereas PV+ fast-spiking interneurons discharge in a strong phase-correlated manner almost at every gamma cycle, CCK+ BCs show a different phase coupling with preferential firing at the beginning of gamma cycles. However, ~50% of these rhythmic oscillatory events are not associated with CCK-BC spikes.

Due to their strongly gamma-associated firing properties, PV+ fast-spiking interneurons appear to be ideally suited for induction of gamma-mediated STDP at their excitatory synapses. In contrast, CCK+ BCs do not satisfy the STDP requirements, as they demonstrate a low frequency gamma-associated firing, which considerably reduces coincidence probability of correlated "pre-before-post" activity at PC/IN synapses within a few milliseconds essential for STDP.

In summary, network oscillations in the gamma frequency range induce postsynaptic mGluR5-mediated LTP of SWR-associated EPSC in PCs, whereas a moderate increase in SWR-associated IPSC appears to be mediated by contra-directional modifications in excitability of two major interneuron classes: CCK+ regular-spiking BC and PV+ fast-spiking interneurons.

Abbreviations

A/C	Associational-commissural
AAC	Axo-axonic cells
AMPA	α-amino-3-hydroxy-5-methyl-4-isoxazolepropionic acid
BC	Basket cells
BSC	Bistratified cells
CA	Cornu ammonis
CB1R	Cannabinoid receptor type 1
CCh	Carbachol
CCK+ BCs	Cholecystokinin-positive basket cells
CP-AMPA	Ca^{2+} permeable AMPA
DG	Dentate gyrus
EC	Entorhinal cortex
EPSC	Excitatory postsynaptic currents
FB	Feedback
FF	Feedforward
HF	Hippocampal formation
HP	Hippocampus proper
IPSC	Inhibitory postsynaptic currents
ISI	Interneurons specific interneurons
KA	Kainate
LEC (A)	Lateral entorhinal cortex (area)
r-EPSC	Reappeared excitatory postsynaptic currents
r-IPSC	Reappeared inhibitory postsynaptic currents

MEC (A)	Medial entorhinal cortex (area)
LTP	Long-term potentiation
mGluR	Metabotropic glutamatergic receptor
mTLE	Mesial temporal lobe epilepsy
NMDA	N-methyl-D-aspartate
O-LM	Oriens-lacunosum moleculare
PaS	Parasubiculum
PC	Pyramidal cell
PER	Perirhinal cortex
PHR	Parahippocampal region
POR	Postrhinal cortex
PP	Perforant path
PPR	Paired pulse ratio
PrS	Presubiculum
PV+ BCs	Parvalbumin-positive basket cells
r-SWR	Reappeared sharp-wave ripples
STD	Short-term depression
STP	Short-term potentiation
SUB	Subiculum
SWR	Sharp-wave ripples

References

1 Lorente de Nó. Studies on the structure of the cerebral cortex II: continuation of the study of the ammonic system. J Physiol Neurol 1934;46:113-77

2 Johnston D, Amaral, DG. The synaptic Organization of the Brain. Shepherd, G.M. (ed.), Oxford University Press: 1997.

3 Van Strien NM, Cappaert NL, Witter MP. The anatomy of memory: an interactive overview of the parahippocampal-hippocampal network. Nat Rev Neurosci. 2009;10:272-82.

4 Amaral DG, Scharfman HE, Lavenex P. The dentate gyrus: fundamental neuroanatomical organization (dentate gyrus for dummies). Prog Brain Res. 2007;163:3-22.

5 O'Mara SM, Commins S, Anderson M, Gigg J. The subiculum: a review of form, physiology and function. Prog Neurobiol. 2001;64:129-55.

6 Canto CB, Wouterlood FG, Witter MP. What does the anatomical organization of the entorhinal cortex tell us? Neural Plast. 2008;2008:381243.

7 Naber PA, Lopes da Silva FH, Witter MP. Reciprocal connections between the entorhinal cortex and hippocampal fields CA1 and the subiculum are in register with the projections from CA1 to the subiculum. Hippocampus. 2001;11:99-104.

8 Wittner L, Henze DA, Záborszky L, Buzsáki G. Three-dimensional reconstruction of the axon arbor of a CA3 pyramidal cell recorded and filled in vivo. Brain Struct Funct. 2007;212:75-83.

9 Myers CE, Scharfman HE. Pattern separation in the dentate gyrus: a role for the CA3 backprojection. Hippocampus. 2011;21:1190-215.

10 Cenquizca LA, Swanson LW. Spatial organization of direct hippocampal field CA1 axonal projections to the rest of the cerebral cortex. Brain Res Rev. 2007;56:1-26.

11 Swanson LW, Köhler C. Anatomical evidence for direct projections from the entorhinal area to the entire cortical mantle in the rat. J Neurosci. 1986;6:3010-23.

12 Kerr KM, Agster KL, Furtak SC, Burwell RD. Functional neuroanatomy of the parahippocampal region: the lateral and medial entorhinal areas. Hippocampus. 2007;17:697-708.

13 Steward O. Topographic organization of the projections from the entorhinal area to the hippocampal formation of the rat. J Comp Neurol. 1976;167:285-314.

14 Witter MP, Wouterlood FG, Naber PA, Van Haeften T. Anatomical organization of the parahippocampal-hippocampal network. Ann N Y Acad Sci. 2000;911:1-24.

15 Kajiwara R, Wouterlood FG, Sah A, Boekel AJ, Baks-te Bulte LT, Witter MP. Convergence of entorhinal and CA3 inputs onto pyramidal neurons and interneurons in hippocampal area CA1--an anatomical study in the rat. Hippocampus. 2008;18:266-80.

16 Gloveli TB. Effects of excluding reticuloseptal input on hippocampal electrical activity in the cat. Fiziol Zh SSSR Im I M Sechenova. 1985;71:80-6.

17 Furtak SC, Wei SM, Agster KL, Burwell RD. Functional neuroanatomy of the parahippocampal region in the rat: the perirhinal and postrhinal cortices. Hippocampus. 2007;17:709-22.

18 Swanson LW, Wyss JM, Cowan WM. An autoradiographic study of the organization of intrahippocampal association pathways in the rat. J Comp Neurol. 1978;181:681-715.

19 Tamamaki N, Nojyo Y. Preservation of topography in the connections between the subiculum, field CA1, and the entorhinal cortex in rats. J Comp Neurol. 1995;353:379-90.

20 Claiborne BJ, Amaral DG, Cowan WM. A light and electron microscopic analysis of the mossy fibers of the rat dentate gyrus. J Comp Neurol. 1986;246:435-58.

21 Freund TF, Buzsáki G. Interneurons of the hippocampus. Hippocampus. 1996;6:347-470.

22 Amaral DG. A Golgi study of cell types in the hilar region of the hippocampus in the rat. J Comp Neurol. 1978;182:851-914.

23 Buckmaster PS, Wenzel HJ, Kunkel DD, Schwartzkroin PA. Axon arbors and synaptic connections of hippocampal mossy cells in the rat in vivo. J Comp Neurol.1996;366:271-92.

24 Ramon Y Cajal S. Histologie du Systeme Nerveux de l'Homme et des Vertebres. 1911; Paris: Maloine.

25 Gulyás AI[1], Tóth K, McBain CJ, Freund TF. Stratum radiatum giant cells: a type of principal cell in the rat hippocampus. Eur J Neurosci. 1998;10:3813-22.

26 Blackstad TW, Kjaerheim A. Special axo-dendritic synapses in the hippocampal cortex: electron and light microscopic studies on the layer of mossy fibers. J Comp Neurol. 1961;117:133-59.

27 Amaral DG, Witter MP. The three-dimensional organization of the hippocampal formation: a review of anatomical data. Neuroscience. 1989;31:571-91.

28 Li XG, Somogyi P, Ylinen A, Buzsáki G. The hippocampal CA3 network: an in vivo intracellular labeling study. J Comp Neurol. 1994;339(2):181-208.

29 Scharfman HE. The CA3 "backprojection" to the dentate gyrus. Prog Brain Res. 2007;163:627-37.

30 Bannister NJ, Larkman AU. Dendritic morphology of CA1 pyramidal neurones from the rat hippocampus: I. Branching patterns. J Comp Neurol. 1995;360:150-60.

31 Deuchars J, Thomson AM. CA1 pyramid-pyramid connections in rat hippocampus in vitro: dual intracellular recordings with biocytin filling. Neuroscience. 1996;74:1009-18.

32 Soussi R[1], Zhang N, Tahtakran S, Houser CR, Esclapez M. Heterogeneity of the supramammillary-hippocampal pathways: evidence for a unique GABAergic neurotransmitter phenotype and regional differences. Eur J Neurosci. 2010;32:771-85.

33 Halasy K, Hajszan T, Kovács EG, Lam TT, Leranth C. Distribution and origin of vesicular glutamate transporter 2-immunoreactive fibers in the rat hippocampus. Hippocampus. 2004;14:908-18.

34 Jones MW, McHugh TJ. Updating hippocampal representations: CA2 joins the circuit. Trends Neurosci. 2011;34(10):526-35.

35 Maccaferri G, Lacaille JC. Interneuron Diversity series: Hippocampal interneuron classifications--making things as simple as possible, not simpler. Trends Neurosci. 2003;26:564-71.

36 Whittington MA, Traub RD. Interneuron diversity series: inhibitory interneurons and network oscillations in vitro. Trends Neurosci. 2003;26:676-82.

37 Klausberger T, Somogyi P. Neuronal diversity and temporal dynamics: the unity of hippocampal circuit operations. Science. 2008;321:53-7.

38 Buhl EH, Han ZS, Lörinczi Z, Stezhka VV, Karnup SV, Somogyi P. Physiological properties of anatomically identified axo-axonic cells in the rat hippocampus. J Neurophysiol.1994;71:1289-307.

39 Gloveli T. Hippocampal spatial navigation: interneurons take responsibility. J Physiol. 2010;588:4609-10.

40 Kosaka T, Katsumaru H, Hama K, Wu JY, Heizmann CW. GABAergic neurons containing the Ca^{2+}-binding protein parvalbumin in the rat hippocampus and dentate gyrus. Brain Res. 1987;419:119-30

41 Freund TF. Interneuron Diversity series: Rhythm and mood in perisomatic inhibition. Trends Neurosci. 2003;26:489-95.

42 Buhl EH, Szilágyi T, Halasy K, Somogyi P. Physiological properties of anatomically identified basket and bistratified cells in the CA1 area of the rat hippocampus in vitro. Hippocampus. 1996;6:294-305.

43 Halasy K, Buhl EH, Lörinczi Z, Tamás G, Somogyi P. Synaptic target selectivity and input of GABAergic basket and bistratified interneurons in the CA1 area of the rat hippocampus. Hippocampus. 1996;6:306-29.

44 Pawelzik H, Hughes DI, Thomson AM. Physiological and morphological diversity of immunocytochemically defined parvalbumin- and cholecystokinin-positive interneurones in CA1 of the adult rat hippocampus. J Comp Neurol. 2002;443:346-67.

45 Maccaferri G, Roberts JD, Szucs P, Cottingham CA, Somogyi P. Cell surface domain specific postsynaptic currents evoked by identified GABAergic neurones in rat hippocampus in vitro. J Physiol. 2000;524:91-116. Erratum in: J Physiol 2000;528(Pt 3):669.

46 Armstrong C, Soltesz I. Basket cell dichotomy in microcircuit function. J Physiol. 2012;590:683-94.

47 Ganter P, Szücs P, Paulsen O, Somogyi P. Properties of horizontal axo-axonic cells in stratum oriens of the hippocampal CA1 area of rats in vitro. Hippocampus. 2004;14:232-43.

48 Buhl EH, Han ZS, Lörinczi Z, Stezhka VV, Karnup SV, Somogyi P. J Neurophysiol. Physiological properties of anatomically identified axo-axonic cells in the rat hippocampus. 1994;71:1289-307.

49 Klausberger T, Magill PJ, Márton LF, Roberts JD, Cobden PM, Buzsáki G, Somogyi P. Brain-state- and cell-type-specific firing of hippocampal interneurons in vivo. Nature. 2003;421:844-8. Erratum in: Nature. 2006;441:902.

50 Li XG, Somogyi P, Tepper JM, Buzsáki G. Axonal and dendritic arborization of an intracellularly labeled chandelier cell in the CA1 region of rat hippocampus. Exp Brain Res. 1992;90:519-25.

51 Fukuda T, Kosaka T. Gap junctions linking the dendritic network of GABAergic interneurons in the hippocampus. J Neurosci. 2000;20:1519-28.

52 Baude A, Bleasdale C, Dalezios Y, Somogyi P, Klausberger T. Immunoreactivity for the GABAA receptor alpha1 subunit, somatostatin and Connexin36 distinguishes axoaxonic, basket, and bistratified interneurons of the rat hippocampus. Cereb Cortex. 2007 Sep;17(9):2094-107. Epub 2006 Nov 22.

53 Katsumaru H, Kosaka T, Heizmann CW, Hama K. Immunocytochemical study of GABAergic neurons containing the calcium-binding protein parvalbumin in the rat hippocampus. Exp Brain Res. 1988;72:347-62.

54 Klausberger T, Márton LF, Baude A, Roberts JD, Magill PJ, Somogyi P. Spike timing of dendrite-targeting bistratified cells during hippocampal network oscillations in vivo. Nat Neurosci. 2004(1):41-7. Erratum in: Nat Neurosci. 2006:979.

55 Ferraguti F, Klausberger T, Cobden P, Baude A, Roberts JD, Szucs P, Kinoshita A, Shigemoto R, Somogyi P, Dalezios Y. Metabotropic glutamate receptor 8-expressing nerve terminals target subsets of GABAergic neurons in the hippocampus. J Neurosci. 2005;25:10520-36.

56 Gloveli T, Dugladze T, Saha S, Monyer H, Heinemann U, Traub RD, Whittington MA, Buhl EH. Differential involvement of oriens/pyramidale interneurones in hippocampal network oscillations in vitro. J Physiol. 2005;562:131-47.

57 Hájos N, Papp EC, Acsády L, Levey AI, Freund TF. Distinct interneuron types express m2 muscarinic receptor immunoreactivity on their dendrites or axon terminals in the hippocampus. Neuroscience. 1998;82:355-76.

58 Martina M, Vida I, Jonas P. Distal initiation and active propagation of action potentials in interneuron dendrites. Science. 2000;287:295-300.

59 Gloveli T, Dugladze T, Rotstein HG, Traub RD, Monyer H, Heinemann U, Whittington MA, Kopell NJ. Orthogonal arrangement of rhythm-generating microcircuits in the hippocampus. Proc Natl Acad Sci U S A. 2005;102:13295-300.

60 Blasco-Ibáñez JM[1], Freund TF. Synaptic input of horizontal interneurons in stratum oriens of the hippocampal CA1 subfield: structural basis of feed-back activation. Eur J Neurosci. 1995;7:2170-80.

61 Elfant D, Pál BZ, Emptage N, Capogna M. Specific inhibitory synapses shift the balance from feedforward to feedback inhibition of hippocampal CA1 pyramidal cells. Eur J Neurosci. 2008;27:104-13.

62 Ferraguti F, Cobden P, Pollard M, Cope D, Shigemoto R, Watanabe M, Somogyi P. Immunolocalization of metabotropic glutamate receptor 1alpha (mGluR1alpha) in distinct classes of interneuron in the CA1 region of the rat hippocampus. Hippocampus. 2004;14:193-215.

63 Buzsáki G, Draguhn A. Neuronal oscillations in cortical networks. Science. 2004;304:1926-9.

64 Somogyi P, Klausberger T. Defined types of cortical interneurone structure space and spike timing in the hippocampus. J Physiol. 2005;562:9-26.

65 Leung LW, Lopes da Silva FH, Wadman WJ. Spectral characteristics of the hippocampal EEG in the freely moving rat. Electroencephalogr Clin Neurophysiol. 1982;54:203-19.

66 Bragin A, Jandó G, Nádasdy Z, Hetke J, Wise K, Buzsáki G. Gamma (40-100 Hz) oscillation in the hippocampus of the behaving rat. J Neurosci. 1995;15:47-60.

67 Chrobak JJ, Buzsáki G. Operational dynamics in the hippocampal-entorhinal axis. Neurosci Biobehav Rev. 1998;22:303-10.

68 Vanderwolf CH. Hippocampal electrical activity and voluntary movement in the rat. Electroencephalogr Clin Neurophysiol. 1969;26:407-18.

69 Buzsáki G, Leung LW, Vanderwolf CH. Cellular bases of hippocampal EEG in the behaving rat. Brain Res. 1983;287:139-71.

70 Csicsvari J, Hirase H, Czurkó A, Mamiya A, Buzsáki G. Oscillatory coupling of hippocampal pyramidal cells and interneurons in the behaving Rat. J Neurosci. 1999;19:274-87.

71 Buhl EH, Tamás G, Fisahn A. Cholinergic activation and tonic excitation induce persistent gamma oscillations in mouse somatosensory cortex in vitro. J Physiol. 1998;513:117-26

72 Maier N, Nimmrich V, Draguhn A. Cellular and network mechanisms underlying spontaneous sharp wave-ripple complexes in mouse hippocampal slices. J Physiol. 2003;550:873-87.

73 Hájos N, Pálhalmi J, Mann EO, Németh B, Paulsen O, Freund TF. Spike timing of distinct types of GABAergic interneuron during hippocampal gamma oscillations in vitro. J Neurosci. 2004;24:9127-37.

74 Dodt HU, Zieglgänsberger W. Infrared videomicroscopy: a new look at neuronal structure and function. Trends Neurosci. 1994;17:453-8.

75 Klausberger T, Márton LF, Baude A, Roberts JD, Magill PJ, Somogyi P. Spike timing of dendrite-targeting bistratified cells during hippocampal network oscillations in vivo. Nat Neurosci. 2004;7:41-7. Erratum in: Nat Neurosci. 2006;9:979.

76 Csicsvari J, Jamieson B, Wise KD, Buzsáki G. Mechanisms of gamma oscillations in the hippocampus of the behaving rat. Neuron. 2003;37:311-22.

77 Whittington MA, Stanford IM, Colling SB, Jefferys JG, Traub RD. Spatiotemporal patterns of gamma frequency oscillations tetanically induced in the rat hippocampal slice. J Physiol. 1997;502:591-607.

78 Towers SK, LeBeau FE, Gloveli T, Traub RD, Whittington MA, Buhl EH. Fast network oscillations in the rat dentate gyrus in vitro. J Neurophysiol. 2002;87:1165-8.

79 Pöschel B, Draguhn A, Heinemann U. Glutamate-induced gamma oscillations in the dentate gyrus of rat hippocampal slices. Brain Res. 2002;938:22-8.

80 Fellous JM, Sejnowski TJ. Cholinergic induction of oscillations in the hippocampal slice in the slow (0.5-2 Hz), theta (5-12 Hz), and gamma (35-70 Hz) bands. Hippocampus. 2000;10:187-97.

81 Fisahn A. Kainate receptors and rhythmic activity in neuronal networks: hippocampal gamma oscillations as a tool. J Physiol. 2005;562:65-72.

82 Mann EO, Radcliffe CA, Paulsen O Hippocampal gamma-frequency oscillations: from interneurones to pyramidal cells, and back. J Physiol. 2005;562:55-63.

83 Wang XJ[1], Buzsáki G. Gamma oscillation by synaptic inhibition in a hippocampal interneuronal network model. J Neurosci. 1996;16:6402-13.

84 Vida I, Bartos M, Jonas P. Shunting inhibition improves robustness of gamma oscillations in hippocampal interneuron networks by homogenizing firing rates. Neuron. 2006;49:107-17

85 Debanne D, Campanac E, Bialowas A, Carlier E, Alcaraz G. Axon physiology. Physiol Rev. 2011;91:555-602.

86 Dugladze T, Schmitz D, Whittington MA, Vida I, Gloveli T. Segregation of axonal and somatic activity during fast network oscillations. Science. 2012;336:1458-61.

87 Sohal VS, Zhang F, Yizhar O, Deisseroth K. Parvalbumin neurons and gamma rhythms enhance cortical circuit performance. Nature. 2009;459:698-702.

88 Tukker JJ, Fuentealba P, Hartwich K, Somogyi P, Klausberger T. Cell type-specific tuning of hippocampal interneuron firing during gamma oscillations in vivo. J Neurosci. 2007;27:8184-9.

89 Freund TF, Katona I. Perisomatic inhibition. Neuron. 2007;56:33-42.

90 Glickfeld LL, Scanziani M. Distinct timing in the activity of cannabinoid-sensitive and cannabinoid-insensitive basket cells. Nat Neurosci. 2006;9:807-15.

91 Mátyás F, Freund TF, Gulyás AI. Convergence of excitatory and inhibitory inputs onto CCK-containing basket cells in the CA1 area of the rat hippocampus. Eur J Neurosci. 2004;19:1243-56.

92 Hájos N, Katona I, Naiem SS, MacKie K, Ledent C, Mody I, Freund TF. Cannabinoids inhibit hippocampal GABAergic transmission and network oscillations. Eur J Neurosci. 2000;12:3239-49.

93 Robbe D, Montgomery SM, Thome A, Rueda-Orozco PE, McNaughton BL, Buzsaki G. Cannabinoids reveal importance of spike timing coordination in hippocampal function. Nat Neurosci. 2006;9:1526-33.

94 Jouvet M. Biogenic amines and the states of sleep. Science. 1969;163:32-41.

95 Petsche H, Stumpf C, Gogolak G. The significance of the rabbit's septum as a relay station between the midbrain and the hippocampus. I. The control of hippocampus arousal activity by the septum cells. Electroencephalogr Clin Neurophysiol. 1962 ;14:202-11

96 Buzsáki G. Theta oscillations in the hippocampus. Neuron. 2002;33:325-40.

97 Pignatelli M, Beyeler A, Leinekugel X. Neural circuits underlying the generation of theta oscillations. J Physiol. 2012;106:81-92.

98 Rotstein HG, Pervouchine DD, Acker CD, Gillies MJ, White JA, Buhl EH, Whittington MA, Kopell N. Slow and fast inhibition and an H-current interact to create a theta rhythm in a model of CA1 interneuron network. J Neurophysiol. 2005;94:1509-18..

99 Mizuseki K, Diba K, Pastalkova E, Buzsáki G. Hippocampal CA1 pyramidal cells form functionally distinct sublayers. Nat Neurosci. 2011;14:1174-81.

100 Dragoi G, Buzsáki G. Temporal encoding of place sequences by hippocampal cell assemblies. Neuron. 2006;50:145-57.

101 Maccaferri G, McBain CJ. The hyperpolarization-activated current (Ih) and its contribution to pacemaker activity in rat CA1 hippocampal stratum oriens-alveus interneurones. J Physiol. 1996;497:119-30.

102 Savić N, Pedarzani P, Sciancalepore M. Medium afterhyperpolarization and firing pattern modulation in interneurons of stratum radiatum in the CA3 hippocampal region. J Neurophysiol. 2001;85:1986-97.

103 Buzsáki G. Two-stage model of memory trace formation: a role for "noisy" brain states. Neuroscience. 1989;31:551-70.

104 Miles R, Wong RK. Excitatory synaptic interactions between CA3 neurones in the guinea-pig hippocampus. J Physiol. 1986;373:397-418.

105 Traub RD, Whittington MA, Buhl EH, LeBeau FE, Bibbig A, Boyd S, Cross H, Baldeweg T. A possible role for gap junctions in generation of very fast EEG oscillations preceding the onset of, and perhaps initiating, seizures. Epilepsia. 2001;42:153-70.

106 Draguhn A, Traub RD, Schmitz D, Jefferys JG. Electrical coupling underlies high-frequency oscillations in the hippocampus in vitro. Nature. 1998;394:189-92.

107 Papatheodoropoulos C, Kostopoulos G. Spontaneous GABA(A)-dependent synchronous periodic activity in adult rat ventral hippocampal slices. Neurosci Lett. 2002;319:17-20.

108 Hájos N, Karlócai MR, Németh B, Ulbert I, Monyer H, Szabó G, Erdélyi F, Freund TF, Gulyás AI. Input-output features of anatomically identified CA3 neurons during hippocampal sharp wave/ripple oscillation in vitro. J Neurosci. 2013;33:11677-91.

109 Schlingloff D, Káli S, Freund TF, Hájos N, Gulyás AI. Mechanisms of sharp wave initiation and ripple generation. J Neurosci. 2014;34:11385-98.

110 Ylinen A, Bragin A, Nádasdy Z, Jandó G, Szabó I, Sik A, Buzsáki G. Sharp wave-associated high-frequency oscillation (200 Hz) in the intact hippocampus: network and intracellular mechanisms. J Neurosci. 1995;15:30-46.

111 Hebb, D; 1949, the organisation of the behavior: New York: Wiley

112 Bienenstock EL, Cooper LN, Munro PW. Theory for the development of neuron selectivity: orientation specificity and binocular interaction in visual cortex. J Neurosci. 1982 ;2:32-48.

113 Zucker RS, Regehr WG. Short-term synaptic plasticity. Annu Rev Physiol. 2002;64:355-405.

114 Salin PA, Scanziani M, Malenka RC, Nicoll RA. Distinct short-term plasticity at two excitatory synapses in the hippocampus. Proc Natl Acad Sci U S A. 1996;93:13304-9.

115 Sjöström PJ, Nelson SB. Spike timing, calcium signals and synaptic plasticity. Curr Opin Neurobiol. 2002;12:305-14.

116 Jonas P, Major G, Sakmann B. Quantal components of unitary EPSCs at the mossy fibre synapse on CA3 pyramidal cells of rat hippocampus. J Physiol. 1993;472:615-63.

117 Reid CA, Fabian-Fine R, Fine A. Postsynaptic calcium transients evoked by activation of individual hippocampal mossy fiber synapses. J Neurosci. 2001;21:2206-14.

118 Nevian T, Sakmann B. Spine Ca^{2+} signaling in spike-timing-dependent plasticity. J Neurosci. 2006;26:11001-13.

119 Astori S, Pawlak V, Köhr G. Spike-timing-dependent plasticity in hippocampal CA3 neurons. J Physiol. 2010;588:4475-88.

120 Debanne D, Gähwiler BH, Thompson SM. Long-term synaptic plasticity between pairs of individual CA3 pyramidal cells in rat hippocampal slice cultures. J Physiol. 1998;507:237-47.

121 McNaughton BL, Battaglia FP, Jensen O, Moser EI, Moser MB. Path integration and the neural basis of the 'cognitive map'. Nat Rev Neurosci. 2006;7:663-78.

122 Sjöström PJ, Turrigiano GG, Nelson SB. Rate, timing, and cooperativity jointly determine cortical synaptic plasticity. Neuron. 2001;32:1149-64.

123 Cormier RJ, Greenwood AC, Connor JA. Bidirectional synaptic plasticity correlated with the magnitude of dendritic calcium transients above a threshold. J Neurophysiol. 2001;85:399-406.

124 Malenka RC, Bear MF. LTP and LTD: an embarrassment of riches. Neuron. 2004;44:5-21.

125 Nicoll RA, Schmitz D. Synaptic plasticity at hippocampal mossy fibre synapses. Nat Rev Neurosci. 2005;6:863-76.

126 McMahon DB, Barrionuevo G. Short- and long-term plasticity of the perforant path synapse in hippocampal area CA3. J Neurophysiol. 2002;88:528-33.

127 Urban NN, Barrionuevo G. Induction of hebbian and non-hebbian mossy fiber long-term potentiation by distinct patterns of high-frequency stimulation. J Neurosci. 1996;16:4293-9.

128 Rebola N, Carta M, Lanore F, Blanchet C, Mulle C. NMDA receptor-dependent metaplasticity at hippocampal mossy fiber synapses. Nat Neurosci. 2011;14:691-3.

129 Kobayashi K, Poo MM. Spike train timing-dependent associative modification of hippocampal CA3 recurrent synapses by mossy fibers. Neuron. 2004;41:445-54.

130 Nakazawa K, Quirk MC, Chitwood RA, Watanabe M, Yeckel MF, Sun LD, Kato A, Carr CA, Johnston D, Wilson MA, Tonegawa S. Requirement for hippocampal CA3 NMDA receptors in associative memory recall. Science. 2002;297:211-8.

131 Kullmann DM, Lamsa KP. Long-term synaptic plasticity in hippocampal interneurons. Nat Rev Neurosci. 2007;8:687-99.

132 Bartos M, Elgueta C. Functional characteristics of parvalbumin- and cholecystokinin-expressing basket cells. J Physiol. 2012;590:669-81.

133 Lamsa KP, Heeroma JH, Somogyi P, Rusakov DA, Kullmann DM. Anti-Hebbian long-term potentiation in the hippocampal feedback inhibitory circuit. Science. 2007;315:1262-6.

134 Lei S, McBain CJ. Distinct NMDA receptors provide differential modes of transmission at mossy fiber-interneuron synapses. Neuron. 2002;33:921-33.

135 Le Roux N, Cabezas C, Böhm UL, Poncer JC.Input-specific learning rules at excitatory synapses onto hippocampal parvalbumin-expressing interneurons. J Physiol. 2013;591:1809-22.

136 Oren I, Nissen W, Kullmann DM, Somogyi P, Lamsa KP. Role of ionotropic glutamate receptors in long-term potentiation in rat hippocampal CA1 oriens-lacunosum moleculare interneurons. J Neurosci. 2009;29:939-50.

137 Nissen W, Szabo A, Somogyi J, Somogyi P, Lamsa KP. Cell type-specific long-term plasticity at glutamatergic synapses onto hippocampal interneurons expressing either parvalbumin or CB1 cannabinoid receptor. J Neurosci. 2010 Jan;30:1337-47.

138 Kullmann DM, Moreau AW, Bakiri Y, Nicholson E. Plasticity of inhibition. Neuron. 2012;75:951-62.

139 Perez Y, Morin F, Lacaille JC. A hebbian form of long-term potentiation dependent on mGluR1a in hippocampal inhibitory interneurons. Proc Natl Acad Sci U S A. 2001;98:9401-6.

140 Woodhall G, Gee CE, Robitaille R, Lacaille JC. Membrane potential and intracellular Ca^{2+} oscillations activated by mGluRs in hippocampal stratum oriens/alveus interneurons. J Neurophysiol. 1999;81:371-82.

141 Ouardouz M, Lacaille JC. Mechanisms of selective long-term potentiation of excitatory synapses in stratum oriens/alveus interneurons of rat hippocampal slices. J Neurophysiol. 1995;73:810-9.

142 Topolnik L, Chamberland S, Pelletier JG, Ran I, Lacaille JC. Activity-dependent compartmentalized regulation of dendritic Ca^{2+} signaling in hippocampal interneurons. J Neurosci. 2009;29:4658-63.

143 Sambandan S, Sauer JF, Vida I, Bartos M. Associative plasticity at excitatory synapses facilitates recruitment of fast-spiking interneurons in the dentate gyrus. J Neurosci. 2010;30:11826-37.

144 Jung MW, McNaughton BL. Spatial selectivity of unit activity in the hippocampal granular layer. Hippocampus. 1993;3:165-82.

145 Meyer AH, Katona I, Blatow M, Rozov A, Monyer H. In vivo labeling of parvalbumin-positive interneurons and analysis of electrical coupling in identified neurons. J Neurosci. 2002;22:7055-64.

146 Fan W, Ster J, Gerber U. Activation conditions for the induction of metabotropic glutamate receptor-dependent long-term depression in hippocampal CA1 pyramidal cells. J Neurosci. 2010;30:1471-5.

147 Hájos N, Mody I. Establishing a physiological environment for visualized in vitro brain slice recordings by increasing oxygen supply and modifying aCSF content. J Neurosci Methods. 2009;183:107-13.

148 Maier N, Morris G, Johenning FW, Schmitz D. An approach for reliably investigating hippocampal sharp wave-ripples in vitro. PLoS One. 2009;4:e6925.

149 Chrobak JJ, Lörincz A, Buzsáki G. Physiological patterns in the hippocampo-entorhinal cortex system. Hippocampus. 2000;10:457-65.

150 Axmacher N, Mormann F, Fernández G, Elger CE, Fell J. Memory formation by neuronal synchronization. Brain Res Rev. 2006;52:170-82

151 Abel T, Havekes R, Saletin JM, Walker MP. Sleep, plasticity and memory from molecules to whole-brain networks. Curr Biol. 2013;23(17):R774-88.

152 Baranyi A, Feher O. Long-term facilitation of excitatory synaptic transmission in single motor cortical neurones of the cat produced by repetitive pairing of synaptic potentials and action potentials following intracellular stimulation. Neurosci Lett. 1981;23:303-8.

153 Feldman DE. The spike-timing dependence of plasticity. Neuron. 2012;75:556-71.

154 Girardeau G, Benchenane K, Wiener SI, Buzsáki G, Zugaro MB. Selective suppression of hippocampal ripples impairs spatial memory. Nat Neurosci. 2009;12:1222-3.

155 Jadhav SP, Kemere C, German PW, Frank LM. Awake hippocampal sharp-wave ripples support spatial memory. Science. 2012;336:1454-8.

156 Zylla MM, Zhang X, Reichinnek S, Draguhn A, Both M. Cholinergic plasticity of oscillating neuronal assemblies in mouse hippocampal slices. PLoS One. 2013;8:e80718.

157 Bartos M, Vida I, Frotscher M, Meyer A, Monyer H, Geiger JR, Jonas P. Fast synaptic inhibition promotes synchronized gamma oscillations in hippocampal interneuron networks. Proc Natl Acad Sci U S A. 2002;99:13222-7.

158 Doischer D, Hosp JA, Yanagawa Y, Obata K, Jonas P, Vida I, Bartos M. Postnatal differentiation of basket cells from slow to fast signaling devices. J Neurosci. 2008;28:12956-68.

159 Jutras MJ, Buffalo EA. Synchronous neural activity and memory formation. Curr Opin Neurobiol. 2010;20:150-5.

160 Markram H, Lübke J, Frotscher M, Sakmann B. Regulation of synaptic efficacy by coincidence of postsynaptic APs and EPSPs. Science. 1997;275:213-5.

161 Hájos N, Paulsen O. Network mechanisms of gamma oscillations in the CA3 region of the hippocampus. Neural Netw. 2009;22:1113-9.

162 Vinck M, Lima B, Womelsdorf T, Oostenveld R, Singer W, Neuenschwander S, Fries P. Gamma-phase shifting in awake monkey visual cortex. J Neurosci. 2010;30:1250-7.

163 Fries P. A mechanism for cognitive dynamics: neuronal communication through neuronal coherence. Trends Cogn Sci. 2005;9:474-80.

164 Dan Y, Poo MM. Spike timing-dependent plasticity: from synapse to perception. Physiol Rev. 2006;86:1033-48.

165 Nowak L, Bregestovski P, Ascher P, Herbet A, Prochiantz A. Magnesium gates glutamate-activated channels in mouse central neurones. Nature. 1984;307:462-5.

166 Kampa BM, Clements J, Jonas P, Stuart GJ. Kinetics of Mg2+ unblock of NMDA receptors: implications for spike-timing dependent synaptic plasticity. J Physiol. 2004;556:337-45..

167 Caporale N, Dan Y. Spike timing-dependent plasticity: a Hebbian learning rule. Annu Rev Neurosci. 2008;31:25-46.

168 Kwag J, Paulsen O. Gating of NMDA receptor-mediated hippocampal spike timing-dependent potentiation by mGluR5. Neuropharmacology. 2012;63:701-9.

169 Conn PJ, Pin JP. Pharmacology and functions of metabotropic glutamate receptors. Annu Rev Pharmacol Toxicol. 1997;37:205-37.

170 Hermans E, Challiss RA. Structural, signalling and regulatory properties of the group I metabotropic glutamate receptors: prototypic family C G-protein-coupled receptors. Biochem J. 2001;359:465-84.

171 Hainmüller T, Krieglstein K, Kulik A, Bartos M. Joint CP-AMPA and group I mGlu receptor activation is required for synaptic plasticity in dentate gyrus fast-spiking interneurons. Proc Natl Acad Sci U S A. 2014;111:13211-6

172 Shigemoto R, Kinoshita A, Wada E, Nomura S, Ohishi H, Takada M, Flor PJ, Neki A, Abe T, Nakanishi S, Mizuno N. Differential presynaptic localization of metabotropic glutamate receptor subtypes in the rat hippocampus. J Neurosci. 1997;17:7503-22

173 Hestrin S, Nicoll RA, Perkel DJ, Sah P. Analysis of excitatory synaptic action in pyramidal cells using whole-cell recording from rat hippocampal slices. J Physiol. 1990;422:203-25.

174 Anwyl R. Metabotropic glutamate receptor-dependent long-term potentiation. Neuropharmacology. 2009;56:735-40.

175 Hunt DL, Castillo PE. Synaptic plasticity of NMDA receptors: mechanisms and functional implications. Curr Opin Neurobiol. 2012;22:496-508.

176 Kwon HB, Castillo PE. Long-term potentiation selectively expressed by NMDA receptors at hippocampal mossy fiber synapses. Neuron. 2008;57:108-20.

177 Marino MJ, Conn PJ. Direct and indirect modulation of the N-methyl D-aspartate receptor. Curr Drug Targets CNS Neurol Disord. 2002;1:1-16.

178 Awad H, Hubert GW, Smith Y, Levey AI, Conn PJ. Activation of metabotropic glutamate receptor 5 has direct excitatory effects and potentiates NMDA receptor currents in neurons of the subthalamic nucleus. J Neurosci. 2000;20:7871-9.

179 Attucci S, Carlà V, Mannaioni G, Moroni F. Activation of type 5 metabotropic glutamate receptors enhances NMDA responses in mice cortical wedges. Br J Pharmacol. 2001;132:799-806.

180 Pisani A, Gubellini P, Bonsi P, Conquet F, Picconi B, Centonze D, Bernardi G, Calabresi P. Metabotropic glutamate receptor 5 mediates the potentiation of N-methyl-D-aspartate responses in medium spiny striatal neurons. Neuroscience. 2001;106:579-87.

181 Jia Z, Lu Y, Henderson J, Taverna F, Romano C, Abramow-Newerly W, Wojtowicz JM, Roder J. Selective abolition of the NMDA component of long-term potentiation in mice lacking mGluR5. Learn Mem. 1998;5:331-43.

182 Campbell UC, Lalwani K, Hernandez L, Kinney GG, Conn PJ, Bristow LJ. The mGluR5 antagonist 2-methyl-6-(phenylethynyl)-pyridine (MPEP) potentiates PCP-induced cognitive deficits in rats. Psychopharmacology (Berl). 2004;175:310-8.

183 Nickols HH, Conn PJ. Development of allosteric modulators of GPCRs for treatment of CNS disorders. Neurobiol Dis. 2014;61:55-71.

184 Auerbach BD, Osterweil EK, Bear MF. Mutations causing syndromic autism define an axis of synaptic pathophysiology. Nature. 2011;480:63-8.

185 Naie K, Manahan-Vaughan D. Regulation by metabotropic glutamate receptor 5 of LTP in the dentate gyrus of freely moving rats: relevance for learning and memory formation. Cereb Cortex. 2004;14:189-98.

186 Zhang S, Manahan-Vaughan D. Place field stability requires the metabotropic glutamate receptor, mGlu5. Hippocampus. 2014;24:1330-40.

187 Sík A, Hájos N, Gulácsi A, Mody I, Freund TF. The absence of a major Ca^{2+} signaling pathway in GABAergic neurons of the hippocampus. Proc Natl Acad Sci U S A. 1998;95:3245-50.

188 McBain CJ, Freund TF, Mody I. Glutamatergic synapses onto hippocampal interneurons: precision timing without lasting plasticity. Trends Neurosci. 1999;22:228-35.

189 Lamsa KP, Kullmann DM, Woodin MA. Spike-timing dependent plasticity in inhibitory circuits. Front Synaptic Neurosci. 2010;2:8.

190 Lamsa K, Heeroma JH, Kullmann DM. Hebbian LTP in feed-forward inhibitory interneurons and the temporal fidelity of input discrimination. Nat Neurosci. 2005;8:916-24.

191 Le Vasseur M, Ran I, Lacaille JC. Selective induction of metabotropic glutamate receptor 1- and metabotropic glutamate receptor 5-dependent chemical long-term potentiation at oriens/alveus interneuron synapses of mouse hippocampus. Neuroscience. 2008;151:28-42.

192 Galván EJ, Calixto E, Barrionuevo G. Bidirectional Hebbian plasticity at hippocampal mossy fiber synapses on CA3 interneurons. J Neurosci. 2008;28(52):14042-55.

193 Sarihi A, Jiang B, Komaki A, Sohya K, Yanagawa Y, Tsumoto T. Metabotropic glutamate receptor type 5-dependent long-term potentiation of excitatory synapses on fast-spiking GABAergic neurons in mouse visual cortex. J Neurosci. 2008;28:1224-35.

Eidesstattliche Versicherung

„Ich, Shota Zarnadze, versichere an Eides statt durch meine eigenhändige Unterschrift, dass ich die vorgelegte Dissertation mit dem Thema: „Gamma Oscillation-Induced Plasticity in Area CA3 of the hippocampus" selbstständig und ohne nicht offengelegte Hilfe Dritter verfasst und keine anderen als die angegebenen Quellen und Hilfsmittel genutzt habe.

Alle Stellen, die wörtlich oder dem Sinne nach auf Publikationen oder Vorträgen anderer Autoren beruhen, sind als solche in korrekter Zitierung (siehe „Uniform Requirements for Manuscripts (URM)" des ICMJE -*www.**icmje**.org*) kenntlich gemacht. Die Abschnitte zu Methodik (insbesondere praktische Arbeiten, Laborbestimmungen, statistische Aufarbeitung) und Resultaten (insbesondere Abbildungen, Graphiken und Tabellen) entsprechen den URM (s.o) und werden von mir verantwortet.

Meine Anteile an etwaigen Publikationen zu dieser Dissertation entsprechen denen, die in der untenstehenden gemeinsamen Erklärung mit dem/der Betreuer/in, angegeben sind. Sämtliche Publikationen, die aus dieser Dissertation hervorgegangen sind und bei denen ich Autor bin, entsprechen den URM (s.o) und werden von mir verantwortet.

Die Bedeutung dieser eidesstattlichen Versicherung und die strafrechtlichen Folgen einer unwahren eidesstattlichen Versicherung (§156,161 des Strafgesetzbuches) sind mir bekannt und bewusst."

Datum 10.06.2015 Unterschrift

Anteilserklärung an etwaigen erfolgten Publikationen

Shota Zarnadze hatte folgenden Anteil an den folgenden Publikationen:
Publikation 1: Zarnadze S, Bäuerle P, Böhm C, Schmitz D, Dugladze T, Gloveli T. Synaptic plasticity induced by gamma oscillations, under review.

S. Zarnadze recorded local field oscillations and single cell activity simultaneously, using patch clamp technics and analyzed obtained data. He further identified recorded cells morphologically by immunohistochemical/biocytin staining and confocal microscopy. He designed the figures and took part in the writing of the manuscript.

Publikation 2: Eller J, Zarnadze S, Bäuerle P, Dugladze T, Gloveli T. Cell type-specific separation of subicular principal neurons during fast network oscillations. PLoS One. 2015;10:e0123636.

S. Zarnadze prepared horizontal and sagittal hippocampal slices and recorded network gamma frequency oscillations in the intact and isolated subiculum. He analyzed and compared the power and frequency of gamma rhythm between dorsal, ventral and intermediate horizontal as well as medial and lateral sagittal subicular slices.

Unterschrift, Datum und Stempel des betreuenden Hochschullehrers/der betreuenden Hochschullehrerin

Unterschrift des Doktoranden/der Doktorandin

Curriculum vitae

Shota Zarnadze

Mein Lebenslauf wird aus datenschutzrechtlichen Gründen in der elektronischen Version meiner Arbeit nicht veröffentlicht.

List of publications

1. **Zarnadze S**, Bäuerle P, Böhm C, Schmitz D, Dugladze T, Gloveli T. Synaptic plasticity induced by gamma oscillations, under review.

2. Eller J, **Zarnadze S**, Bäuerle P, Dugladze T, Gloveli T. Cell type-specific separation of subicular principal neurons during fast network oscillations. PLoS One. 2015;14;10(4):e0123636.

Acknowledgment

I would like to pay special thankfulness and appreciation to the persons who helped me during this important period of my life, made my research successful and assisted me at every point to cherish my goal.

I would firstly like to express the deepest appreciation to my supervisor Prof. Dr. Tengis Gloveli for his guidance and persistent help, his great generosity of time and patience. He continually and convincingly conveyed a spirit of adventure in regard to research and excitement in regard to teaching. Without his support this dissertation would not have been possible.

I would like to thank Dr. Tamar Dugladze for her assistance with certain experiments. She helped me to overcome substantial challenges and provided me with valuable practical tips and suggestions from her ample experience in electrophysiology and immunostaining procedures.

I am particularly grateful to my dear colleges and friends Dr. Nino Maziashvili and Shalva Gurgenidze whose help enabled me to take first steps to perform neurophysiological experiments.

For his invaluable intellectual input and encouragement, I am very grateful to Dr. Peter Bäuerle.

Special thanks are due to my companions during the working hours and my friends Joanna Eller, Katja Luther, Linda Brenndörfer and Melanie Timmler for their professional support and great sense of humor creating a pleasant working atmosphere.

I would also like to thank Sonja Frosinski, Pamela Glowaki and Dr. Katrin Schulze for their great administrative assistance whose reminders and constant motivation encouraged me to meet the deadlines.

For their technical support, I am very grateful to Bernd Schacht and Janine Tyra.

I also thank my friends Dr. Birgit Voigt and Tobias Albert for their moral and emotional support.

Finally, I want to thank my parents and my wife whose help over the last few years has been immense and invaluable.